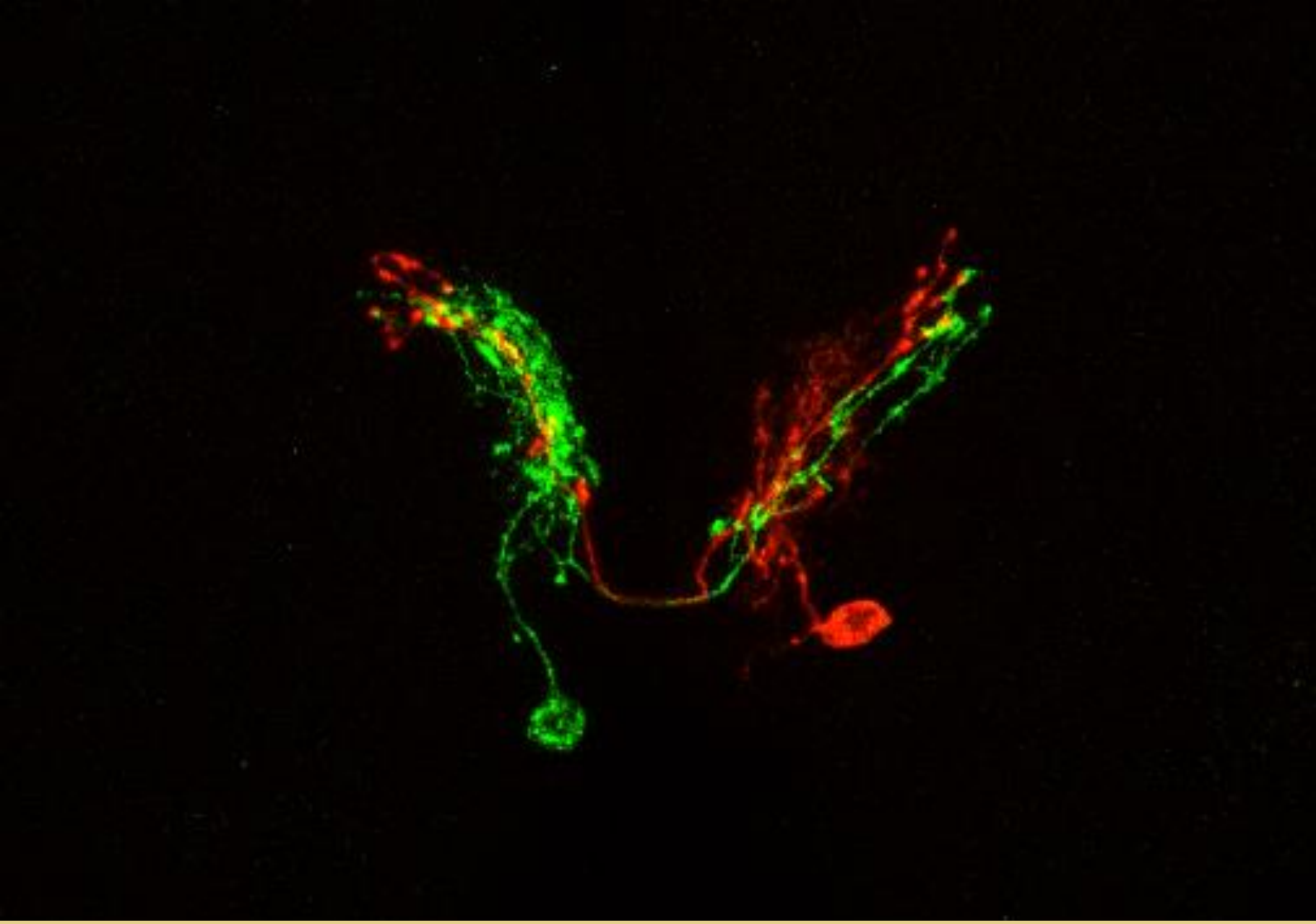

Joana Sofia Costa Pereirinha

Cell type-specific drivers to study the Dilp8-sensitive neuroendocrine circuit

Tese de Mestrado em Biologia Celular e Molecular, realizada sob a orientação científica do Doutor Alisson Gontijo (CEDOC-Centro de Estudos de Doenças Crónicas da Universidade Nova de Lisboa) e orientação interina da Professora Doutora Emília Duarte (Centro de Neurociências e Biologia Celular da Universidade de Coimbra), e apresentada ao Departamento de Ciências da Vida da Faculdade de Ciências e Tecnologia da Universidade de Coimbra (DCV-FCTUC)

Setembro de 2017

· U C ·

Universidade de Coimbra

ACKNOWLEDGMENTS

Após o esforço e dedicação de tantas pessoas, a tese está finalmente acabada.

Agradeço ao meu orientador Alisson. Obrigada por me ter dado a oportunidade de entrar no Integrative Biomedicine Laboratory e de fazer parte da fabulosa equipa que o constitui. Quero também agradecer-lhe por ter dado o mote e me ensinar a fazer boa ciência. À Fabiana, agradeço-lhe tudo o que me ensinou, desde o inicio até ao fim, toda a paciência que teve e todas as vezes que me incentivou. Agradeço aos dois a confiança que depositaram em mim e a oportunidade que me deram. Obrigada.

Agradeço também a todos os meus colegas do IBL. André, Andreia, Ângela, Ivana, Raquel, Filipe, Yanel, Ana, Cláudia e Ednilson, obrigada por fazerem do nosso grupo uma equipa onde todos se ajudam e onde se trabalha com gosto. Agradeço principalmente ao André e à Andreia por toda a paciência que tiveram para mim e para me ensinar e todas as vezes que responderam aquelas minhas perguntas.

Aos meus amigos, agradeço-vos por continuarem a ser meus amigos após quase um ano de ausência e negligência. À Sara, por estares sempre lá para mim. Agradeço à Joana e à Mariana por me darem força e por não deixarem que o meu dramatismo leve a melhor.

À Catarina, por teres tido um ano de paciência, por teres tomado conta de mim e por teres feito deste ano que passou um ano muito melhor.

Agradeço aos meus pais e ao resto da minha família, tudo o que fizeram para eu ter tido as oportunidades que tive, por nunca terem posto entraves ao meu futuro e por me terem apoiado sempre. Agradeço à minha irmã, Inês, por seres minha irmã e me dizeres sempre a verdade.

Ao Fábio, obrigada pela paciência que tiveste para mim, por aguentares o stress todo e por me apoiares sempre. Sem ti não teria sido possível.

Muito obrigada.

CONTRIBUTIONS

This master thesis resulted from a common effort of the IBL team, in particular I would like to point out the following contributions:

The results represented in Figure 4.2 and 4.5 were generated by me, Fabiana Herédia and Andreia Casimiro.

The results represented in Table 4 were generated by Andrés Garelli and Andreia Casimiro.

The results represented in Figure 4.12 were generated by me and André Macedo.

Work in the Integrative Biomedicine Laboratory during my thesis was supported by the FCT and the EU, via the 7th Framework Programme (CIG).

ABSTRACT

Body organs of animals coordinate their growth through autonomous and non-autonomous programs, which together produce individuals with organs of a size and proportion typical of a species. The ability of animals to achieve this developmental program even in the face of severe developmental and/or environmental perturbations is termed developmental stability. In Drosophila, an insulin-like peptide, Dilp8, mediates interorgan growth coordination during larval development. Dilp8 is produced whenever abnormal growth occurs in peripheral epithelial tissues (imaginal discs) of developing larvae. Dilp8 activity induces a delay in the onset of metamorphosis by antagonizing the metamorphosis-inducing ecdysone signalling pathway, providing extra time for the developing larvae to compensate for the growth of abnormally growing tissues, promoting developmental stability. This Dilp8 activity is absolutely dependent on the presence of a conserved relaxin receptor-like protein, Lgr3, in the larval CNS. Two bilateral brain interneurons, named *pars intercerebralis Lgr3*-positive (PIL) neurons, have been hypothesized to be the critical neurons mediating the Lgr3-dependent response to the Dilp8 peripheral tissue stress signal. The model is that the Dilp8 signal activates Lgr3 receptor expressed in the PIL neurons. This leads to an increase in cAMP signalling and PIL neuron activation, which somehow leads to a delay in the biosynthesis of ecdysone by the ring gland and a consequential delay in the onset of metamorphosis. The main aim of this thesis is to test this model by generating PIL neuron-specific genetic drivers. For this, we used four different strategies: 1) genetic dissection of a regulatory element previously shown to drive expression in PIL neurons (*RB19B09>*); 2) searching for at least four independent sparse gene drivers that drive expression in PIL neurons to constitute a Versatile Entry Code (VEnCode) for PIL neurons in order to generate an exquisitely-specific VEnCode-based PIL neuron driver based on a new quadruply-split GAL4 (4x-split VEnC-GAL4); 3) using these REs to generate Split GAL4-based PIL neuron drivers; and 4) using recombinase-mediated Flp-out intersectional strategies to manipulate PIL neurons using the *MZ699>* and *RB19B09>* drivers (*MZ699* ∩ *RB19B09>*). With strategy 1 and 2 we obtained four elements, *R19B09.3A, R19B09.3C, R29B09* and *R25E10*, all of which drive expression in PIL neurons and are being used to develop VEnCode- or Split GAL4-based drivers for PIL neurons. By removing *Lgr3* using RNAi (*Lgr3-IR*) or thermogenetically activating neurons with TrpA1 in subpopulations of cells under the control of these and other drivers developed in strategy 4, I made a series of key findings that challenge the current model of how the Dilp8-Lgr3 pathway works: while the data still support the fact that Lgr3 is required in PIL neurons to convey the Dilp8 peripheral stress signal and delay development, I gathered enough evidence to reject the hypothesis that PIL neurons are activated following Dilp8 signalling. Rather, TrpA1 thermogenetic neuronal activation and Kir2.1-mediated neuronal silencing of the few *MZ699* ∩ *RB19B09>*-expressing cells, suggest a model where PIL neurons have a constitutive activity that promotes pupariation, which is temporarily silenced upon Dilp8-Lgr3 signalling. In addition to these functional studies,

I further defined PIL neuron neuroanatomy, observing that the bilateral pairs of PIL neurons are not identical: while both send ipsilateral and contralateral projections to the anterior-dorsal most compartments of the neuropil, only one of the bilateral PIL neuron sends ipsilateral projections towards the subesophageal zone. Finally, by exploring an imaging-based screen for drivers putatively driving expression in PIL neurons, I discovered novel cell populations, characterized by the drivers *R48H10>* and *R69F02>,* which induce a delay in pupariation upon TrpA1 thermogenetic activation. I found no evidence that any of these cells act in the Dilp8-Lgr3 pathway, but it is possible that they might act downstream of PIL neurons. I also found a restricted population of elav-GAL80 resistant *R19B09>* and *R69F02>*-expressing cells that cause a delay in pupariation upon TrpA1 thermogenetic activation. I end my thesis by proposing a revised model of how the Dilp8-Lgr3 pathway works to promote developmental stability, which hopefully could be tested with the new VEnCode- and Split GAL4-based PIL neuron drivers that my work opens up the possibility to develop.

Key-words: Developmental stability, Dilp8, Lgr3, neuroanatomy, *D. melanogaster*

SUMÁRIO

Os órgãos dos animais coordenam o seu crescimento através de programas autónomos e não autónomos, que juntos originam adultos com órgãos de tamanho e proporção típicos da espécie. A capacidade dos animais de recorrerem a este programa de desenvolvimento, mesmo encarando graves perturbações ambientais e/ou de desenvolvimento, é chamada estabilidade do desenvolvimento. Em *Drosophila,* Dilp8, um péptido tipo-insulina, medeia a coordenação do desenvolvimento inter-orgão durante o desenvolvimento larval. Dilp8 é produzido sempre que ocorre crescimento anormal nos tecidos epiteliais periféricos (discos imaginais) em larvas em desenvolvimento. A atividade de Dilp8 induz um atraso no começo da metamorfose por ser antagonista da via de sinalização da ecdisona, indutora da metamorfose. Portanto a atividade de Dilp8 proporciona tempo adicional para o desenvolvimento larval de forma a compensar o crescimento dos tecidos a crescer irregularmente, promovendo a estabilidade do desenvolvimento. Tem-se descrito que Dilp8 atua no SNC através de um novo circuito neuronal que inclui dois interneurónios bilaterais (neurónios PIL) que expressam Lgr3, uma proteína conservada tipo-recetor de relaxina. Como Dilp8, Lgr3 é essencial para prevenir a variabilidade no desenvolvimento. Foi colocada a hipótese de que os neurónios PIL são essenciais para mediar a resposta, dependente de Lgr3, ao sinal de stress Dilp8. O modelo proposto é que o sinal periférico Dilp8 ativa o recetor Lgr3 expresso nos interneurónios PIL. Isto induz um aumento na sinalização de cAMP e a atividade dos neurónios PIL, o que leva ao atraso na biossíntese de ecdisona pela glândula anelar e por consequência um atraso no começo da metamorfose. O principal objetivo desta tese é testar este modelo, caracterizando elementos regulatórios (ERs) específicos para os neurónios PIL ao usar quatro estratégias distintas: 1) dissecar um elemento regulatório, com capacidade de regular a expressão nos neurónios PIL, previamente testado (R19B09>); 2) procurar pelo menos quatro ERs genéticos que levam à expressão nos neurónios PIL, para integrar o Versatile Entry Code (VEnCode) especifico para os neurónios PIL, recorrendo a uma nova estratégia de GAL4 dividido em 4 (4x-split VEnC-GAL4); 3) usar estes ERs para conduzir a expressão genética de neurónios PIL baseados no Split-GAL4; e 4) usar estratégias de interseção Flp-out mediadas por recombinação para manipular os neurónios PIL usando os ERs *MZ699>* e *RB19B09>* (*MZ699* ∩ *RB19B09>*). Usando as estratégias 1 e 2 obtivemos quatro elementos, *R19B09.3A, R19B09.3C, R29B09* e *R25E10,* em que todos levam à expressão nos neurónios PIL e são usados para o desenvolvimento de condutores de expressão genética nos neurónios PIL, baseados no VEnCode ou no Split-GAL4. Ao remover Lgr3, usando RNAi (Lgr3-IR) ou ativando termogeneticamente neurónios com TrpA1 em subpopulações de células sob o controlo destes ERs ou de outros desenvolvidos na estratégia 4, nós fizemos diversas descobertas que desafiam o modelo atual de funcionamento da via Dilp8-Lgr3: enquanto os nossos resultados sustentam o facto de que Lgr3 é necessário nos neurónios PIL para transmitir o sinal de Dilp8 e atrasar o desenvolvimento, os nossos resultados rejeitam

a hipótese de que os neurónios PIL são ativados depois da sinalização de Dilp8. A ativação neuronal termogenética por TrpA1 e o silenciamento neuronal mediado por Kir2.1 das poucas células onde ambos os ERs *MZ699* e *RB19B09* regulam a expressão genética, sugerindo um novo modelo onde os neurónios PIL têm atividade constitutiva que promove a pupariação, que é temporariamente silenciada em resposta à sinalização Dilp8-Lgr3. Adicionalmente a estes estudos funcionais, nós definimos a neuroanatomia dos neurónios PIL, observando que o par bilateral de neurónios PIL não é idêntico: enquanto ambos revelam projeções ipsilaterais e contralaterais para a maioria dos compartimentos anterior-dorsal do neurópilo, um dos neurónios PIL bilaterais revela projeções ipsilaterais para a zona subesofagial, enquanto que o outro não. Por ultimo, ao explorar uma seleção com base em imagiologia para os ERs que hipoteticamente conduzem expressão genética nos neurónios PIL, nós descobrimos novas populações celulares, caracterizadas pelos ERs *R48H10>* e *R69F02>,* que induzem um atraso na pupariação após ativação termogenética por TrpA1. Nós não encontrámos evidencias de que estas células atuam na via Dilp8-Lgr3, mas é possível que atuem a jusante dos neurónios PIL. Nós descobrimos populações restritas de células R19B09 e R69F02 resistentes a elav-GAL80 que causam um atraso na pupariação após ativação por TrpA1. No final desta tese proponho um modelo revisto de como a via Dilp8-Lgr3 atua para promover a estabilidade do desenvolvimento, o que no futuro poderá ser estudado usando os novos ERs de neurónios PIL baseados no VEnCode e no Split-GAL4, ao qual os resultados deste trabalho permitem dar continuidade.

Palavras-chave: Estabilidade no desenvolvimento, Dilp8, Lgr3, neuroanatomia, *D. melanogaster*

TABLE OF CONTENTS

Acknowledgments ..... **I**
Contributions ..... **II**
Abstract ..... **III**
Sumário ..... **V**
Table of Contents ..... **VII**
Figure Index ..... **IX**
Abbreviations ..... **X**
1 Introduction **11**
1.1 Developmental stability in *Drosophila* 2
1.2 Dilp8-dependent delay of developmental progression 4
1.3 VEnCode, a new technology for cellular targeting 6
2 Objectives **10**
3 Materials and Methods **12**
3.1 *Drosophila melanogaster* as a genetic tool 13
3.1.1 *Drosophila melanogaster* stocks 14
3.1.2 Larval dissection and Immunohistochemistry 16
3.1.3 Developmental time assay 17
3.1.4 Generation of transgenic flies 18
3.2 Cell culture 18
3.2.1 DL2 cells 18
3.2.2 Cell transfection 19
3.2.3 Cell preparation and Immunocytochemistry 19
3.3 Molecular Biology 20
3.3.1 Cloning Techniques 20
3.3.2 Gateway Cloning Technology 22
3.3.3 Construction of the pENTR plasmids 23
3.3.4 Construction of the Split-Gal4 plasmids 27
4 Results and Discussion **29**
4.1 Dissection of the R19B09 enhancer 30
4.2 New methodologies – VEnCode 37
4.2.1 Identification of candidates for PIL neuron-specific drivers 37
4.2.2 VEnCode for PIL neurons 38
4.2.3 VEnCode for PTTH-producing neurons 42
4.2.4 Quadruply-split GAL4 pieces for the VEnCode-based gene drivers 43
4.3 PIL neuron anatomical considerations 45
4.4 Backup methodologies 48
4.4.1 Recombination mediated (R19B09-MZ699) expression restriction 48
4.4.2 Split GAL4 52

4.5 New elements of the Dilp8-dependent delay 53
5 Major conclusions 59
References 64

FIGURE INDEX

Figure 1.1. Ecdysone pulses induce each of the major developmental transitions in the *Drosophila* life cycle.....3
Figure 1.2. Dilp8-sensitive neuroendocrine pathway coupling growth and maturation timing.....6
Figure 1.3. VEnCode model. 7
Figure 1.4. Schematic representation of the GAL4-UAS system of Drosophila, a binary system for targeting expression in vivo.....7
Figure 3.1 The life cycle of *Drosophila melanogaster*.....14
Figure 3.2. Schematic representation of phiC31-mediated integration. 18
Figure 3.3. Model of Gateway Technology system. 22
Figure 3.4. Model of pENTR construction with the designed MCS. 23
Figure 3.5. 4x split VEnC-GAL4 developed with three specific split-inteíns.....24
Figure 3.6. Strategy for RE cloning. 26
Figure 3.7. Final model of pENTRs cloning and the final plasmids detailed. 27
Figure 3.8. Strategy for Split-Gal4 cloning.. 28
Figure 3.9. Final model of the Split GAL4 plasmids. 28
Figure 4.1. Schematic representation of the *Lgr3* gene. 30
Figure 4.2. Functional dissection of the R19B09 regulatory element identifies two independent regions that redundantly control *Lgr3* expression in cells that are relevant for the Dilp8-dependent delay.....31
Figure 4.3. *Lgr3* R19B09.3 fragments drive expression in PIL neurons. 33
Figure 4.4. Two independent REs within the R19B09 element drive gene expression in the PIL neurons. 34
Figure 4.5. Lgr3 R19B09.3 fragments drive expression in TrpA1-sensitive cells, inducing a developmental timing delay.....36
Figure 4.6. The *Lgr3* gene has at least two shadow enhancers that are active in the PIL neurons. 37
Figure 4.7. Images from FlyLight representing the described GAL4 drivers pattern in the larval CNS. 38
Figure 4.8. New TrpA1-sensitive cells delay the onset of metamorphosis. 40
Figure 4.9. New REs are expressed in a subset of cells that include the PIL neurons. 41
Figure 4.10. Specific REs selected to construct a VEnCode for PIL neurons. 42
Figure 4.11. Specific REs selected to constitute a VEnCode for PTTH-producing neurons. 43
Figure 4.12. *4x-split VEnC-GAL4* activates gene transcription. 45
Figure 4.13. PIL neuron neuroanatomy. 47
Figure 4.14. PIL neuron neuroanatomy during larval development. 48
Figure 4.15. R19B09 ∩ MZ699> drives gene expression in PIL neurons. 49
Figure 4.16. R19B09 ∩ MZ699 cells are not sufficient to induce a delay upon TrpA1 thermogenetic activation.. 51
Figure 4.17. Kir2.1 silencing of R19B09 ∩ MZ699 cells does not rescue the Dilp8-dependent delay. 52
Figure 4.18. Discovery of new cell populations able to induce an Lgr3-independent delay in developmental timing. 56
Figure 4.19. Lgr3 is not required in *R48H10*>- or *R69F02*>-expressing cells to delay development in response to Dilp8 activity. 56
Figure 4.20. Preliminary evidence that some TrpA1-sensitive 2x-elav-GAL80-resistant cells drive developmental delays. 58
Figure 5.1. Models of the Dilp8-Lgr3 pathway, leading to a delay in the developmental progression.....53
Figure 5.2. Summary of the cell populations found that mediate the Dilp8-dependent delay.....54

ABBREVIATIONS

20E	20-hydroxyecdysone
AD	Activation domain
AEL	After egg laying
attB	Bacterial attachment site
attP	Phage attachment site
BDSC	Bloomington *Drosophila* Stock Center
Brp	Bruchpilot
BSA	Bovine serum albumin
cAMP	Cyclic adenosine monophosphate
CNS	Central nervous system
DAPI	4',6-diamidino-2-phenylindole
DBD	Binding domain
Dilp	*Drosophila* insulin-like peptides
DL2	*Drosophila* line 2
DNA	Deoxyribonucleic acid
DPE	Downstream promoter element
DSCP	*Drosophila* synthetic core promoter
EF	Esophageal forame
FBS	Fetal bovine serum
Flp	Flippase
FRT	Flippase recognition target
GFP	Green fluorescence protein
HA	Human influenza hemagglutinin
IIS	Insulin/insulin-like growth factor signalling
Inr	Initiator element
InR	Insulin receptor
IPC	Insulin-producing cells
IQR	Interquartile range
JAK	Janus kinase
JH	Juvenile hormone
JNK	c-Jun N-terminal kinases
LB	Lysogeny broth
Lgr3	Leucine-rich repeat G protein-coupled receptor 3
MCFO	Multicolor flp-out
MCS	Multiple-cloning site
mRNA	Messenger RNA
MTE	Motif ten element
PBS	Phosphate-buffered saline
PBST	PBS triton

PCR Polymerase chain reaction

PFA Paraformaldehyde

PG Prothoracic gland

PIL *pars intercerebralis* Lgr3-positive

PTTH Prothoracicotropic hormone

RE Regulatory elements

RFP Red fluorescence protein

RNA Ribonucleic acid

RNAi RNA interference

RT Room temperature

RXFPs Relaxin family peptides

SEZ Subesophageal zone

sfGFP super folder GFP

SL2 Schneider line 2

smGFP spaghetti monster GFP

SOC Super Optimal broth with Catabolite repression

STAT Signal transducer and activator of transcription

Tb Tubby marker

TGP Terminal growth period

TrpA1 Transient receptor potential cation channel A1

UAS Upstream activating sequence

VNC Ventral nerve cord

1 INTRODUCTION

1.1 DEVELOPMENTAL STABILITY IN *DROSOPHILA*

The regulation of final organ size is fundamental to ensure normal development. Organ size is coordinated with organ function and if organ size is not regulated correctly, this function can be compromised (Shingleton 2010; Gokhale & Shingleton 2015). Flies and mammals share many conserved genes and signalling pathways, so that *Drosophila* becomes a great model to study how organ size is regulated, being informative about how organ size is regulated in animals in general. While organ growth has many autonomous components, it also has to be coordinated across the whole organism, to assure fine proportionality and buffer development against variations in the environment or in intrinsic errors of development (Davidowitz et al. 2003; Tennessen & Thummel 2011; Gokhale & Shingleton 2015). The development of individual organs may be slowed by localized abnormalities in cell proliferation, such as tumours or injuries that trigger tissue repair and/or regeneration (Thornhill & Møller 1997). Hormones have been shown to play an important role in assuring that each organ reaches its normal size at the normal time during development (Shingleton 2010).

The life history of animals typically has discrete stages representing embryonic development, a juvenile growth phase, sexual maturation and reproductive adulthood. In *Drosophila*, post-embryonic development is characterized by a succession of well-defined stages. It begins as a worm-like larvae that develops through three stages (instars) separated by two molts. At the end of the third instar, larvae enter the pupal stage, in which they undergo complete metamorphosis into the adult form (Soller et al. 1999). Many adult structures and appendages (e.g. antennas, eyes, wings and legs) originate from the imaginal discs of the larvae. These discs are simple epithelial sacs that grow discretely during the larval stage. At the onset of metamorphosis, the discs stop growing and undergo final differentiation, evagination and fusion. Premetamorphic growth therefore determines final adult body size and imaginal disc growth determines adult organ size. Imaginal disc growth is influenced by many of the same humoral factors and signalling pathways that regulate growth in larval tissues. When disc growth is compromised, the duration of the larval stage increases, allowing extra time for the tissues to regenerate and achieve their target size before the onset of metamorphosis (Poodry & Woods 1990).

Some of the most well studied hormones that control the larval growth are ecdysone (and its active form, 20-hydroxyecdysone (20E)), the prothoracicotropic hormone (PTTH) and the juvenile hormone (JH). Neurosecretory cells in the brain produce PTTH, which is responsible for positively regulating the timing of molting by stimulating the biosynthesis and release of ecdysone from the prothoracic gland (PG) into the hemolymph (Agui et al. 1979). Progression through all of the developmental stages is dictated by pulses of 20E (Thummel 2001) **(Figure 1.1)**. JH is thought to promote larval molts and inhibit the metamorphosis program. During the final larval instar, JH levels decline. This is thought to license the next major 20E pulse to induce the onset of the metamorphosis program. As PTTH feeds into the ecdysone biosynthesis program, manipulations of the PTTH levels or ablation of PTTH-producing neurons delay the 20E pulse and extends the larval growth stage, leading to larger flies (Nijhout & Williams 1974). In summary, these and other hormonal

cascades coordinate critical *Drosophila* developmental stage transitions and thereby final body and organ size.

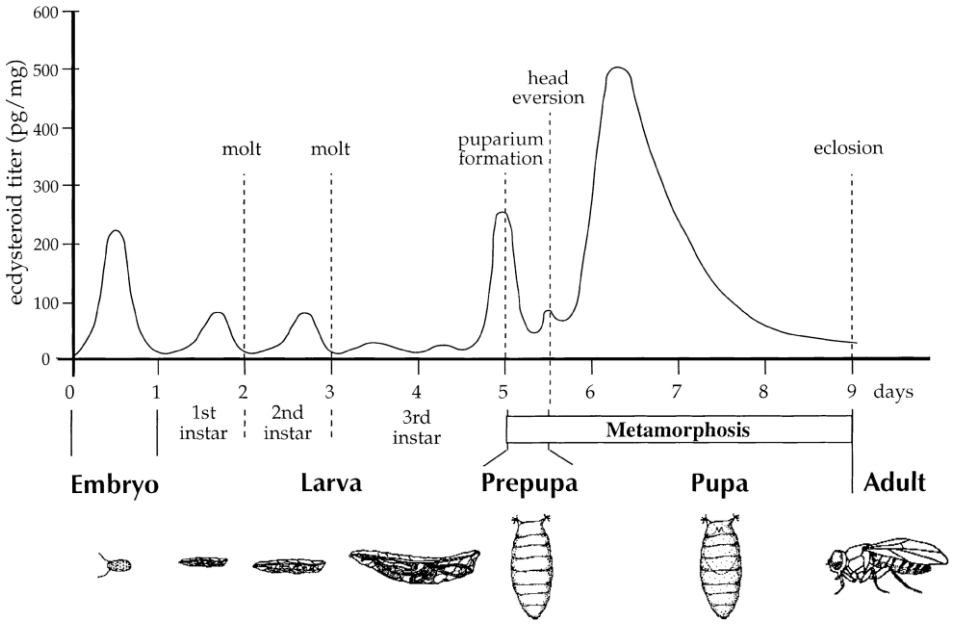

Figure 1.1. Ecdysone pulses induce each of the major developmental transitions in the *Drosophila* life cycle (Thummel 2001).

Various types of damage can trigger a response that results in prolonged larval or pupal stages. The extent of this developmental delay is correlated with two factors: 1) the amount of damaged tissue and 2) the developmental phase in which the damage has occurred (Simpson et al. 1980; Stieper et al. 2008). The amount of damaged tissue is positively correlated to the length of the delay (Simpson et al. 1980) and damage in any stage of development only induces a delay of the onset of metamorphosis at the third instar stage (Halme et al. 2010). These findings suggested the presence of a developmental checkpoint in the last larval instar. This checkpoint is thought to extend larval growth by inhibiting the transcription of the gene encoding PTTH, which will lead to reduced ecdysone biosynthesis and consequently a delayed onset of metamorphosis (Halme et al. 2010; Hackney et al. 2012). Consistently, developmental delays induced by X-irradiation are associated with a decrease in *ptth* expression and this can be reverted via ectopic feeding of 20E (Halme et al. 2010).

The timing of insect metamorphosis is also known to be regulated by the larva reaching the critical weight in the final larval instar. Once the larva achieves critical weight, the PG begins to release small amounts of ecdysone, that promotes growth of imaginal tissues (Herboso et al. 2015), preparing the animal for the termination of larval development. Achievement of critical weight is related with the beginning of the hormonal cascade that culminates in metamorphosis (Mirth et al. 2016). However, there is a temporal delay between the achievement of critical weight and the elevation of ecdysone levels that causes the larva to stop feeding and end body growth. During this period, called terminal growth period (TGP), *Drosophila* larvae can more than triple their mass (Stieper et al. 2008). In *Drosophila*, both body and organ sizes are regulated by the critical weight plus the growth achieved during the TGP (Davidowitz et al. 2003).

Some factors as malnutrition or starvation can delay the achievement of critical weight in *Drosophila*. If animals encounter poor nutrient conditions prior to the onset of critical weight, larval development will stall and subsequent increases in ecdysone levels will be delayed until growth conditions become appropriate again (Mirth & Riddiford 2007; Edgar 2006). This mechanism ensures the storage of sufficient nutrients for survival during the pupal stage. Larvae that have achieved critical weight have sufficient stored energy to complete metamorphosis. The main signalling pathway regulating growth related to nutrition is the insulin/insulin-like growth factor signalling (IIS) pathway. Reduction of IIS early in development can delay the achievement of critical weight (Shingleton et al. 2005). Inversely, upregulating the synthesis of *Drosophila* insulin-like peptides (Dilps) from insulin-producing cells (IPCs) results in elevated ecdysone signalling and precocious initiation of metamorphosis (Walkiewicz & Stern 2009). Manipulation of IPCs by starvation or mutations leads to the generation of animals with smaller size (Zhang et al. 2009; Ikeya et al. 2016). The *Drosophila* genome encodes eight Dilps (Dilp1-8), Dilp2, 3 and 5 are produced by IPCs of the brain (Cao & Brown 2001) and Dilp6 is produced by fat body (Slaidina et al. 2009). Recent reports demonstrated *dilp8* expression in abnormally-growing in larval imaginal discs (Colombani et al. 2012; Garelli et al. 2012).

1.2 DILP8-DEPENDENT DELAY OF DEVELOPMENTAL PROGRESSION

Imaginal discs play an important role in coordinating the developmental processes leading to metamorphosis. In 1927, it was observed that x-ray irradiation of *Drosophila* larvae delayed pupariation (Hussey et al. 1927). This delay has been found to be proportional to the amount of regenerating imaginal disc tissue triggered by the damage inflicted to the imaginal discs by irradiation. Importantly, larvae with damaged imaginal discs metamorphose at the correct size, suggesting that a mechanism exists that promotes developmental stability by coupling the status of the imaginal disc growth to the activity of the neuroendocrine centres controlling developmental timing (Stieper et al. 2008). Subsequent research showed that tumorous growth of imaginal discs also strongly delays metamorphosis (Menut et al. 2007). This led to the hypothesis that aberrant imaginal disc growth produces a diffusible factor that is able to inhibit the larva to pupa transition. Garelli *et al.* tried to identify this factor by looking for genes up-regulated in delay-producing eye-disc tumours (Garelli et al. 2012). They identified *dilp8*, a gene encoding a small prepropeptide of about 150 amino acids, which shares many similarities with insulin-like peptides. Dilp8 has homology to the human relaxin peptides (Garelli et al. 2012; Bathgate et al. 2013). *dilp8* mutants showed a reduced developmental delay in response to imaginal disc abnormal growth. This study together with a study by Colombani *et al*., demonstrated that Dilp8 is the signal produced by growing imaginal tissues that relays the growth status of the discs to the neuroendocrine centres controlling the onset of metamorphosis (Colombani et al. 2012). Colombani *et al*. also showed that *dilp8* induction in the damaged discs is dependent on JNK signalling (Colombani et al. 2012). JAK/STAT signalling, which is activated by JNK signalling, is then required for *dilp8* expression in conditions of aberrant tissue growth (Katsuyama et al. 2015). Dilp8 acts on the brain

to suppress ecdysone production and activity (Colombani et al. 2012; Garelli et al. 2012) by delaying and/or inhibiting the biosynthesis of ecdysone by the prothoracic gland, a part of a composite endocrine organ called the ring gland (Colombani et al. 2012; Garelli et al. 2012). It was unclear exactly how Dilp8 interacted with the PTTH-producing neurons (Garelli et al. 2012).

Garelli *et al*. found a neuronal receptor, leucine-rich repeat G protein-coupled receptor 3 (Lgr3), that plays a critical role in the Dilp8-dependent developmental stability circuit (Garelli et al. 2015). Lgr3 is an orphan receptor that belongs to the relaxin family peptides receptors (RXFPs), with 34% of identity with human RXFP1 and RXFP2 (Bathgate et al. 2013). Lgr3 acts in the Dilp8 pathway, where, like Dilp8, it mediates the communication between damaged imaginal discs and the PG. Lgr3 protein is detectable in the central nervous system (CNS), in about 180 neurons, 50 of which are located in the brain. Four of these Lgr3-positive neurons are a pair of bilateral *pars intercerebralis* Lgr3-positive (PIL) neurons, that are good candidate neurons to mediate the Dilp8-dependent developmental delay (Garelli et al. 2015). PIL neurons require Lgr3 to respond to Dilp8 by increasing cAMP levels (Garelli et al. 2015; Vallejo et al. 2015). Similar results were reported in other study (Colombani et al. 2015). Dilp8 was shown to bind directly to different receptors, including the Insulin Receptor (InR) (Garelli et al. 2015) and Lgr3 itself (Vallejo et al. 2015). It therefore remains to be determined whether Dilp8 can penetrate the blood-brain-barrier separating the brain and the peripheral tissues and act by directly activating Lgr3 in the PIL neurons. Moreover, the path the Dilp8 "tissue stress" signal follows PIL neuron activation remains to be clearly defined. Even though it is known that ultimately Dilp8 will affect the levels of ecdysone, how exactly PIL neuron activation affects the ecdysone production is unknown because PIL neurons do not seem to project to the PG. This suggests that there must be other neurons interacting with PIL neurons and sending information downstream. PTTH neurons are one of the candidate neurons that could interact with PIL neurons and send the information of delay to the ring gland, inhibiting the synthesis of ecdysone (Garelli et al. 2015). However, the IPCs, which are known to modulate developmental timing (Rulifson et al. 2002), can also the mediate PIL neuron-PG interaction. These results demonstrate that the Dilp8/Lgr3 neuroendocrine circuit is involved in a feedback that guarantees the coordination between developmental transitions and organ growth **(Figure 1.2)**. Our work intends to contribute to the understanding of how exactly the peripheral Dilp8 signal reaches the PIL neurons and how these activated PIL neurons influence ecdysone production. Specifically, we hope to build the tools to test the role of PIL and PTTH neurons in this neuroendocrine circuit responsive to abnormal tissue growth.

The similarities between the Dilp8-Lgr3-PG circuitry and the hypothalamic-pituitary axis in humans has become visible. The Dilp8-responding and Lgr3-expressing PIL neurons are located in the *pars intercerebralis*, a brain region which is anatomically and functionally analogous to the vertebrate hypothalamus. While the *Drosophila pars intercerebralis* connects the CNS to the ring gland, in vertebrates, the hypothalamus connects the CNS to the endocrine system via the pituitary gland, relaying information about the state of the body.

The hypothalamus also expresses relaxin receptors including RXFP1, an Lgr3-homologue, increasing the similarities between the Dilp8-Lgr3 pathway and the vertebrate relaxin pathway.

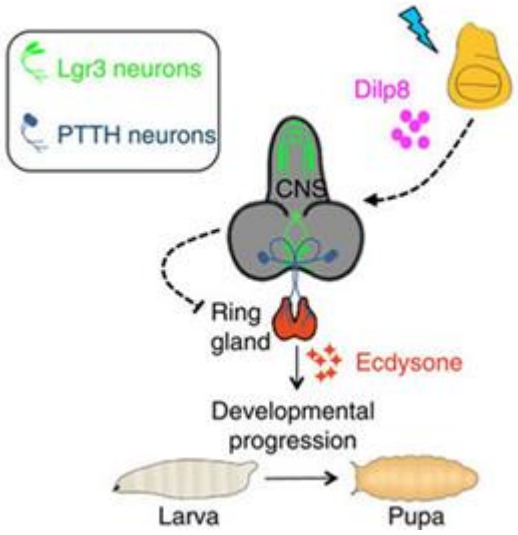

Figure 1.2. Dilp8-sensitive neuroendocrine pathway coupling growth and maturation timing (adapted from Garelli et al. 2015).

1.3 VEnCode, a new technology for cellular targeting

Currently, there is no technique that allows specific targeting of any single cell type in a complex living organism. Most gene delivery systems are limited by the technology and knowledge available to distinguish cellular types from others prior to gene delivery, typically depending on cell-surface markers for this selection. One of the major problems with this strategy is that most cell surface markers are not absolutely cell-specific, which inevitably leads to DNA delivery and subsequent cellular response in unwanted cells. An alternative to these "pre-DNA delivery" selectivity is to use DNA delivery systems that achieve specificity post-delivery, exploring the transcription profile of the target cell. The transcriptional program of any cell reflects a unique combination of binary on/off states of gene regulatory elements (RE) present in the genome. Most REs capable of driving expression of genetic information are used several times by a restricted number of cell types or cell states during the life of an organism. Therefore, it is frequently difficult to define a single RE that drives gene expression in a single population of cells. However, using intersectional methods, the desired target-cell specificity of gene drivers can be achieved by anatomical overlap between expression patterns driven by two or more REs. We call these REs combinations that carry cellular diagnostic value, Versatile Entry Codes (VEnCodes). VEnCode has as a main goal the delivery of one or more genes to any cell type or state, e.g., differentiated or tumoral. What distinguishes VEnCode from other techniques for cellular targeting is that VEnCode, using the natural gene expression signature consisting of multiple active REs, should be able to differentiate a target cell type among other cells. VEnCode can overcome the major drawback in gene therapy and/or genetic modification by allowing cell-restricted delivery of genetic material.

Due to a combination of carefully-chosen REs, VEnCode acts as a highly specific transcriptional program sensor, being adaptable to complex organisms or disease states **(Figure 1.3)**.

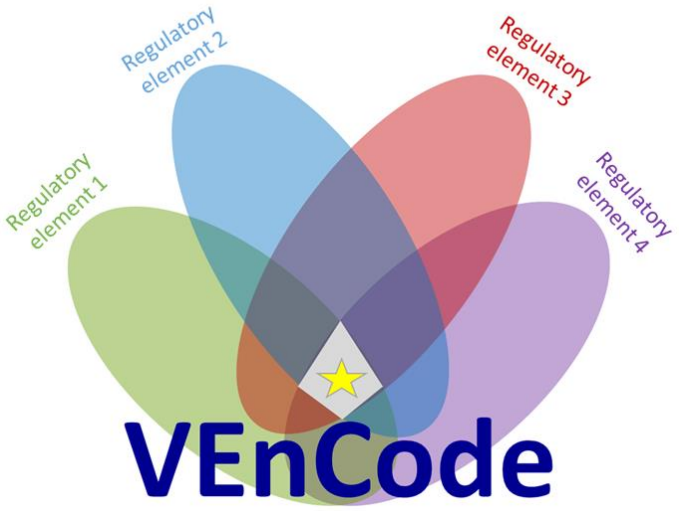

Figure 1.3. VEnCode model. The VEnCode technology is based on the intersection of chosen REs, that overlap in a specific cell type or state.

The proof of concept of VEnCode in *D. melanogaster* takes advantage of powerful tools for targeted gene expression highly used in fruitflies. The characterization of VEnCode function is related to previous work of gene expression restriction (Luan et al. 2006; Barret D. Pfeiffer et al. 2010a). In *Drosophila*, the systems used to manipulate specific cells, do not guarantee exclusively in the target. These systems use GAL4 or LexA transcription activators and VEnCode can be used with the Gal4 system or with the LexA system to answer to this problem. Gal4 is a transcription activator from *Saccharomyces cerevisiae*, which has been used extensively in *Drosophila* (Fischer et al. 1988). The Gal4/UAS binary expression system, where UAS is the Gal4 binding site, has become a powerful tool for directed gene expression **(Figure 1.4)** (Duffy 2002). In this system and similar ones, like the LexA/LexAop system, one transgenic construct drives the expression of a transcriptional activator and a second construct contains its binding sites upstream of a reporter gene. LexA is a regulator of the SOS response to DNA damage in *Escherichia coli* (Walker 1984) and it consists of a DNA-binding domain and a dimerization domain that binds to LexA DNA-binding motifs (LexAop) found upstream of its target genes (Butala et al. 2009).

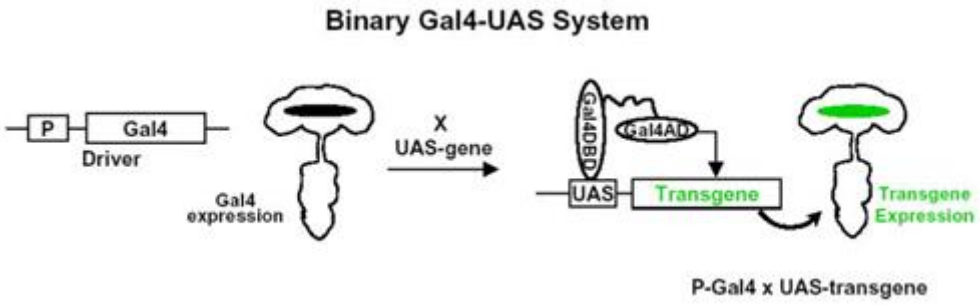

Figure 1.4. Schematic representation of the GAL4-UAS system of Drosophila, a binary system for targeting expression in vivo. P is a RE that drives expression of yeast transcription factor Gal4. Flies bearing a transgene containing Gal4 downstream of a P in a cell-

The DNA-binding and transcription-activating functions of Gal4 are accomplished through different functional domains of the protein that can be separated into distinct polypeptides. Luan *et al*. demonstrated that it is possible to drive Gal4 DNA-binding domain and activation domain separately, under the control of different enhancers (Luan et al. 2006). With this method, termed "split-Gal4", the reporter expression was restricted to the overlap of the two patterns, where an active Gal4 was reconstituted. However, the major drawback with split-protein strategies is leakiness, the fact that the majority of genes are reused and expressed in different tissues and at different times during an organism's lifetime. Regarding this issue, there might be no combination of two genes in the human genome that are co-expressed only in a type of cancer cells or genes in the *Drosophila* genome that are co-expressed in one of all of the neuronal types of the *Drosophila* brain. However, a wisely-chosen combination of three or more REs could provide sufficient specificity to target cancer cells or any specific neuron or population of neurons in the fly. VEnCode-based gene delivery strategies can achieve this specificity by splitting Gal4 or LexA into up to four pieces, each of which is expressed via a different RE. The REs are chosen based on their known expression pattern, so that their expression overlaps exclusively in the target cell type, where the four protein pieces will reconstitute an active Gal4 (or LexA). To guaranty the desired specificity, each protein piece should be unreactive on its own and assembly into an active Gal4 (or LexA) should occur exclusively when and where the protein pieces are co-expressed in the target cell. To this purpose, a protein process called intein-mediated protein splicing (Anraku et al. 2005; Evanko 2007) was used to generate a quadruply-split system. An intein is a protein segment that has the ability of self-cleaving from a protein while joining the remaining portions, the "exteíns", with a peptide bond (Mills et al. 1998; Saleh & Perler 2006; Li 2015). Split-inteíns are a subset of inteíns which contain two fragments expressed from independent units, which, when present in the same cell, reassemble into a functional intein that excises itself and covalently joins the exteín fragments into a single protein (Truong et al. 2015). The split-intein fragments are called N-terminal intein fragment (IntN) and C-terminal intein fragment (IntC).

The mechanism by which damaged tissues trigger developmental delays associated with inhibition of ecdysone remain poorly understood. The injury-response checkpoint at the third larval instar involves humoral signals including insulin-like peptides, as Dilp8, which appear to act on the PIL neurons, PTTH neurons and/or the ring gland (Colombani et al. 2015; Garelli et al. 2015). However, the nature of this interaction remains unknown. Additional questions need to be answered, such as: how the imaginal disc-derived Dilp8 can pass through the brain-blood-barrier and act on PIL neurons, whether the interaction between Lgr3 and Dilp8 is direct or not and how Lgr3-expressing neurons relay information to the ring gland. More research is required to understand if other neurons are also involved in these mechanisms and their functions.

It is known that injury in *Drosophila* triggers developmental delays. Similarly, in vertebrates, severe injury, chronic disease and infection can each lead to developmental delays like disruptions in gamete development

and a delayed onset of puberty (Pozo & Argente 2002). Understanding how injured tissues trigger changes in endocrine function is essential to understanding several disease states. The analysis of the injury-induced molting checkpoint in insects can provide valuable insights into the interactions between injured tissues and endocrine centres.

We hypothesize that PIL neurons are critical cells in this pathway, mediating the response to Dilp8, requiring Lgr3. But are PIL neurons the only cells with this role? Are they sufficient to cause a developmental timing delay? Are all the four PIL neurons functionally and neuroanatomically redundant? How do they interact with other cells? The answer of these questions is dependent of the exclusive target of PIL neurons. In this thesis, my main aim is to restrict gene expression to the PIL neurons. Our approach is to find REs that can be coupled with intersectional genetics approaches to drive expression specifically in the PIL neurons.

2 OBJECTIVES

Our main objectives in this thesis are to:

1. Generate PIL neuron specific drivers.
2. Understand the role of PIL neurons in the Dilp8-developmental delay pathway.
3. Characterize new neurons in the Dilp8-Lgr3 delay pathway.

To achieve these objectives, we will:

1.1. Define PIL neuron drivers.

1.2. Test different strategies, including VEnCode, to target specifically not only PIL neurons, but also other neurons involved in the Dilp8-sensitive neuroendocrine pathway.

2.1. Manipulate PIL neuron function by activating and silencing PIL neurons.

2.2. Manipulate PIL neuron activity by removing Lgr3 using RNAi.

2.3. Understand PIL neuron anatomy and its interaction with neighbouring cells.

3.1. Find new populations of cells (supposedly neurons distinct from PIL neurons) that are involved in the Dilp8-Lgr3-dependent coupling of growth and developmental timing.

3 MATERIALS AND METHODS

3.1 *DROSOPHILA* MELANOGASTER AS A GENETIC TOOL

Drosophila melanogaster, commonly known as vinegar flies or fruit flies, are a group of small dipteran insects (with about 3 mm of length), belonging to the family Drosophilidae. Characteristics such as the small size, relatively large brood and short generation time makes *Drosophila* one of the most valuable organisms in biological research. The extensive knowledge of *Drosophila* genetics allows its common use as model organism in developmental biology. In 2000, the *Drosophila* genome was completely sequenced by Adams and colleagues (Adams et al. 2000), demonstrating it has 122 million base pairs (approximately 5% of the size of human genome) and only four pairs of chromosomes: one pair of heterosomes (X, Y) and three autosomal chromosomes (Henderson 2004). The second and third chromosomes are metacentric and are divided by the centrosome into the left (L) and right (R) arms. The fourth chromosome is the smallest, representing only 2% of the *Drosophila* genome. It has been estimated that about 75% of known human disease genes have a recognisable match in the *Drosophila* genome (Reiter et al. 2001). This high degree of gene homology observed between Drosophila and Human grants the former an unparalleled value in the study of human protein function, localization and interactions.

Other factors contributing to the long and distinguished history of *Drosophila* research are: 1) fruit flies are hardy, with simple food requirements and occupy little space; 2) their generation time is about 10 days at 25 °C **(Figure 3.1)** or 12 days at room temperature (RT) and development may be shorter or longer in higher or lower temperatures, respectively; 3) a large number of offspring are easily produced allowing sufficient data to be quickly collected; 4) a large number of genetically defined mutants are available; 5) the presence of balancer chromosomes that can be followed by easily observed physical characteristics; 6) the possibility of targeting mutations to specific genes; 7) and the sophisticated genetic tools that are available (Barret D. Pfeiffer et al. 2010b; del Valle Rodriguez et al. 2012), such as P-elements, transgenic flies carrying RNAi, targeted gene expression through the binary Gal4-UAS system (Brand & Perrimon 1993) and the ternary Split-Gal4 system (Luan et al. 2006). Together, these advantages make genetic experiments in *Drosophila* fast, cheap and easy relative to others *in vivo* models.

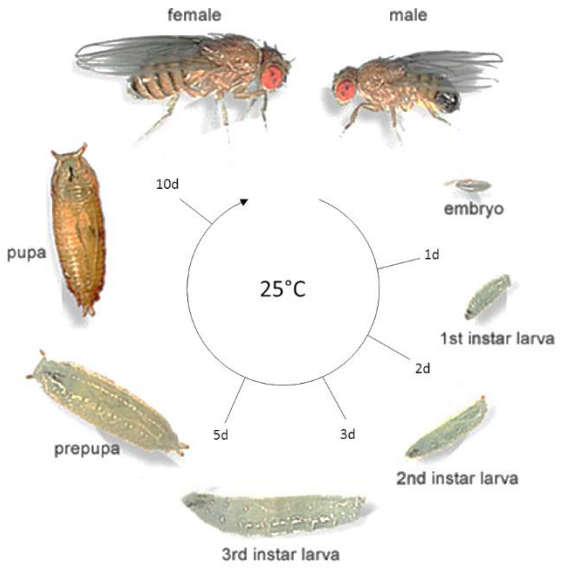

Figure 3.1 The life cycle of *Drosophila melanogaster* (adapted from Parvathi V *et al*. 2009).

3.1.1 Drosophila melanogaster stocks

All fly stocks used in this work were maintained in vials with standard cornmeal-agar medium at 25°C for most experiments or at 18° for stock maintenance, in 70% humidity-controlled conditions/atmosphere.

All stocks used in this work are described in table 1, with the complete genotype and origin. These stocks were acquired from the Bloomington *Drosophila* Stock Centre (BDSC) (http://flystocks.bio.indiana.edu/), offered by other laboratories as generous gifts, or generated in the lab by injection and/or genetic crosses, using balancer chromosomes.

Table 1. *Drosophila melanogaster* stocks.

Number	Genotype	Origin	Stock
1	w[1118];; P{10XUAS-IVS-myr::GFP}su(Hw)attP5	BDSC	32199
2	w[1118];; P{y[+t7.7] w[+mC]=GMR43A12-GAL4}attP2	BDSC	47357
3	w[1118];: P{y[+t7.7] w[+mC]=GMR84E05-GAL4}attP2	BDSC	40395
4	w[1118];; P{y[+t7.7] w[+mC]=GMR54C08-GAL4}attP2	BDSC	47946
5	w[1118];; P{y[+t7.7] w[+mC]=GMR46C11-GAL4}attP2	BDSC	50262
6	w[1118];; P{y[+t7.7] w[+mC]=GMR82G10-GAL4}attP2	BDSC	50262
7	w[1118];; P{y[+t7.7] w[+mC]=GMR24H12-GAL4}attP2	BDSC	49101
8	w[1118];; P{y[+t7.7] w[+mC]=GMR48H10-GAL4}attP2	BDSC	50395
9	w[1118];; P{y[+t7.7] w[+mC]=GMR52E10-GAL4}attP2	BDSC	38835
10	w[1118];; P{y[+t7.7] w[+mC]=GMR64G08-GAL4}attP2	BDSC	39319

11	w[1118];; P{y[+t7.7] w[+mC]=GMR69F02-GAL4}attP2	BDSC	39494
12	w[1118];; P{y[+t7.7] w[+mC]=GMR78F10-GAL4}attP2	BDSC	40007
13	w[1118];; P{y[+t7.7] w[+mC]=GMR87B08-GAL4}attP2	Janelia Farm	
14	w[1118];; P{y[+t7.7] w[+mC]=GMR25E10-GAL4}attP2	BDSC	49320
15	w[1118];; P{y[+t7.7] w[+mC]=GMR28E05-GAL4}attP2	BDSC	49459
16	w[*];; P{y[+t7.7] w[+mC]=20XUAS-IVS-mCD8::GFP}attP2	BDSC	32194
17	w*; P{10XUAS-IVS-mCD8::RFP}attP40	BDSC	32219
18	w[*];; P{w[+mC]=UAS-Hsap\KCNJ2.EGFP}7 - aka Kir2.1	BDSC	6595
19	w[*]; Bl[1]/CyO; P{w[+mC]=alphaTub84B(FRT.GAL80)}3	BDSC	38881
20	w[1118];; P{10XUAS(FRT.stop)GFP.Myr}su(Hw)attP1	BDSC	55811
21	w[*];; P{y[+t7.7] w[+mC]=20XUAS-IVS-mCD8::GFP}attP2	BDSC	32194
22	w[1118]	Maria Dominguez's lab	
23	w; if/CyO; MKRS/TM6B, Hu	António Jacinto's lab	
24	yw;; ptth-HA (III)	Michael O´Connor's lab	
25	w;; GMR19B09.3.1-Gal4	Bruce Baker's lab	
26	w;; GMR19B09.3A-G-Gal4/TM6B	Bruce Baker's lab	
27	w; if/CyO; GMR19B09.3C.1-Gal4	Bruce Baker's lab	
28	w; Sp/CyO; GMR19B09.3D.1-Gal4	Bruce Baker's lab	
29	w;; GMR19B09.1.1-Gal4	Bruce Baker's lab	
30	w;; GMR19B09.2.1-Gal4	Bruce Baker's lab	
31	UAS-TRPA1/TM6B	Christen Mirth's lab	
32	UAS-TRPA1/CyO	Christen Mirth's lab	
33	w; UAS>stop>Trpa1/CyO	Maria Luisa Vasconcelos's lab	
34	11340-1-1M tub-dilp8(1) on II	Generated at the lab	
35	w[1118];; Lgr3-IR V22/TM6B	Generated at the lab	
36	w; P{10XUAS-IVS-myr::GFP}su(Hw)attP5; ptth-HA	Generated at the lab	
37	w[*]; P{w[+mW.hs]=GawB}4G	Generated at the lab	
38	if/CyO; sfGFP-Lgr3-V22/TM6B	Generated at the lab	
39	Lgr3[ag1]/TM6B, Hu	Generated at the lab	
40	Lgr3[ag2]/TM6B, Hu	Generated at the lab	
41	w*; UAS-myr::tdTomato/CyO; Lgr3[ag5]/TM6B	Generated at the lab	
42	w[1118]; +/+; Lgr3[ag1],P{y[+t7.7]w[+mC]=GMR48H10-GAL4}attP2(I)/TM6B	Generated at the lab	
43	w[1118]; +/+; Lgr3[ag1],P{y[+t7.7]w[+mC]=GMR69F02-GAL4}attP2(I)/TM6B	Generated at the lab	
44	w[1118]; +/+; Lgr3[ag1],P{y[+t7,7]w[+mc]=GMR19b09-Gal4}attP2(IV)/TM6B	Generated at the lab	

45	w[1118]; +/+; Lgr3[ag1], GMR19B09.3C.1-Gal4(V)/TM6B	Generated at the lab	
46	UAS-TRPA1/CyO; Lgr3[ag1]/TM6B	Generated at the lab	
47	Lgr3[ag1]/TM6B,Hu	Generated at the lab	
48	Lgr3[ag2]/TM6B,Hu	Generated at the lab	
49	UAS-TRPA1/CyO; Lgr3[ag2]/TM6B	Generated at the lab	
50	UAS-TRPA1; Lgr3-IR V22/TM6B	Generated at the lab	
51	If/CyO; UAS-TRPA1/TM6B	Generated at the lab	
52	w; elavGal80/CyO; UAS-TRPA1/TM6B	Generated at the lab	
53	w; elavGal80/CyO; P{y[+t7.7] w[+mC]=GMR48H10-GAL4}attP2	Generated at the lab	
54	w; elavGal80/CyO; P{y[+t7.7] w[+mC]=GMR69F02-GAL4}attP2	Generated at the lab	
55	w; elavGal80/CyO; GMR19b09-Gal4/TM6B	Generated at the lab	
56	UAS-TRPA1; Lgr3_sfGFP[ag5]	Generated at the lab	
57	GMR19B09-LexA; LexAop2-FLPL, MZ699-Gal4/TM6B	Generated at the lab	
58	UAS-TRPA1; P{w[+mC]=alphaTub84B(FRT.GAL80)}3/TM6B	Generated at the lab	
59	UAS>stop>kir2.1-GFP; +; tub-dilp8/TM6B	Generated at the lab	
60	w; elavGal80/CyO; UAS-mCherry	Generated at the lab	

3.1.2 Larval dissection and Immunohistochemistry

To collect larvae, female and male adult flies were crossed and maintained in a vial at 25°C in standard fly food with a controlled number of animals, five males and five females, to avoid overcrowding. The larvae used were wandering third instar larvae with approximately 5 days after egg laying.

a) **Dissection**

Tissues were dissected from larvae in cold S2 cell culture medium (Schneider's Insect Medium, Sigma Aldrich), fixed in 4% paraformaldehyde (PFA) (Sigma Aldrich) in PBS for 30 min at RT and permeabilized with PBS containing 0,3% Triton-X-100 (PBST) 3 times during 20 min.

b) **Antibody staining**

After permeabilization, blocking was performed for 2 h in PBST supplemented with 1% bovine serum albumin (BSA) to reduce nonspecific binding of the antibodies. Larval tissues were incubated with the primary antibodies (Table 2) diluted in blocking solution overnight at 4 °C. The next day, tissues were washed in PBST 3 times during 30 min, incubated with the respective secondary antibodies (Table 2), and diluted in blocking solution for 2 h at RT, protecting the samples from the light exposure from this step on. After washing, nuclei were counterstained with 1:1000 DAPI (Sigma Aldrich) for 10 min, washed again with PBST, and with PBS 1x.

Table 2. List of primary and secondary antibodies used in immunofluorescence assays.

Primary Antibodies			
Protein	Host	Concentration	Origin
GFP	Rabbit	1:200	Life technologies, A11122
GFP	Mouse	1:20	DSHB, 12E6
HA	Mouse	1:50	Santa-Cruz Biotech, 57592
Fasciclin II	Mouse	1:20	DSHB, 1DA
Brp	Mouse	1:100	DSHB, nc82
V5	Mouse	1:200	eBioscience, 14-6796-82
Secondary Antibodies			
Protein	Anti	Concentration	Origin
Alexa fluor 488	Rabbit	1:250	Invitrogen, A11070
Alexa fluor 488	Mouse	1:250	Life technologies, A11029
Alexa fluor 594	Mouse	1:250	Invitrogen, A11020

c) **Mounting and Imaging**

All samples were mounted in DABCO mounting medium (16 mL glycerol, 4 mL 1x PBS, and 0,4 g DABCO) in microscope slides and stored at 4°C, protected from light. Images were obtained with a Zeiss LSM 710 Confocal Microscope (x 20 and x 40 objectives) and processed using Fiji.

3.1.3 Developmental time assay

To verify if the specific REs studied in this work are involved, or not, in the Dilp8-dependent delay in the onset of metamorphosis, we performed pupariation timing assays. The flies of the desired genotypes, aged 3-15-days old, were crossed and maintained in laying pots with apple juice agar plates for 48 h, so that the flies could adapt to the environment. When the experiment began, all the apple plates were exchanged for new ones with a small amount of yeast-sucrose paste. The plates were exchanged every 2 h, 4-5 times a day. Second instar larvae (48 h after egg laying [AEL]) were transferred to vials containing standard *Drosophila* food. The number of larvae per each vial were between 20 to 30, never exceeding 30 larvae to avoid competition, which could negatively affect developmental timing. Survey of pupae consists in counting the number of puparia in each time interval. At 9 am, 15 pm, and 21 pm, the number of pupae formed were counted, until all larvae pupariated or died. The final total N of pupae for each genotype is depicted in the respective figures. Pupariation was defined as cessation of movement with evaginated spiracles and a darker colour of the puparium. These experiments were performed at 25 °C, except for experiments using flies carrying the TrpA1 transgene. *Drosophila* Transient Receptor Potential channel (TrpA1) (an ortholog of the

mammalian TrpA1 channel) is a temperature and voltage-gated cation channel that regulates *Drosophila* thermotactic behaviour (Rosenzweig et al. 2005). Previous work has shown that neurons expressing TrpA1 fire action potentials when temperatures exceed 22°C (Hamada et al. 2008). By ectopically expressing TrpA1 (using the GAL4-UAS system) and then delivering modest heat pulses, sets of neurons can be remotely activated (Hamada et al. 2008; Pulver et al. 2009). Experiments done with this construct were performed at 18°C until the second instar (day 3 AEL), after which the larvae were transferred to 29°C to activate the system.

Data were plotted as box plots representing median and the 25 and 75% quartiles. The whiskers extend to data points that are less than 1.5x the interquartile range (IQR) away from the 1st/3rd quartile. Data points falling outside of the interval defined by the whiskers were plotted as outliers.

3.1.4 Generation of transgenic flies

To generate transgenic lines, we used the ϕC31 integrase mediated insertion method (Groth et al. 2004). The *Streptomyces* phage ϕC31 has biological characteristics that is similar with the movement of transposons in *Drosophila*. The phage is capable of inserting its own genomic DNA into bacterial genomes using an integrase (Combes et al. 2002). This serine integrase mediates recombination between a bacterial attachment site (*attB*) and a phage attachment site (*attP*) (Thorpe et al. 2000), represented in the **Figure 3.2**. The *Drosophila* community has generated various stocks harbouring *attP* site at characterized genome locations (Groth et al. 2004). The following *Drosophila* lines, from Bloomington, were used to inject the plasmids of interest: Dmel\P{CaryP}attP2 localized at the 3L chromosome, and Dmel\P{CaryP}attP40 localized at the 2L chromosome. The plasmid containing both transgene and donor sequence (*attB*) was co-injected with ϕC31 integrase into embryos from the previous lines (Fish et al. 2007). These injections were carried out using the Champalimaud microinjection service.

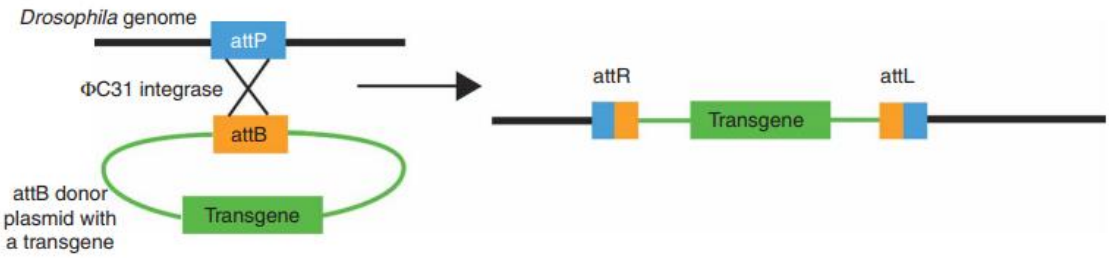

Figure 3.2. Schematic representation of phiC31-mediated integration (Fish et al. 2007).

3.2 CELL CULTURE

3.2.1 DL2 cells

Drosophila Line 2 (otherwise known as Schneider Line 2) abbreviated as DL2 or SL2, respectively, is one of the most common *D. melanogaster* cell lines. DL2 cells are derived from a primary culture of late stage (20–

24-h old) *D. melanogaster* embryos, likely from a macrophage-like lineage. These cells grow in an intermediary state of adherent and suspension. They are cultured in Schneider's *Drosophila* medium supplemented with 10% of heat-inactivated Fetal Bovine Serum (FBS) and 1% of Penicillin-Streptomycin, in tissue culture T25-flasks at 25°C. The cultures were split twice a week in 1:10 dilution.

3.2.2 Cell transfection

Plasmids were transfected into DL2 cells using FuGENE® HD Transfection Reagent (Promega), a non-liposomal reagent designed to transfect DNA into a large variety of cell lines.

One day before the transfection, 1.5 x 10^5 cells were seeded in coverslips and grown with Schneider's medium supplemented with 10% of FBS to reach 80% of confluency the next day. For transfection, a mix of DNA plasmids was produced with equimolar amounts of all the plasmids. A total of 1 µg of plasmid DNA was used *per* transfection. FuGENE® was added to the DNA mix in a 3:1 FuGENE®:DNA ratio and incubated for 15 min at RT. After this period, the mix was added to the cells, which were then incubated at 25°C for 48 h. All the transfections were made in duplicates.

3.2.3 Cell preparation and Immunocytochemistry

In order to prepare cells for immunofluorescence assays, the culture medium was removed and cells were fixed with 4% PFA in 1x PBS for 20 min. The PFA solution was then removed and the cells were washed with 1x PBS. Cells were permeabilized with 0,1% Triton X-100 in PBS for 10 min and washed in 1x PBS before the blocking step.

a) **Antibody staining**

The cells were blocked in PBS-BSA (1%) for 1 h and then incubated overnight at 4°C with the primary antibody (table 2) diluted in PBS-BSA (1%). The next day, cells were washed with 1x PBS and incubated for 2 h with the secondary antibody diluted in PBS-BSA (1%). From this point forward, all the steps were done away from the light. After washing with 1x PBS, nuclei were counterstained with DAPI (Sigma Aldrich) for 10 min and washed again with 1x PBS.

b) **Mounting and Imaging**

All samples were mounted in DABCO mounting medium (16 mL glycerol, 4 mL 1x PBS and 0.4 g DABCO) in microscope slides and stored at 4°C, protected from light. Images were obtained with a Zeiss Z2 Fluorescence Microscope (20x and 40x objectives) and processed using Fiji.

3.3 MOLECULAR BIOLOGY

3.3.1 Cloning Techniques

a) **Regulatory elements sequence amplification by PCR**

The REs necessary to construct a VEnCode system to target the PIL neurons were chosen after multiple experiments done with these REs driving GAL4, as described in the Results section. The lines were obtained from the GAL4 Janelia collection. The sequences of each RE were amplified from *D. melanogaster* genomic DNA, using Supreme NZYTaq II DNA polymerase (NZyTech). Briefly, initial denaturation was performed during 5 min at 95°C, followed by 35 cycles of 30 s of denaturation at 95°C, 30 s for primer annealing at 60°C and 1 min *per* 1 kb of extension at 72°C. The final extension was done during 10 min at 72°C. This protocol was used for all amplification steps.

b) **Enzymatic Restriction Digestion**

For restriction enzyme-mediated cloning, digestions of plasmids or PCR fragments with BglII, XhoI, KpnI and/or NotI, (New England Biolabs) were performed at 37°C during 2h. After the digestion reaction, the digestion products were separated in agarose gel and the band of the expected size was cut and purified as described below.

c) **Agarose gel electrophoresis**

After a PCR reaction or an enzymatic digestion, samples were loaded into an agarose gel and run either to confirm the expected size from PCR amplification or to separate the digested fragments, respectively. Subsequently, the DNA was recovered from the agarose gel, as described in the next section. All agarose gels were prepared with 1.2% in TAE 1x buffer. Two µL of Green Safe Premium (NZYTech) per 50 mL of agarose gel were added to allow the visualization of the DNA products. The molecular marker NZYDNA Ladder III (NZYTech) was run along with the samples to identify the molecular weight of the DNA bands after migration. The images were acquired with ChemiDoc™ XRS+ system (Bio-Rad Laboratories).

d) **DNA purification**

Purification of either PCR products, DNA from enzymatic digestions, or plasmid DNA from agarose gels was performed with NZYGelpure kit (NZYTech), as described by the manufacturer. For the DNA purification from an agarose gel, the desired DNA band was cut out of the agarose gel and purified to obtain DNA samples. The DNA concentration and quality were measured by Thermo Scientific NanoDrop™ 2000 Spectrophotometer and stored at -20°C.

e) **DNA Ligation**

DNA ligation was performed using T4 DNA Ligase (NZYTech) at RT, overnight. The DNA ligase catalyses the formation of covalent phosphodiester linkages, that permanently join the fragments together. This was used

to generate recombinant plasmids. To perform the ligation reaction, 50 ng of the vector were used, plus an amount of insert to achieve a 5:1 insert:vector molar ratio. After the ligation, the final plasmid is complete, being then transformed into competent cells for propagation.

f) **Transformation of Competent Cells**

Following DNA ligation, bacterial competent cells were transformed with the resultant plasmid by heat-shock (45 s at 42 °C followed 2 min at 0 °C). Then, SOC medium was added to the bacteria to allow them to grow during by incubating them for 1 h at 37 °C with shaking. This step is important to allow time for the bacteria to express the antibiotic resistance proteins encoded on the plasmid backbone, which will allow their selection as resistant colonies when they are plated on agar plates containing antibiotics. Half the volume or all transformation was plated on LB agar plates supplemented with the appropriated antibiotic (100 µg/ml of Ampicillin or 50 µg/ml of Kanamycin, depending on the plasmid transformed), and incubated at 37 °C, overnight. For the construction of the typical plasmids we used NZY5α Competent Cells (NZYTech). For the construction of the pENTRs we used Stbl3 Chemically Competent *E. coli* (prepared in our lab), chosen due to its reduced frequency of recombination. For the selective reactions of Gateway Technology we used One Shot TOP10 Chemically Competent *E. coli* cells (Thermo Fisher) due to their high transformation efficiency and sensitivity to CCDB protein.

g) **Colony PCR screening**

Upon transformation, the resulting colonies were tested by a colony PCR screening to select the colonies that contained the vector of interest. This screening was done by PCR using specific primers for each construct, allowing to differentiate the colonies that do not have the insert from the colonies that have it, and the ones that have the insert in the wrong orientation. After the PCR, the products were run in an agarose gel. A single colony of each construct, apparently positive, was chosen for plasmid DNA isolation and purification.

h) **Plasmid DNA isolation and purification**

To obtain a high density of the positive colony plasmid DNA, the colony was inoculated overnight at 37 °C in liquid LB medium containing antibiotic. The plasmid DNA was then purified from the bacterial culture using the NZYMiniprep kit (NZYTech). After the purification, the concentration of the plasmid was assessed by Thermo Scientific NanoDrop™ 2000 Spectrophotometer, and posteriorly sent for sequencing.

i) **Sanger sequencing**

To confirm the sequence of the final plasmid, a reaction of 100 ng/µl of plasmid DNA with 10 ρmol/µl of primer was sent to Stab Vida for sequencing. Unless the fragments were small, two different primers, one of each side of the fragment, were chosen to start the sequencing. Due to the low quality of the sequencing methods at the beginning and at the end of the sequence, with one primer at each side it is possible to compare the results and obtain high-quality sequence for the whole construct.

3.3.2 Gateway Cloning Technology

The Gateway Cloning Technology is based on the site-specific recombination used by phage λ to integrate its DNA in the *E. coli* chromosome. Both have specific recombination sites: in phage λ, it is called *att*P; in *E. coli,* it is called *att*B. During the integration, the recombination between attP (243 nt) and attB (25 nt) sites creates attL (100 nt) and attR (168 nt) sites flanking the region where the phage λ was integrated. This strategy has been used for cloning processes, as described in **Figure 3.3.** The canonical strategy for Gateway cloning is characterized by two main steps: In step 1 (BP reaction), the gene of interest is subcloned into a Donor Vector (pDONR), generating an Entry Clone. The gene of interest is flanked by attB sites, while the donor vector has attP sites. After recombination, the entry cloned obtained has attL sites. In step 2 (LR reaction), the gene of interest is cloned from the Entry Clone into a Destination Vector. In this case, the destination vector has attR sites to recombine with the attL sites from the entry clone.

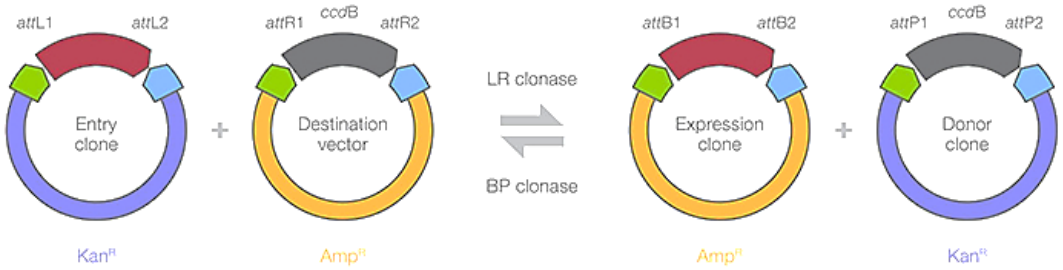

Figure 3.3. Model of Gateway Technology system (from ThermoFisher Scientific).

One of the main advantages and goals of this technique is that we can generate many different expression clones from having developed just one entry clone with our region of interest. A wide number of Gateway-compatible vectors have been established worldwide and tested for expression of genes in *Drosophila*, plants, bacteria, vertebrates, and mammalian cell lines, containing a variety of promoters, enhancers, and terminators. The vectors can also contain fluorescent protein tags and selectable markers, either upstream or downstream of the open reading frames. Another positive characteristic of the Gateway Technology is the possibility of multisite cloning. Through the different recombination sites, it is possible to assemble up to 4 fragments in one final destination vector.

However, our strategy consisted of a non-canonical use of the gateway technology. We sought to develop a type of Gateway-related vectors, called pENTR. These plasmids allow one to generate Entry clones, suitable for downstream Gateway cloning into Destination vectors, by restriction enzyme reactions instead of the above-described recombination steps. Such strategy grants a more flexible and affordable method to generate subsequent Entry clones containing our genes of interest. Our custom pENTRs vectors were designed based on pDONR (Donor Vector) together with our collaborator Dr. José Ramalho. For this purpose, the attP sites from pDONR were recombined with a custom de novo-generated sequence containing attB sites flanking a multiple-cloning site (MCS) **(Figure 3.4)**, generating a pENTR vector with attL sites. This vector

allows the cloning of any gene of interest by restriction enzymes and then the generation of an expression clone by performing the LR reaction, as shown in Figures 3 and 4.

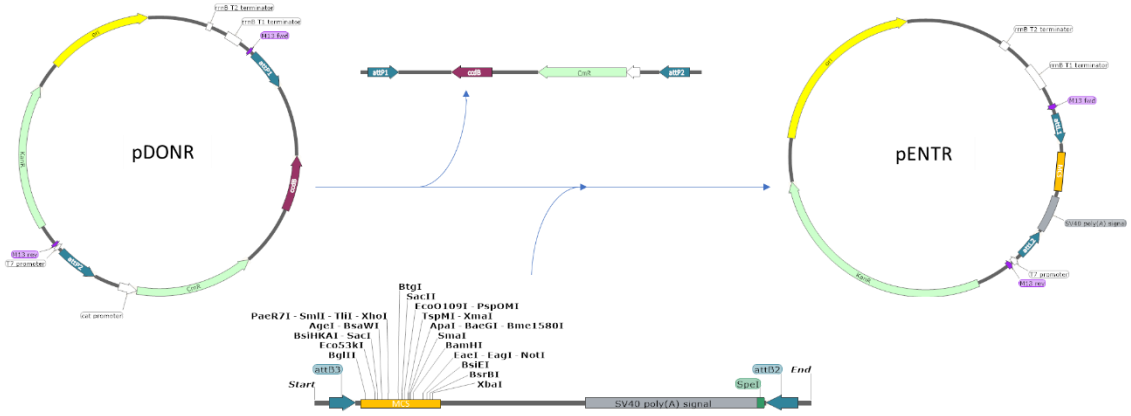

Figure 3.4. Model of pENTR construction with the designed MCS. The pDONRs were modified, replacing by recombination, the ccdB gene and the chloramphenicol resistance for the MCS and the polyA signal. With this reaction, the attPs present at the pDONR recombined with the attBs from the designed MCS and resulting in attLs.

3.3.3 Construction of the pENTR plasmids

The region of interest cloned into the the pENTRs (see section 2.3.2) will contain three modules: the RE, the *Drosophila* synthetic core promoter (DSCP) (Pfeiffer et al. 2008), and one piece of the quadruply-split Gal4 developed at our laboratory. The purpose of this setup was to place the yeast transcriptional activator GAL4 under the control of these endogenous REs.

The REs are short fragments of genomic DNA that can be used as drivers for mRNA expression. Nevertheless, to guarantee robust transcription in *Drosophila*, some REs may require the presence of a core promoter with specific sequence motifs. The DSCP is the core promoter used in the Janelia Gal4 collection (Pfeiffer et al. 2008). The DSCP developed contains the TATA, Inr, MTE, and DPE sequence motifs. As the REs used in our study were selected from the Janelia Gal4 collection, we also used the DSCP core promoter in our pENTR constructs, in order to increase the chances of obtaining the same expression pattern as the lines used from Janelia, as described below.

In this work, as will be further described below, we attempted to PCR-amplify eight different REs (four REs that drive mRNA expression in cells including the PIL neurons and four REs that drive expression in cells including the PTTH-producing neurons), and separately place each of them upstream of a synthetic gene encoding a protein piece of the quadruply-split GAL4 **(Figure 3.5)**. Quadruply-split GAL4 was made by splitting the transcription factor GAL4 into its DNA binding domain (DBD) and activation domain (AD), while polypeptide sequences (exteíns) flanked by inteíns (see Introduction) were added in the middle. In sum, this

approach consists of the following: a segment containing the GAL4 DNA-binding domain (GAL4dbd) (B D Pfeiffer et al. 2010) bound to the N-terminal piece of the split intein AceL-TerL (Thiel et al. 2014); a second segment including the C-terminal of the split intein AceL-TerL bound to the N-terminal of another split intein, gp41-1 (Carvajal-Vallejos et al. 2012; Dassa et al. 2009); a third segment comprising the C-Terminal of gp41-1 and the N-Terminal of NpuDnaE split intein (Cheriyan et al. 2013); and finally, a fourth segment containing the C-Terminal of NpuDnaE followed by the VP48 activation domain (Zhou et al. 2006). Each RE drives the expression of one piece of the GAL4, but the transcription activation only occurs when the four pieces are bound together.

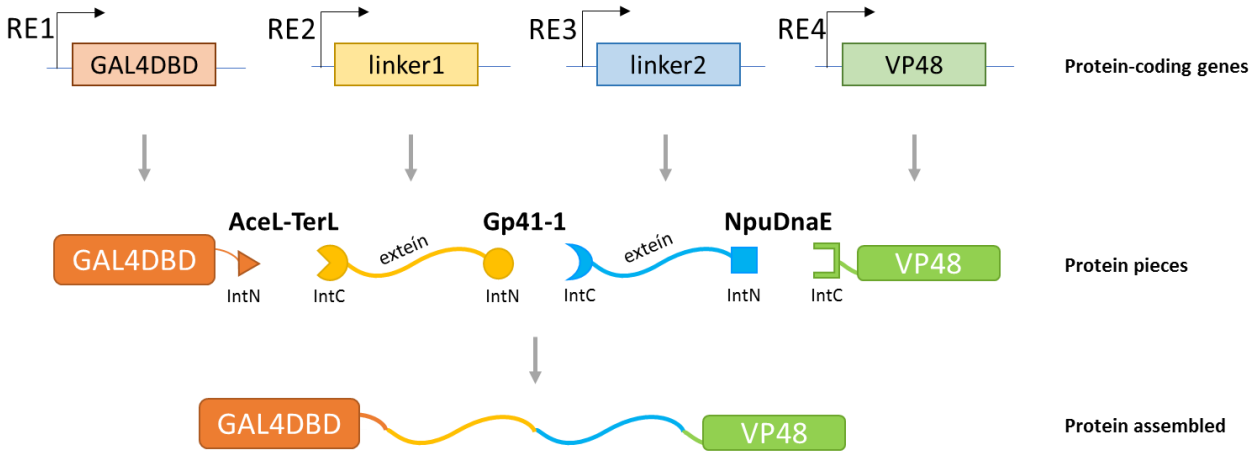

Figure 3.5. 4x split VEnC-GAL4 developed with three specific split-inteíns. The transcription factor GAL4 can be split into two domains, the DBD and the AD (in this case VP48), and its function can be restored when the DBD and its AD are brought together by sustained interaction. To connect the functional domains, three different split-inteíns were added: AceL-TerL, Gp41-1, and NpuDnaE, excising themselves and leaving the exteins with peptide bonds, thereby reconstituting a functional GAL4 transcription factor. Each RE drives the expression of each piece of the 4x split VEnC-GAL4. At the protein-coding genes, GAL4DBD is the simplification for Gal4DBD-AceL-TerL-IntN; linker1 is the simplification for AceL-TerL-IntC-Gp41-1-IntN; linker2 is the simplification for Gp41-1-IntC-NpuDnaE-IntN; and VP48 is the simplification for NpuDnaE-IntC-VP48.

a) **Regulatory element cloning**

The FlyLight database contains anatomical patterns of larval and adult brain of thousand transgenic GAL4 lines of *D. melanogaster* from the Janelia GAL4 collection, in which the expression of an exogenous gene is directed to a small subset of cells in the fly brain. The REs chosen from the FlyLight database, after multiple experiments as described in Chapter 3-Results and Discussion, were: R29B09, R25E10, R19B09.3A, and R19B09.3C, to construct a VEnCode for PIL neurons; and R43A12, R54C08, and R84E05, to construct a VEnCode for PTTH neurons. The primers (numbers 1-16 at table 3) used for the amplification of each RE had a restriction site for BglII or for XhoI, as described in **Figure 3.6.** PCR products were run in an agarose gel to confirm the correct size, and the corresponding bands were isolated from the gel and purified, as described above. The PCR products were composed by the RE sequence plus the restriction site of BglII on the 5'end, and the restriction site of XhoI on 3'end. Thus, restriction enzyme digestion was needed to create the respective sticky ends to further clone the RE into pENTR. In parallel, the pENTRs were digested with the

same restriction enzymes, BglII and XhoI, leaving the same sticky ends to perform the ligation step to make the different pENTR plasmids containing a single RE, such as pENTR-R29B09, pENTR-R25E10, and so on. This class of plasmids can be generally called “pENTR-RE”. To confirm if the colonies obtained from the transformation were correct, we performed colony PCR screening using one primer in the insert and the other primer in the backbone plasmid (number 22 or 23 at Table 3). This strategy allowed us to confirm that the insert was located inside the vector and in the correct orientation.

Table 3. List of primers used in molecular biology techniques**.**

Number	Target	Direction	Sequence
Primers used for REs amplification			
1	R19B09.3A	Forward	GTCGAGAGATCTGATAAACCTGTTCGATCATTGGAGAT
2	R19B09.3A	Reverse	GGTACCCTCGAGGATCCTACCCGGCGGCCAAATGA
3	R19B09.3C	Forward	GTCGAGAGATCTAGCCGAATAACTTTCTCCACA
4	R19B09.3C	Reverse	GGTACCCTCGAGACTCCTTAATGGGATTACCGACA
5	R25E10	Forward	GTCGAGAGATCTATCGCCGAAACGCTCGGTGTGCCTG
6	R25E10	Reverse	GGTACCCTCGAGCTCGAAGACCTGTTCATAACAACCG
7	R29B09	Forward	GTCGAGAGATCTGGTATGGCACCATCGTATCCCAAGT
8	R29B09	Reverse	GGTACCCTCGAGCGGGTATTTCGCAGCGTTTACAAAT
9	R43A12	Forward	GTCGAGAGATCTCTGCTGAGTAAGCCGAGAAACGGAG
10	R43A12	Reverse	GGTACCCTCGAGTTGCCACCAGCTTGTCGACTGTAGC
11	R84E05	Forward	GTCGAGCTCGAGGATGGCCTACTCAAGGAATGTCCGC
12	R84E05	Reverse	GGTACCAGATCTGGCCACCCAGCACATGGAGATGATG
13	R54C08	Forward	GTCGAGAGATCTCGAAGTGGCTATCAGGTTGCTAACC
14	R54C08	Reverse	GGTACCCTCGAGGTGCGGATCGGAAAAAGTAGACACA
15	*ptth* promoter	Forward	GTCGAGAGATCTGGATTTCCACGGGGAACAG
16	*ptth* promoter	Reverse	GGTACCCTCGAGCTGTACTCCTTCTGCAGCTCTGG
Primers used for DSCP amplification and cloning			
17	DSCP	Forward	GTCGAGCTCGAGGAGCTCGCCCGGGGATCGAG
18	DSCP	Reverse	GGTACCGGTACCGTTTGGTATGCGTCTTGTGA
Primers used for Split-Gal4 cloning			
19	R19B09.3A	Forward	CACCGATAAACCTGTTCGATCATTGGAGAT
20	R19B09.3C	Forward	CACCAGCCGAATAACTTTCTCCACA

21	R29B09	Forward	CACCGGTATGGCACCATCGTATCCCAAGT
Primers for sequencing			
22	M13	Forward	GTAAAACGACGGCCAGT
23	M13	Reverse	CAGGAAACAGCTATGAC
24	T7 promoter	Forward	TAATACGACTCACTATAGGG

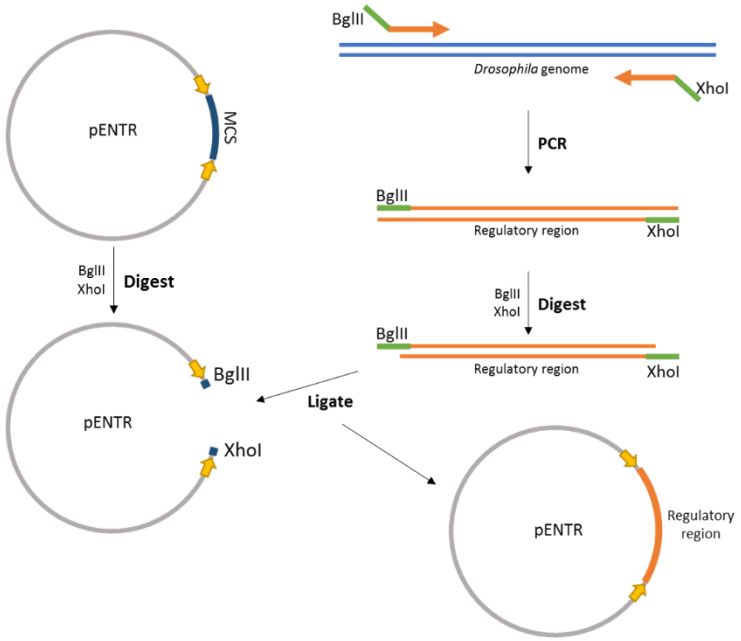

Figure 3.6. Strategy for RE cloning. The pENTRs were digested with BglII and XhoI, releasing a small fragment (MCS, dark blue). At the same time the chosen REs were amplified from the *D. melanogaster* genome (double blue lines) with specific primers (orange+green arrows), containing a restriction site for the enzymes BglII and XhoI (green fragments). Then, the PCR reactions were purified, and digested with BglII and XhoI, leaving overhangs compatible with the overhangs of the plasmids. After purification, the insert and the plasmid were ligated, generating a pENTR with a specific RE (named "pENTR-RE", regulatory region, orange), flanked by attL sites (yellow arrows).

b) **DSCP and Gal4 piece cloning**

DSCP was amplified from pBPGAL4.2Uw-2 plasmid, a gift from Gerald Rubin (Addgene plasmid # 26227) using primers 17 and 18 (table 3), which contained restriction sites for the enzymes XhoI and KpnI, respectively. DSCP amplification by PCR resulted in a product of 155 bp, confirmed by agarose gel electrophoresis. This fragment was digested with XhoI and KpnI during 2 h at 37 °C. After this preparation, the DSCP was subcloned in XhoI+KpnI-digested and purified pCaSpeR4 plasmids containing the 4x-split VEnC-GAL4. XhoI+KpnI-digested insert (DSCP) and vector (pCaSpeR4) were ligated, transformed in NZY5α cells, and plated in LB agar with ampicillin resistance. For each 4x-split VEnC-GAL4 piece cloning, colonies were tested by PCR and sequenced as described above to generate four different pCaSpeR4-DSCP+GAL4_piece plasmids. Each pCaSpeR4-DSCP+GAL4_piece plasmid was then digested with XhoI and NotI, to release a fragment containing the DSCP and the GAL4 piece, which was subcloned into the different XhoI+NotI-digested pENTR-REs to make

pENTR-RE-DSCP-GAL4_piece. In total, we constructed eight of these pENTR-RE-DSCP-GAL4_piece, each one with one specific RE, the DSCP, and one of the four pieces from the 4x-split VEnC-GAL4 **(Figure 3.7)**.

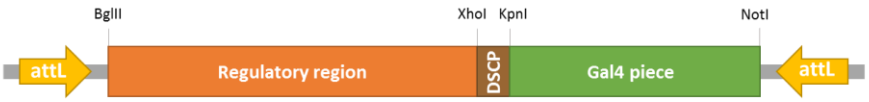

Plasmids for PIL neurons specific VEnCode	
pENTR1-PILa-VEnC-GAL4-p1	pENTR-attL1-R19B09.3A-DSCP-Gal4DBD-AceL-TerL-IntN-attL5R
pENTR2-PILb-VEnC-GAL4-p2	pENTR-attL5-R19B09.3C-DSCP-AceL-TerL-IntC-Gp41-1-IntN-attL4
pENTR3-PILc-VEnC-GAL4-p3	pENTR-attL4R-R29B09-DSCP-Gp41-1-IntC-NpuDnaE-IntN-attL3R
pENTR4-PILd-VEnC-GAL4-p4	pENTR-attL3-R25E10-DSCP-NpuDnaE-IntC-VP48-attL2
Plasmids for PTTH neurons specific VEnCode	
pENTR1-PTTHa-VEnC-GAL4-p1	pENTR-attL1-R43A12-DSCP-Gal4DBD-AceL-TerL-IntN-attL5R
pENTR2-PTTHb-VEnC-GAL4-p2	pENTR-attL5-R84E05-DSCP-AceL-TerL-IntC-Gp41-1-IntN-attL4
pENTR3-PTTHc-VEnC-GAL4-p3	pENTR-attL4R-R54C08-DSCP-Gp41-1-IntC-NpuDnaE-IntN-attL3R
pENTR4-PTTHd-VEnC-GAL4-p4	pENTR-attL3-*ptth*promoter-DSCP-NpuDnaE-IntC-VP48-attL2

Figure 3.7. Model of final pENTR structure, and details of the PIL Neuron and PTTH neuron VEnCode plasmids. All pENTRs constructed have one regulatory region, the DSCP, and one of the four 4x-split VEnC-Gal4 pieces. Also described are all plasmids constructed for the PIL neuron-specific VECode and for the PTTH neuron-specific VEnCode, indicating the short plasmid name (left column) and the detailed plasmid name (right column).

3.3.4 Construction of the Split-Gal4 plasmids

As a backup strategy to generate a PIL-neuron specific driver, we attempted to generate a Split-Gal4 system (Pfeiffer *et al*. 2010) for PIL neurons. Different REs were cloned into the two vectors, pBPZpGAL4DBDUw and pBPp65ADZpUw, in several combinations **(Figure 3.8)**. We first cloned the REs into pENTR/D-TOPO (figure 10). For this, we designed primers to amplify the REs from the *D. melanogaster* genome and added a 4-bp sequence (CACC) at the 5'prime of the left primer, as described in figure 10. This 4-bp sequence is necessary for directional TOPO cloning, a very efficient cloning technique that capitalizes on topoisomerase I activity (Shuman 1991; Shuman 1994). The overhang in the cloning vector (GTGG) occupies the 5' end of the PCR product, annealing with the added bases and stabilizing the fragment in the correct orientation. To generate different possibilities for a PIL neuron-specific split-GAL4 driver, we amplified the R19B09.3A, R19B09.3C, and R29B09 REs, and generated the pENTR/D-TOPO-R19B09.3A, pENTR/D-TOPO-R19B09.3C, pENTR/D-TOPO-R29B09 plamids. We then performed an LR reaction to clone these fragments into the two Split-GAL4 vectors (pBPZpGAL4DBDUw and pBPp65ADZpUw).

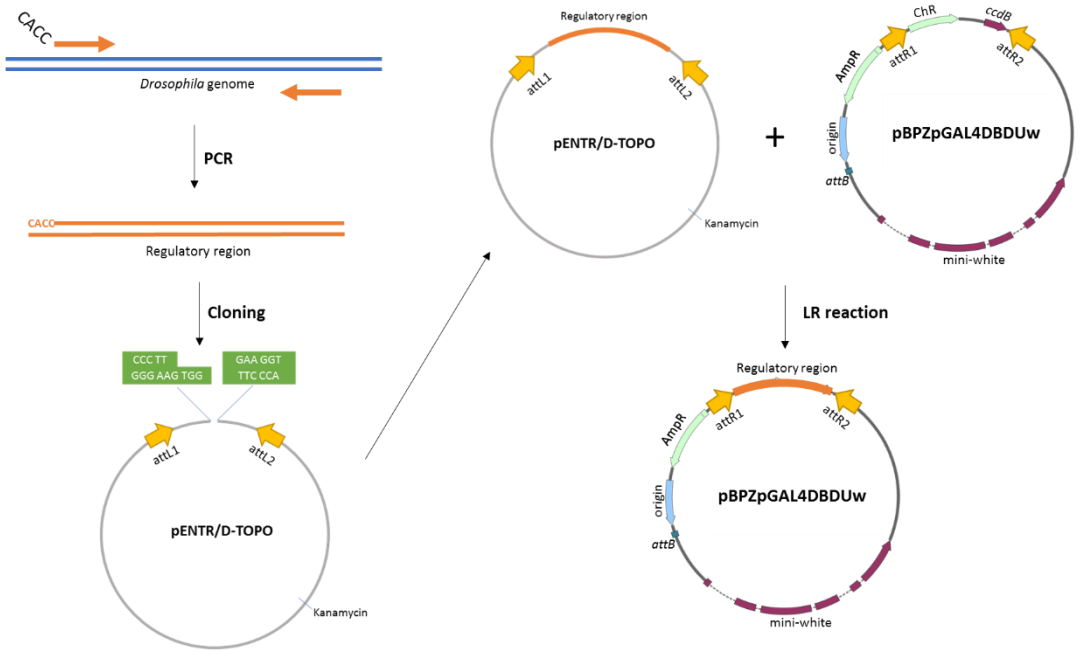

Figure 3.8. Strategy for Split-Gal4 cloning. The regulatory regions were amplified from the *Drosophila* genome (double blue lines) with specific primers (orange arrows) in which the right primer had a CACC specific for TOPO cloning, then the regulatory region after purified was cloned into the pENTR/D-TOPO as described by the manufacturer. After it has been confirmed the sequence by sequencing, the LR reaction was performed between the pENTR/D-TOPO and the destination vectors chosen, the both plasmids with the split-Gal4.

In total, we constructed four different Split-GAL4 plasmids (**Figure 3.9)**. The GAL4DBD plasmids were injected to be inserted in the attP2 site, localized at the 3rd chromosome, while the GAL4-AD (p65AD) plasmids were injected to be inserted in the attp40 site, localized at the 2nd chromosome. The transgenic flies generated will be crossed as following: flies with the construct R19B09.3C-GAL4DBD will be crossed with flies with the construct R29B09-p65AD, thus the F1 generation will have a functional GAL4 protein reconstituted in cells where both *R19B09.3C>* and *R29B09>* drivers are driving expression.

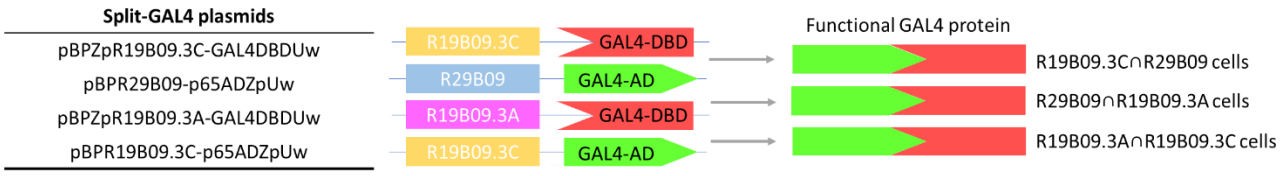

Figure 3.9. Final model of the Split GAL4 plasmids. Each plasmid constructed contains one RE, R19B09.3C, R29B09 or R19B09.3A and one functional domain of the GAL4 protein, GAL4-DBD or GAL4-AD (p65AD). The GAL4-DBD binds to GAL4-AD, creating a functional GAL4 protein that is only expressed in cells where both REs drive each domain.

4 RESULTS AND DISCUSSION

As described above, PIL neurons are strong candidates to mediate the Dilp8- and Lgr3-dependent developmental delay, but this has never been formally tested, because PIL neurons have always been genetically manipulated together with other cells due to the lack of PIL neuron-specific gene drivers. Our main hypothesis is that Lgr3 is required in PIL neurons in order for animals to respond to the Dilp8 peripheral stress signal. To test this hypothesis, we attempted to generate PIL neuron-specific drivers, as described below. We designed four independent strategies (sections 4.1-4.4) to achieve this goal.

4.1 DISSECTION OF THE R19B09 ENHANCER

The enhancer fragment GMR19B09 (Jenett et al. 2012) (hereafter referred to as R19B09) drives gene expression in cells where Lgr3 is required to transduce the Dilp8-dependent delay in the onset of metamorphosis (Garelli et al. 2015; Colombani et al. 2015; Vallejo et al. 2015; Jaszczak et al. 2015). Of the ~270 *R19B09-GAL4* (*R19B09*>)-expressing neurons (Li et al. 2014), four are the PIL neurons (Garelli et al. 2015). R19B09 is a 3-kb fragment corresponding to the seventh intron and part of the flanking exons of the *Lgr3* locus **(Figure 4.1A).** Here, we asked two major questions: First, which region or regions of R19B09 drives expression in the cells in which Lgr3 is required to delay development in response to Dilp8, being functionally relevant in the pathway? Secondly, which region or regions of R19B09 drive expression in the PIL neurons, being anatomically relevant for this work? Our hypothesis is that these regions will be the same, but we must consider the formal possibility that the PIL neurons might not be the critical cells in which Lgr3 is required for the Dilp8-dependent delay, so the regions we identify while answering both question might differ. Our main strategy to address these questions was to test a series of R19B09 fragments generated by Meissner *et al*. (Meissner et al. 2016) **(Figure 4.1B)**.

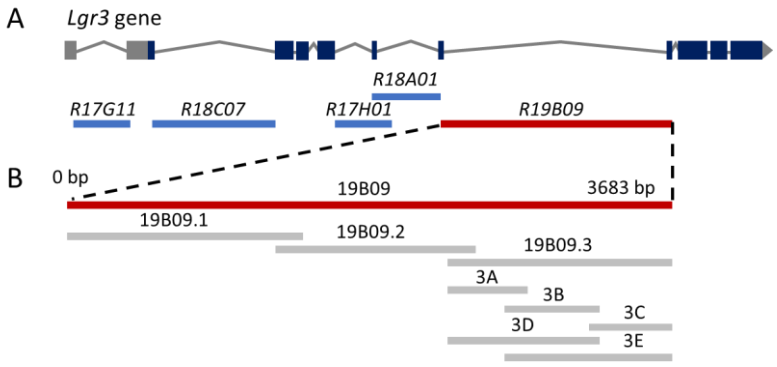

Figure 4.1. Schematic representation of the *Lgr3* gene. (A) Five large non-coding regions (introns) of the *Lgr3* gene (R17G11, R18C07, R17H01, R18A01, and R19B09), containing putative Lgr3 regulatory elements (REs) have been placed upstream of GAL4, and their expression in the CNS has been characterised at FlyLight (Jenett et al. 2012; Li et al. 2014). R19B09 (red bar), but not the other drivers (blue bars), drives expression in a population of cells, englobing the PIL neurons, in which Lgr3 is necessary to transduce the Dilp8-dependent delay. (B) R19B09 was divided into multiple fragments, each of which was also placed upstream of GAL4 (Meissner et al. 2016). Here we will use these fragments to map the R19B09 region(s) that drive(s) expression in cells were Lgr3 is necessary to convey the Dilp8-dependent delay and/or region(s) that drive(s) expression in PIL neurons.

To answer the first question of which R19B09 region(s) drive(s) expression in cells were Lgr3 is necessary to convey the Dilp8-dependent delay, we expressed RNAi against Lgr3 (*Lgr3-IR*) under the control of the

different R19B09 fragments, and assayed for their ability to suppress the delay produced by constitutive expression of Dilp8 under the control of the *Tubulin* promoter (*Tub-dilp8*) **(Figure 4.2A)**. For this, we crossed each *R19B09 fragment-GAL4* (*Rf>*) line with a stock of the genotype *Tub*-dilp8/S-*T*/*UAS-Lgr3-IR-V22* (*S-T* is a balancer with translocations between 2nd and 3rd marked with the dominant Tubby (Tb) marker), and scored the pupariation time of the non-Tb larvae of the genotype: *Tub-dilp8; Rf>Lgr3-IR*. The positive control for the delay was the F1 of a cross between the line *Tub-dilp8/S-T/UAS-Lgr3-IR-V22* and *w[1118]*, and the negative control was the F1 larvae of a cross between the *Rf>* line *R19B09>* and *w[1118]*. Consistent with previous results (Garelli et al. 2015), *Tub-dilp8* induced an 18-h median delay ($P < 0.0001$, Dunn's post hoc test), and both *Lgr3-GAL4::VP16>* (Colombani et al. 2015) and the *R19B09>* (Garelli et al. 2015; Colombani et al. 2015) control drivers significantly rescued this delay when driving *Lgr3-IR* ($P < 0.0001$, for both, Dunn's post hoc test). The *Lgr3-GAL4::VP16* line drives GAL4 expression in most Lgr3-positive cells, being an additional control for Lgr3 activity. These results confirm that the Lgr3 receptor is necessary in *Lgr3-GAL4-VP16>*- and *R19B09>*-expressing cells to delay the onset of metamorphosis in response to Dilp8. Regarding the R19B09 fragments, all fragments, except R19B09.1, showed significant suppression of the Dilp8-induced delay when driving Lgr3-IR ($P < 0.0001$, Dunn's post hoc test). As the R19B09.3A and R19B09.3C regions correspond to non-overlapping segments of the seventh intron of *Lgr3* **(Figure 4.1)**, our result suggests there are at least two independent regions within the *R19B09* element driving gene expression in cells requiring Lgr3 for the Dilp8-dependent delay.

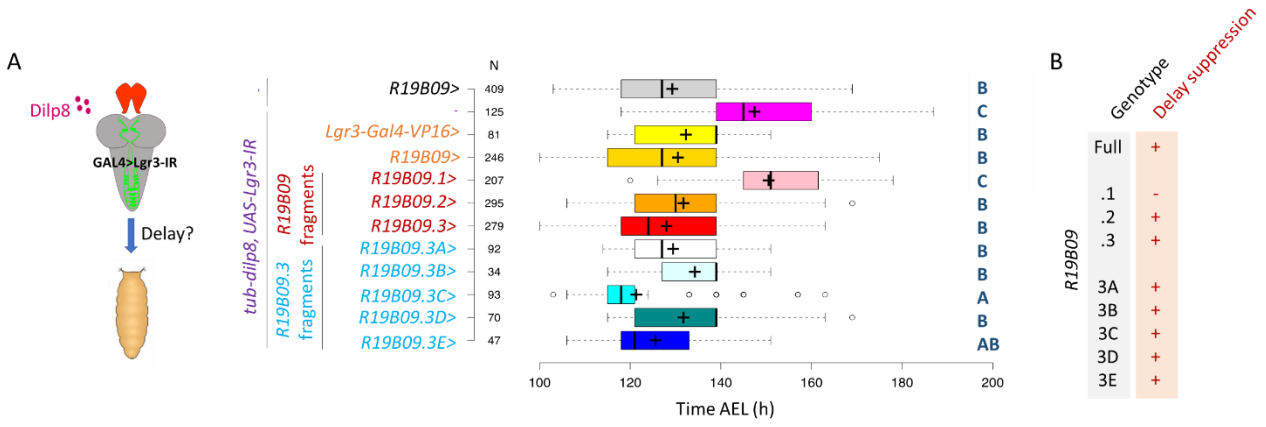

Figure 4.2. Functional dissection of the R19B09 regulatory element identifies two independent regions that redundantly control *Lgr3* expression in cells that are relevant for the Dilp8-dependent delay. (A) Box plot showing pupariation time (Time after egg laying (AEL)) in h of (N) larvae expressing Dilp8 under the control of *Tubulin* promoter (*Tub-dilp8*) and RNAi against *Lgr3* (*Lgr3-IR*) under control of *Lgr3-GAL4-VP16>* (control for suppression), the *Lgr3* RE R19B09 (*R19B09>*, another control for suppression), and various R19B09 fragments. As a negative control, a stock carrying *R19B09>* was crossed with *w[1118]* animals, and F1 larvae were scored. As a positive control for the delay, *Tub-dilp8, UAS-Lgr3-IR-V22* animals were crossed with *w[1118]* animals, and F1 larvae were scored. Whiskers extend to data points that are less than 1.5x interquartile range (IQR) away from 1st/3rd quartile, dots are outliers, the black vertical bars represent the median, and the plus sign represents the mean. $P < 0.0001$, Kruskal–Wallis one-way ANOVA test. Genotypes sharing the same letter (blue) are not statistically different at $\alpha = 0.01$, Dunn's *post hoc* test. (B) Summary of the phenotype of *Tub-dilp8* suppression for each R19B09 fragment. In the table "+" denotes a positive finding, and "-" denotes a negative finding.

To answer the second question of which R19B09 region(s) drive(s) expression in PIL neurons, we expressed *myr::tdTomato* under the control of the different R19B09 fragments in animals carrying the *sfGFP::Lgr3*

endogenous marker, which labels all Lgr3-positive neurons, including the PIL neurons **(Figure 4.3A)**. We crossed the different *Rf>* lines with a stock carrying *UAS-myr::tdTomato; sfGFP::Lgr3*, and then performed immunohistochemistry of the F1 larval CNS to analyse the colocalization between *sfGFP::Lgr3* and *myr::tdTomato*, detected with an antibody against GFP and the endogenous tdTomato fluorescence, respectively. Therefore, when the *Rf>* drives expression in the PIL neurons, we expect to observe a colocalization of both reporters. Our results show clear colocalization between *sfGFP::Lgr3* and *myr::tdTomato* driven by *R19B09.3>* or all its subfragments (*R19B09.3A-3E*; **Figure 4.3A,** and data not shown). Interestingly, these results show that PIL neuron expression is regulated by two independent and redundant REs contained in the non-overlapping fragments R19B9.3A and R19B09.3C. Redundant REs can be called shadow enhancers (Hong et al. 2008). *Drosophila* Lgr3 has evolved at least two shadow enhancers in its seventh intron to secure Lgr3 protein expression in the PIL neurons. Shadow enhancers can confer precision and robustness to gene expression, albeit complete spatial redundancy is rare (Cannavò et al. 2016). Consistent with this, *R19B9.3A>* and *R19B09.3C>* seem to drive very different patterns aside from the coinciding PIL neuron expression (**Figure 4.3A**). Contrary to *R19B09.3>*, neither *R19B09.1>* nor *R19B09.2>* drove detectable expression of *myr::tdTomato* in the PIL neurons. As the *R19B09.1>* driver also does not suppress the Dilp8-dependent delay when driving *Lgr3-IR*, we can also conclude that Lgr3 is not required in *R19B09.1>*-expressing cells, to convey the delay. However, in contrast to *R19B09.1>*, the *R19B09.2>* driver suppresses the Dilp8-dependent delay when driving Lgr3-IR. These initial results suggest that, contrary to our expectations, the PIL neurons may not be the cells or may not be the only cells requiring Lgr3 in the Dilp8 pathway to induce a developmental timing delay.

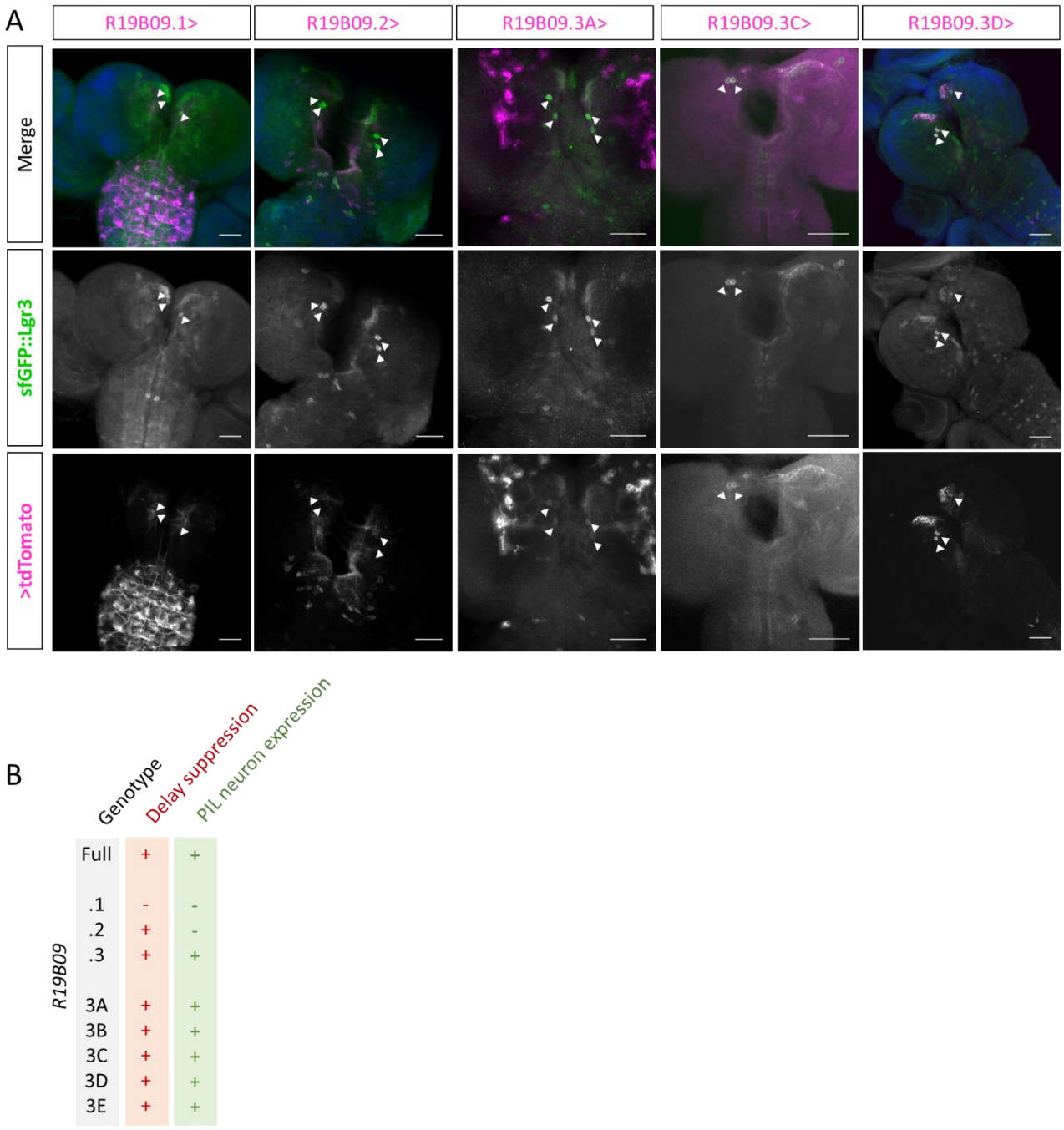

Figure 4.3. *Lgr3* R19B09.3 fragments drive expression in PIL neurons. (A) Sum of confocal z-stack slices stained with anti-GFP (green) to show *sfGFP::Lgr3* expression (Garelli et al. 2015) and with *myr::tdTomato* (magenta) driven by the various R19B09 fragments. DAPI counterstain labels nuclei (blue). Both *R19B09.1>* and *R19B09.2>* do not drive detectable expression in sfGFP::Lgr3-positive PIL neurons, while the *R19B09.3>* fragments drive expression in PIL neurons. PIL neuron cell bodies are highlighted with arrowheads. Scale bars, 50 µm. (B) Summary of the phenotypes of *Tub-dilp8* suppression and PIL neuron expression for each R19B09 fragment. In the table "+" denotes a positive finding and "-" denotes a negative finding.

Surprised by the findings described above, we reasoned that even the slightest expression of *Lgr3-IR* in the PIL neurons could lead to a significant reduction in Lgr3 protein levels, which could be physiologically relevant and sufficient to suppress the Dilp8-dependent delay, yet too weak to be detectable by the myr::tdTomato colocalization strategy. Hence, in order to independently confirm that the *R19B09.1>* and *R19B09.2>* elements do not drive expression in the PIL neurons, and that the *R19B09.3A>* and *R19B09.3C>* elements do, we devised a more sensitive immunofluorescence assay to test the capability of *Rf*-driven *Lgr3-IR* to reduce

sfGFP::Lgr3 protein levels in the PIL neurons. Namely, we crossed animals of the genotype *UAS-Lgr3-IR-V22, sfGFP::Lgr3* with the different *Rf>* lines, and performed immunofluorescence analyses on dissected CNSs from the F1 larvae of the genotype *Rf>Lgr3-IR; sfGFP::Lgr3*, using an antibody against GFP. Consistent with previous results using the myr::tdTomato reporter, no detectable *sfGFP::Lgr3* was observed in cells bdies located in the PIL neuron anatomical region when either *R19B09.3A>* or *R19B09.3C>* were used to express Lgr3-IR (**Figure 4.4**). These results confirm that both *R19B09.3A>* and *R19B09.3C>* elements drive expression in the PIL neurons.

In contrast, when *Lgr3-IR* was driven under the control of *R19B09.1>,* we could still observe PIL neurons expressing *sfGFP::Lgr3*, suggesting that this RE does not drive expression in PIL neurons. This result confirmed our previous observations on the colocalization between *sfGFP::Lgr3* and *R19B09-1>*myr::tdTomato. Interestingly, *sfGFP::Lgr3* expression in PIL neurons seemed weaker in *R19B09.2>Lgr3-IR* brains compared to brains of *R19B09.1>Lgr3-IR* animals*,* suggesting that maybe *R19B09.2>* is indeed capable of driving weak gene expression in PIL neurons, which could be sufficient to suppress the Dilp8-dependent delay **(Figure 4.2A)**. The fact that we could not see colocalization between R19B09.2>myr::tdTomato and sfGFP::Lgr3 with this driver **(Figure 4.3A)**, could be explained if the expression of *myr::tdTomato* is too weak to be detected in our staining conditions. Unfortunately, we did not have time to obtain quantitative measurements of the extent of the *sfGFP::Lgr3* depletion induced by *R19B09.2>Lgr3-IR* in PIL neurons. Nevertheless, with these two experiments, we can be confident about the fact that both the *R19B09.3A>* and *R19B09.3C>* elements are capable of driving gene expression in the PIL neurons.

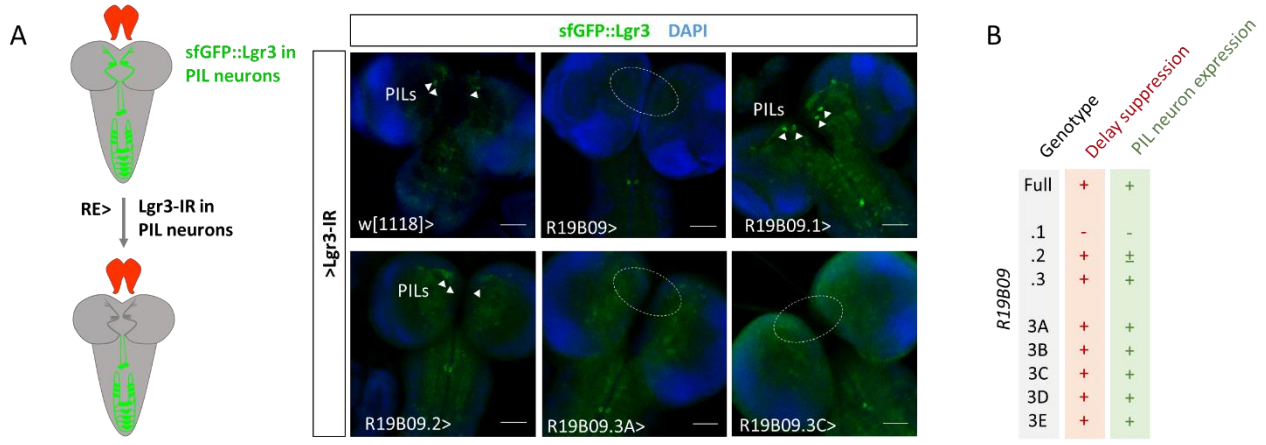

Figure 4.4. Two independent REs within the R19B09 element drive gene expression in the PIL neurons. (A) Sum of confocal z-stack slices stained with anti-GFP (green) and DAPI (blue). The REs drive *Lgr3-IR,* reducing the *sfGFP::Lgr3* expression (green) in the subset of cells where they are expressed. As a negative control, we crossed *w[1118]* animals to *UAS-Lgr3-IR-V22, sfGFP::Lgr3* animals, so that *Lgr3-IR* is not expressed in this condition, and all sfGFP::Lgr3-positive neurons are labelled in green. As a positive control, we used *R19B09>* driving *Lgr3-IR*, expecting the absence of *sfGFP::Lgr3* in the PIL neurons. Dashed white circle denotes the PIL neuron anatomical region (*pars intercerebralis*). Scale bars, 50 µm. (B) Summary of the phenotypes of delay suppression and PIL neuron expression (summary of PIL neuron expression findings using both sfGFP::Lgr3 Lgr3-IR and sfGFP::Lgr3 myr::tdTomato colocalization techniques) for each R19B09 fragment. In the table "+" denotes a positive finding and "-" denotes a negative finding.

The results above showed that sequences located on the last third of the R19B09 RE drive expression in cells where Lgr3 is required to transduce the Dilp8-dependent delay. However, it is not clear if the activation of

the neurons in which these REs are expressed is sufficient or not to generate a delay in the onset of metamorphosis. To answer this question, we drove the transient receptor potential cation channel A1 ortholog (TrpA1) under the control of *R19B09>* to thermogenetically activate the neurons by shifting the animals from 18°C to 29°C at the second larval instar stage **(Figure 4.5A)**. We scored the timing of pupariation of F1 larvae of *R19B09>* animals crossed with three different UAS lines: *UAS-Lgr3-IR-V22*, a condition where we do not expect a delay in the onset of metamorphosis, *UAS-TrpA1,* where *TrpA1* is driven, leading to calcium influx in the cells and an increase in neuronal firing rates in neurons at temperatures above 22°C, and *UAS-TRPA1; UAS-Lgr3-IR-V22,* a condition where both *TrpA1* and *Lgr3-IR* are driven to test their epistasis. The controls used were *R19B09>* crossed with *UAS-Lgr3-IR-V22*, and the UAS lines crossed with *w[1118]*. The results show that the *GAL4* enhancer line *R19B09>,* significantly delays the onset of metamorphosis when driving TrpA1 ($P < 0.0001$, Dunn's *post hoc* test). Furthermore, we find that the TrpA1-induced delay does not require Lgr3 in the *R19B09>*-expressing cells, because the delay is not rescued by co-expression of *Lgr3-IR* ($P > 0.01$, Dunn's *post hoc* test). This suggests that activation of R19B09 neurons is epistatic to Lgr3 activity in these neurons. One possibility is that R19B09 neuronal firing occurs downstream of Lgr3 activation by Dilp8, hence Lgr3 is not required.

Next, we attempted to discover which neuronal population was responsible for the R19B09>TrpA1-induced delay. Our strategy was to thermogenetically activate the different subsets of *R19B09>*-expressing cells using the different *Rf>* lines crossed to *UAS-TrpA1* and score the timing of pupariation in similar temperature-shift conditions as the experiments described above **(Figure 5B)**. As a positive control for the TrpA1-induced delay we used the complete R19B09 element driving TrpA1 (*R19B09>TrpA1*). The results show that all *Rf>* drivers, except *R19B09.3A>*, induced some extent of delay in pupariation time when compared to the *UAS-TrpA1* negative control, although all were weaker than the full R19B09 driver ($P < 0.01$, Dunn's *post hoc* test; **Figure 3A**). The weakest lines were *R19B09.1>* and *R19B09.2>.* The REs R19B09.1 and R19B09.2 can have some basal activity in the cells activated by TrpA1, explaining this result. As all R19B09.3 subfragments, except for the R10B09.3A, induced stronger delays upon TrpA1 activation, we interpret these results as indicative that the most relevant TRPA1-sensitive cells are part of the population of cells in which elements located at the two distal thirds of the *R19B09* element (represented by the REs R19B09.3, 3B, 3C, 3D and 3E) are active. Taking into account that R19B09.3A is active in PIL neurons **(Figure 3A),** but *R19B09.3A>*-expressing cells do not induce a delay when thermogenetically activated with TrpA1, we can argue that there are other *R19B09.3A>*-expressing cells that influence the delay. These may interact with PIL neurons inhibiting the delay, or PIL neurons might not be sufficient to induce a delay when thermogenetically activated with TrpA1. This would mean that the *R19B09.3A>* driver would not drive expression in any other TrpA1-sensitive cell population that influences developmental timing. The *R19B09.3A>TrpA1* result suggests that other, yet unidentified, cells can regulate pupariation timing. It would be very interesting to determine if they are part of the Lgr3-Dilp8 developmental stability pathway or rather represent cells acting in other pathways relevant for

developmental timing control (see Introduction). The exploration of putative new components of this pathway is addressed at the section 4.5.

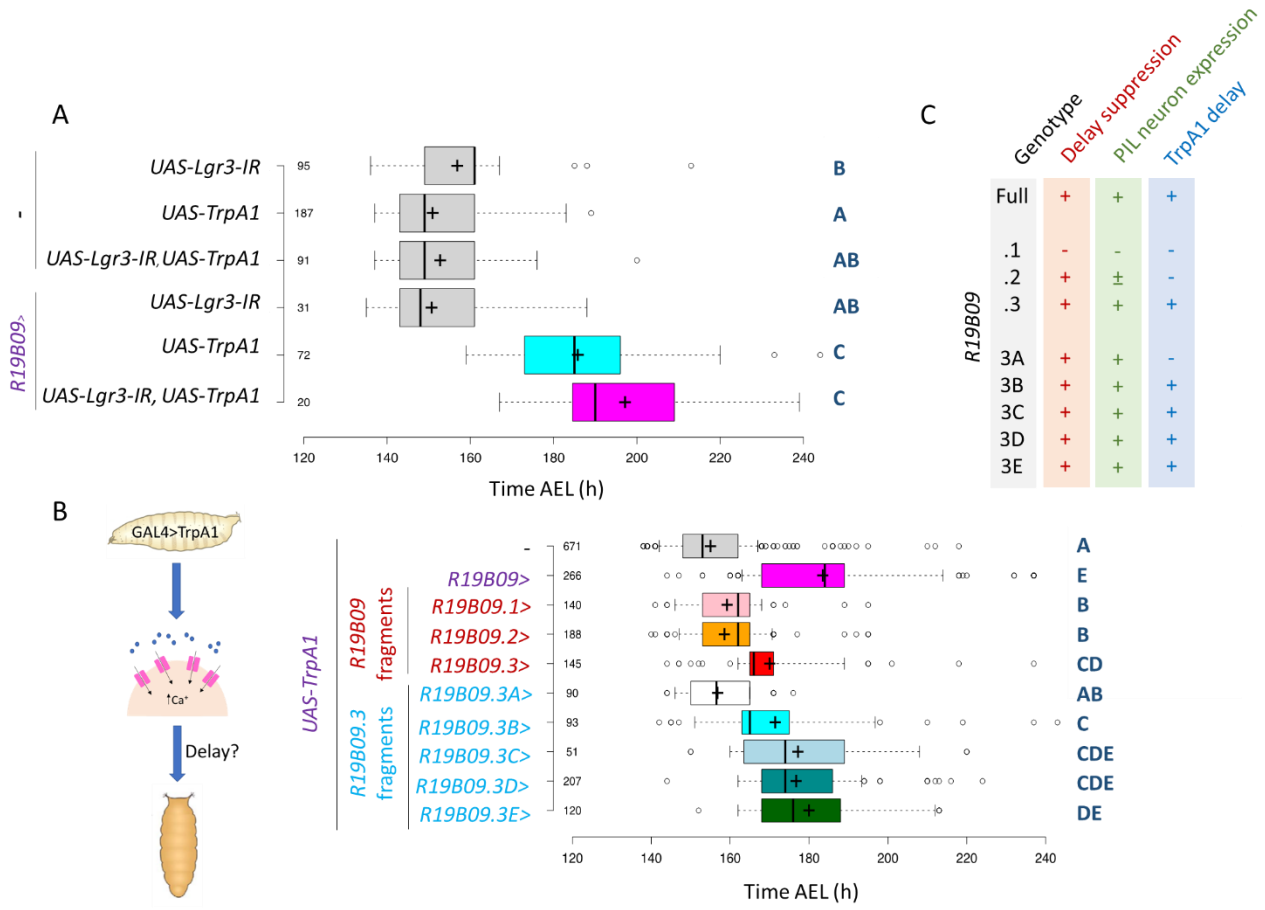

Figure 4.5. Lgr3 R19B09.3 fragments drive expression in TrpA1-sensitive cells, inducing a developmental timing delay. Box plot showing pupariation time (Time after egg laying (AEL)) in h of (N) larvae expressing: (A) The transient receptor potential cation channel A1 ortholog (TrpA1) and Lgr3-IR under the control of the Lgr3 R19B09 (*R19B09>*) driver. As negative control for delay, the same UAS lines were crossed with *w[1118]*. (B) TrpA1 under the control of the Lgr3 R19B09 (*R19B09>*) driver, and various R19B09 fragments. As negative control for delay, TrpA1 was crossed with *w[1118]*. Whiskers are 5 and 95% percentiles, dots are outliers, the black vertical bars represent the median and the plus sign represents the mean. (A,B) Whiskers extend to data points that are less than 1.5 x interquartile range (IQR) away from 1st/3rd quartile, dots are outliers, the black vertical bars represent the median and the plus sign represents the mean. $P < 0.0001$, Kruskal–Wallis one-way ANOVA test. Genotypes sharing the same letter (blue) are not statistically different at $\alpha = 0.01$, Dunn *post hoc* test. (C) Summary of the phenotypes of delay suppression, PIL neuron expression (summary of PIL neuron expression findings using both sfGFP::Lgr3 Lgr3-IR and sfGFP::Lgr3 myr::tdTomato colocalization techniques) and TrpA1 delay for each R19B09 fragment. In the table "+" denotes a positive finding and "-" denotes a negative finding.

Mapping the R19B09 element **(Figure 4.6)** led to the three main conclusions: 1) that at least two PIL neuron shadow enhancers are present in the *Lgr3* gene; 2) that there might be other R19B09-positive cells, besides the PIL neurons, that mediate the Dilp8-response, and 3) that a small R19B09 region (R19B09.3A) that drives expression in PIL neurons is not sufficient to induce a delay upon thermogenetic activation.

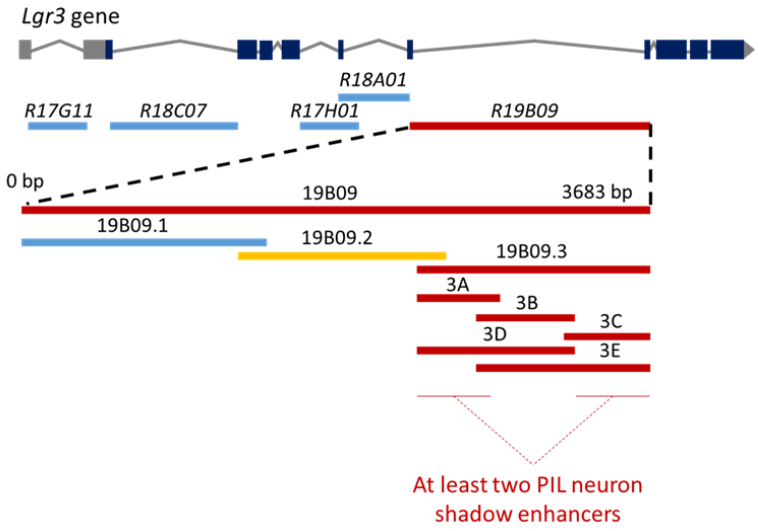

Figure 4.6. The *Lgr3* gene has at least two shadow enhancers that are active in the PIL neurons. The RE R19B09 was fragmented into three small element: the R19B09.1 fragment (blue bar), which neither regulates the response to Dilp8 in Lgr3-positive neurons nor drives expression in PIL neurons; the R19B09.2 fragment (yellow bar), which suppresses the Dilp8-dependent delay when driving *Lgr3-IR*, but its expression in PIL neurons is very weak, at best; and the R19B09.3 fragment and its subfragments (red bars), which drive *Lgr3* in cells that regulate the Dilp8-dependent delay and drive expression in the PIL neurons, constituting at least two redundant "shadow" enhancers.

4.2 New methodologies – VEnCode

The second strategy to find drivers for PIL neurons is using VEnCode, a new approach developed in our laboratory. VEnCodes are natural RE activity signatures that target specifically only one cell type or state. VEnCode explores the intersection of multiple (≥3) active REs that overlap exclusively in the desired cell type or cell state. To apply this strategy to generate a PIL neuron-specific driver, we need to find REs overlapping exclusively in PIL neurons. As it is currently a challenge to determine a lack of overlap in unwanted cells using only functional and image analysis data in *Drosophila*, we first sought to identify multiple drivers that express in PIL neurons and at the same time have sparse expression in the CNS. This was done to reduce the likelihood that the drivers would overlap in other neurons than the target PIL neurons. In this section, we will thus search for, select, and characterise the REs that will be used as promoters to construct a VEnCode for PIL neurons.

4.2.1 Identification of candidates for PIL neuron-specific drivers

a) **Neuroanatomical screen for PIL neuron REs**

To perform a neuroanatomical screen, we searched for neurons that resemble the PIL neuron neuroanatomically (Garelli et al. 2015) at the FlyLight database. In this database, the adult and larval nervous systems of animals carrying different Janelia GAL4 lines expressing GFP have been imaged in high resolution. In this visual screen, we identified five GAL4 driver lines (R52E10, R64G08, R69F02, R78F10 and R48H10) that drove expression in cells that looked like PIL neurons **(Figure 4.7).**

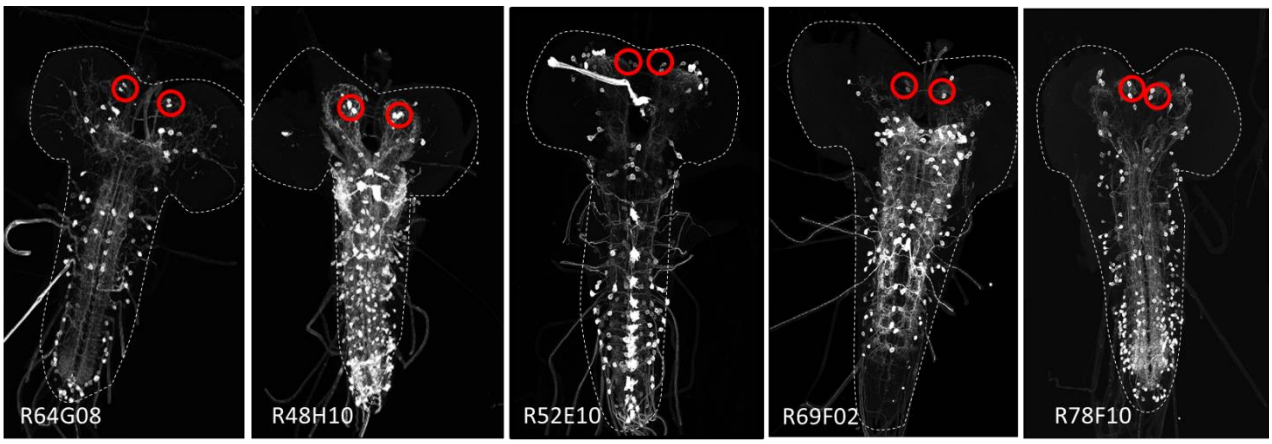

Figure 4.7. Images from FlyLight representing the described GAL4 drivers pattern in the larval CNS. Red circles limit the PIL-like neurons.

b) **Functional screen for PIL neuron REs**

The second strategy to find PIL neuron drivers relies on the assumption that PIL neurons are critical cells amongst those that require Lgr3 to convey the Dilp8-delay signal. We thus removed Lgr3 using *Lgr3-IR* in 68 different neuronal populations using sixty-eight new GAL4 lines from the Janelia Collection and assayed for their ability to suppress the Dilp8-dependent delay caused by *Tub-dilp8* constitutive expression. Namely, we crossed *Tub-dilp8/S-T/UAS-Lgr3-IR-V22* animals with each Janelia GAL4 line and non-Tb F1 larvae of the genotype *Tub-dilp8; GAL4 line>Lgr3-IR* were scored for pupariation time. The *Tub-dilp8/S-T/UAS-Lgr3-IR-V22* stock crossed to *w[1118]* and to a stock carrying a panneuronal driver, *elav-GAL4,* served as negative and positive control for suppression, respectively. A rescue of the delay means that Lgr3 is required in the cells, and that we can use the identified GAL4 driver as a candidate PIL neuron RE in our VEnCode strategy. From the sixty-eight lines analysed, only seven drivers suppressed the delay (**Table 4**, and results not shown).

Table 4. List of identified regulatory elements that rescue the dilp8-dependent delay when driving *Lgr3-IR*.

Regulatory element	Size (bp)	Chromosome	Gene
R87B08	3073	X	***runxb*** (CG15455)
R36A05	3881	X	***ct*** (CG11387)
R64H06	3939	X	***amn*** (CG11937)
R29B09	819	2R	***pkc53e*** (CG6622)
R25E10	1331	2R	***adf1*** (CG15845)
R28E05	3647	2R	***dscam*** (CG17800)
R57F02	2009	2L	***nacralpha-30d*** (CG4128)

4.2.2 VEnCode for PIL neurons

To understand the interaction between Lgr3 and Dilp8 and the role of Lgr3-positive PIL neurons in the Dilp8 pathway, we need to have the means to exclusively manipulate this pair of bilateral neurons. The finding that

R19B09.3C> is a very sparse driver for PIL neurons bring us closer to the main goal of finding specific drivers for PIL neurons. However, a truly exclusive driver is essential to make unequivocal conclusions regarding PIL neuron function. Here, we will try to determine VEnCodes for PIL neurons to generate VEnCode-based PIL neuron-specific driver. The first step to determine a VEnCode in Drosophila is to find at least three or four drivers that are both active in the PIL neurons and have a sparse expression in the CNS. To determine the ability of the five candidate REs identified in the neuroanatomical screen (R52E10, R64G08, R69F02, R78F10, and R48H10**;** see section 4.2.1.a) to drive expression in the PIL neurons, we tested them in the sfGFP::Lgr3 Lgr3-IR assay **(Figure 4.8A)**. If a driver produces gene expression in the sfGFP::Lgr3-positive PIL neurons, we should detect a decrease or an absence of sfGFP::Lgr3 expression in the PIL neuron anatomical region by immunofluorescence using an anti-GFP antibody. The results show a strong expression of *sfGFP::Lgr3* in all the five lines analysed, despite the presence of *Lgr3-IR*. This suggests that none of PIL-like neurons identified in the neuroanatomical screen were actually PIL neurons. Similar results were found using the *UAS-myR:tdTomato* assay for colocalization between *sfGFP::Lgr3* and myr::tdTomato **(Figure 4.8B)**.

Interestingly, despite not driving expression in the PIL neurons, two of these drivers, *R48H10>* and *R69F02>*, produced a delay in the onset of metamorphosis when the cell populations they drive expression in were thermogenetically activated with TrpA1 ($P < 0.0001$, Dunn's *post hoc* test; **Figure 4.8C**). Namely, we crossed each Janelia GAL4 line with *UAS-TrpA1* and performed a developmental time assay. The *UAS-TrpA1* line was crossed with *w[1118]* and with *R19B09>* as negative and positive controls for the delay, respectively. Importantly, the two positive drivers produced a strong delay, proportional to the one produced by the *R19B09>TrpA1* positive control **(Figure 4.8C)**. These results show that *R48H10>* and *R69F02>* cells represent one or more new populations of cells that are TrpA1-sensitive and capable of triggering a delay in the onset of metamorphosis. These cells may or may not be acting in the Dilp8- and Lgr3-dependent developmental stability pathway. Our attempt to characterise these new population of cells is described in section 4.5. We conclude that our neuroanatomical screen unfortunately did not yield any new RE driving expression in PIL neurons.

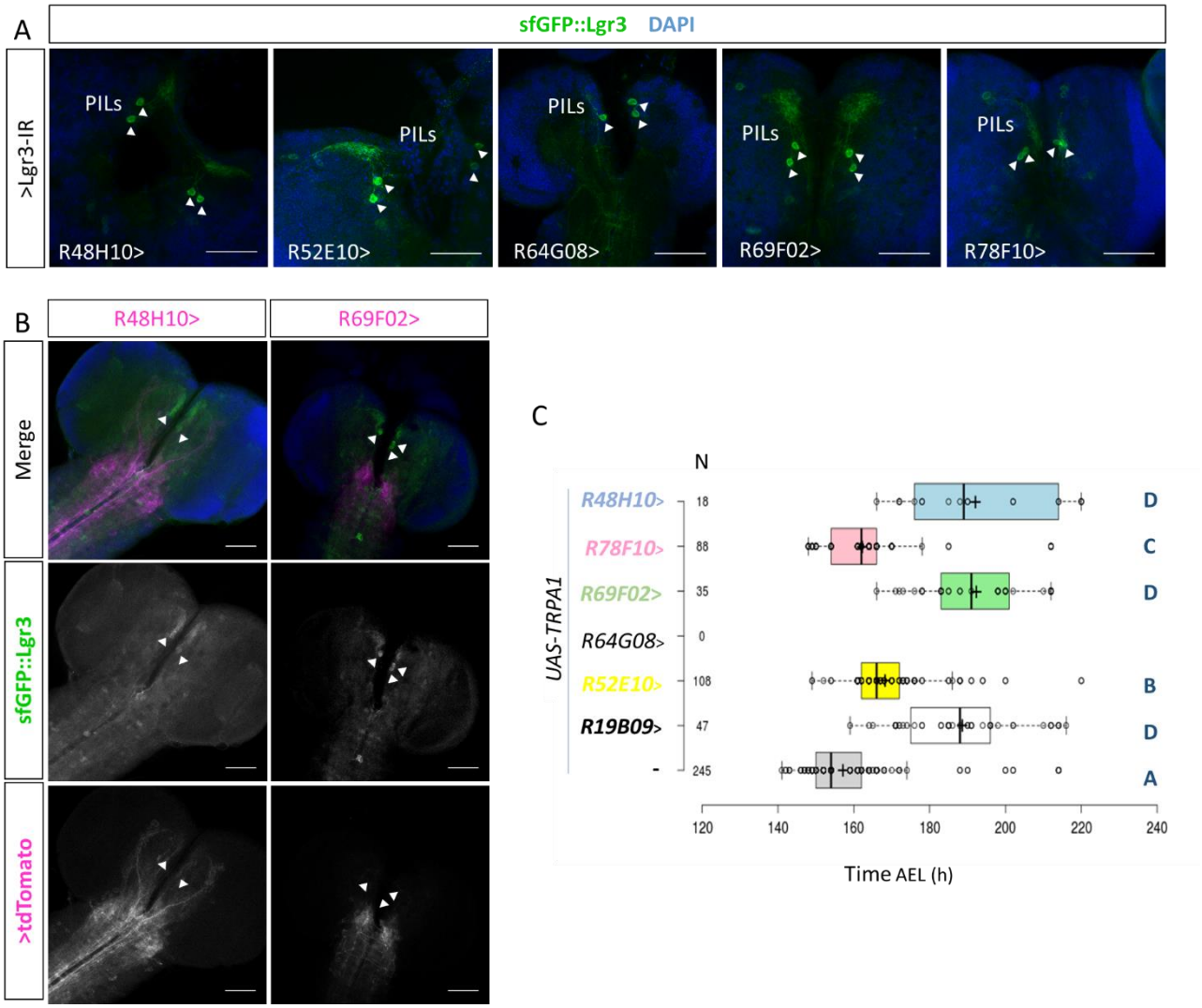

Figure 4.8. New TrpA1-sensitive cells delay the onset of metamorphosis. (A) Sum of confocal z-stack slices stained with anti-GFP (green) and DAPI (blue). The REs described are tested for their ability to reduce the *sfGFP::Lgr3* (green) expression when driving *Lgr3-IR.* (B) Sum of confocal z-stack slices stained with anti-GFP (green) to show *sfGFP::Lgr3* expression (green) and with *myr::tdTomato* (magenta) driven by the *R48H10>* and *R69F02>* and DAPI (blue). PIL neurons are highlighted with arrowheads. (C) Box plot showing pupariation time of (N) larvae expressing TrpA1 driven by the RE *R19B09>* (as positive control for delay), *R52E10>, R64G08>, R69F02>, R78F10>* and *R48H10>*. As a negative control, a stock carrying the *UAS-TrpA1* cassette was crossed with *w[1118]* animals and their F1 larvae were scored. Whiskers extend to data points that are less than 1.5 x IQR away from 1st/3rd quartile, dots represent all data, the black vertical bars represent the median and the plus sign represents the mean. $P < 0.0001$, Kruskal–Wallis one-way ANOVA test. Genotypes sharing the same letter (blue) are not statistically different at $\alpha = 0.01$, Dunn *post hoc* test. (A,B) Scale bars, 50 µm.

To confirm our initial assumption that the GAL4 lines identified in the *Lgr3-IR* functional screen **(Table 4)** suppressed the Dilp8-dependent delay caused by *Tub-dilp8* constitutive expression because they drive expression in PIL neurons, we performed immunofluorescence and colocalization assays, similar to the ones performed in previous experiments. The GAL4 lines *R25E10>*, *R29B09>*, *R28E10>*, and *R87B08>* were crossed with the *UAS-Lgr3-IR-V22, sfGFP::Lgr3* stock, and the resulting F1 larval CNSs were dissected and labelled with an anti-GFP antibody **(Figure 4.9A)**. We observed that all drivers eliminate *sfGFP::Lgr3* expression in PIL neurons, confirming our assumption that all drivers identified in the *Lgr3-IR* functional screen would drive expression in PIL neurons. For VEnCode purposes, we pursued further experiments with the GAL4 lines *R25E10>* and *R29B09>*, due to their smaller size, which facilitates downstream cloning steps required for construct manipulations. It is important to state that both *R29B09>* and *R25E10>* do not drive detectable

UAS-myr::tdTomato in PIL neurons labelled with the *sfGFP::Lgr3* marker **(Figure 4.9B)**. This result contrasts with the previous result, but as the results of the experiment using *Lgr3-IR* are of unequivocal interpretation, we conclude that the *Lgr3-IR sfGFP::Lgr3* assay is more sensitive than the *tdTomato* colocalization experiment, and, consequently, that both REs R48H10 and R69F02 are capable of actively driving enough gene expression in PIL neurons to remove detectable Lgr3 protein and supposedly to suppress the Dilp8-dependent delay (section 4.2.1.b).

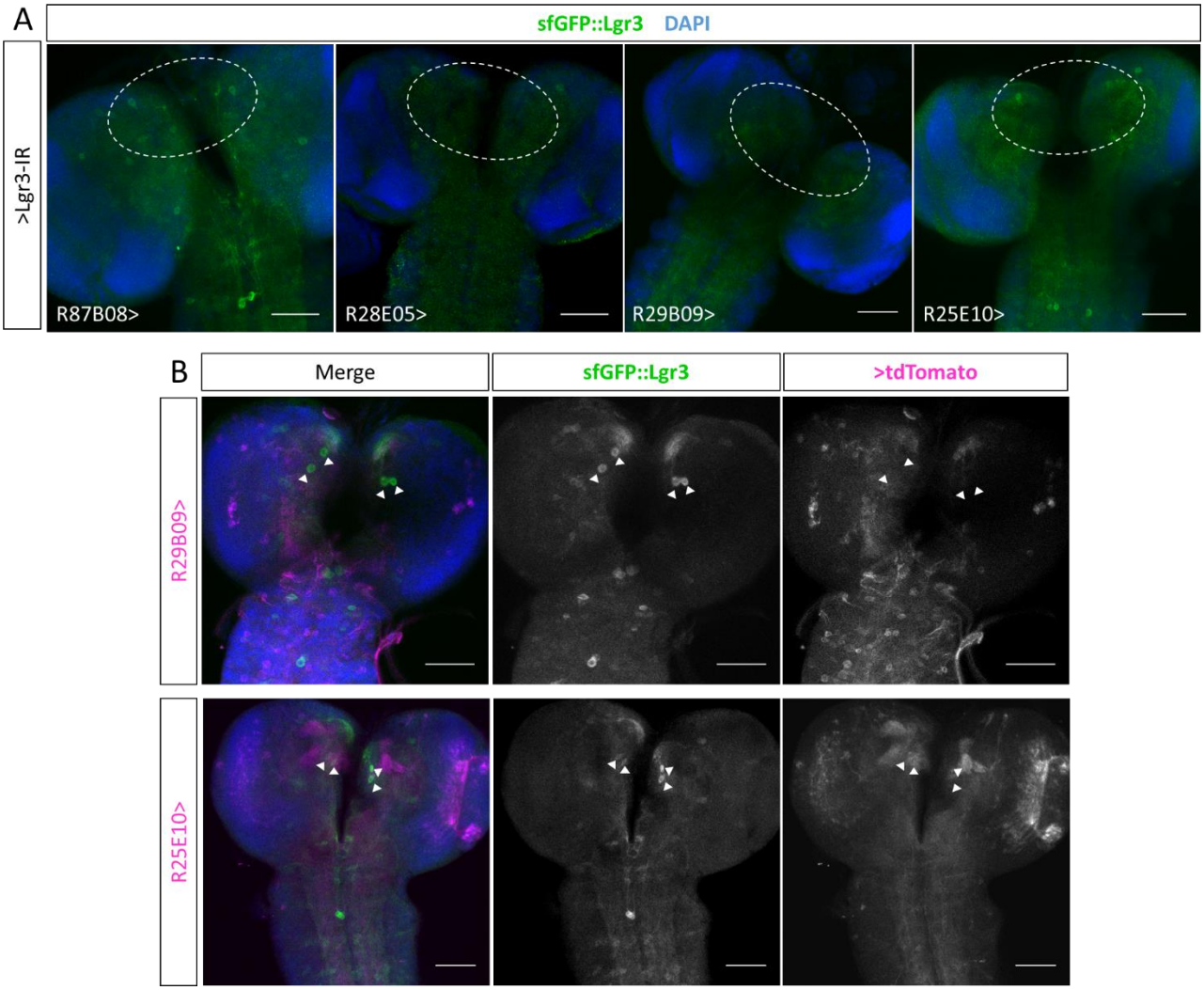

Figure 4.9. New REs are expressed in a subset of cells that include the PIL neurons. (A) Sum of confocal z-stack slices of L3 larval brains stained with anti-GFP (green) and DAPI (blue). The REs *R87B08>, R28E05>, R29B09>,* and *R25E10>* drive*Lgr3-IR* in a subpopulation of cells, and their ability to reduce endogenous sfGFP::Lgr3 expression levels is assayed . Dashed white circle denotes the PIL neuron anatomical region (*pars intercerebralis*). (B) Sum of confocal z-stack slices of L3 larval brains stained with anti-GFP (green) to show sfGFP::Lgr3 expression (green) and DAPI (blue). Endogenous tdTomato fluorescence (magenta) driven by *the R29B09>* or *R25E10>* is also depicted. Both *R29B09> and R25E10>* apparently do not drive detectable expression in sfGFP::Lgr3-positive neurons. The cell bodies of the PIL neurons are highlighted with arrowheads. (A,B) Scale bars, 50 µm.

In summary, we have obtained two REs from the functional screen, R25E10 and R29B09, and two REs, R19B09.3A and R19B09.3C, from the R19B09 fragmentation experiments, all of which drive clear gene expression in PIL neurons. These four REs will constitute the PIL neuron VEnCode. A summary of our results with these four PIL neuron REs, and their localization in the genome are depicted in **Figure 4.10**.

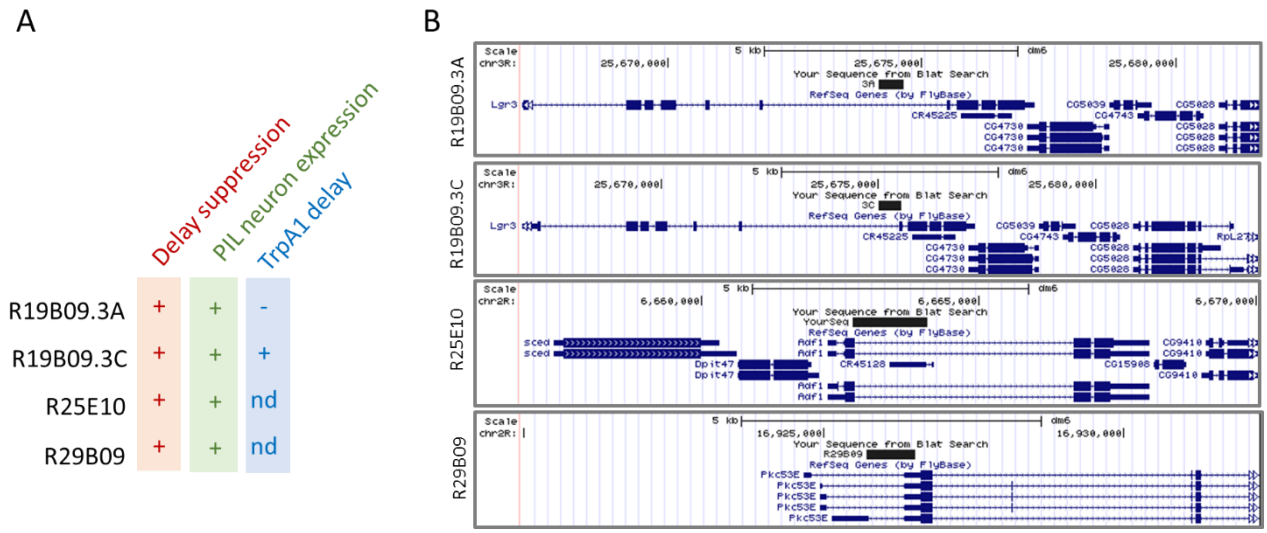

Figure 4.10. Specific REs selected to construct a VEnCode for PIL neurons. (A) Summary of the phenotypes of delay suppression, PIL neuron expression (summary of PIL neuron expression findings using both sfGFP::Lgr3, Lgr3-IR and sfGFP::Lgr3, myr::tdTomato colocalization techniques) and TrpA1 delay for each PIL neuron-specific driver. In the table "+" denotes a positive finding, "-" denotes a negative finding, and "nd" denotes 'not done'. (B) Genome localization of the four selected REs.

To construct a VEnCode-based PIL neuron-specific gene driver for fly neurogenetics, the four selected REs, R19B09.3A, R19B09.3C, R29B09 or R25E10, need to be assembled into plasmids additionally containing the DSCP, one of the 4x-split VEnC-GAL4 pieces (see Methods section), and an attB site for the specific insertion in the Drosophila genome using one of the many available attP landing sites. I have begun assembling these plasmids, as described in the Methods section, but unfortunately, we were not able to finish their assembly and generate the transgenic lines in time for the writing up of this thesis. Once the plasmids are complete, they will be injected in fly embryos carrying four different attP sites, generating four stocks of transgenic flies. After this, we will use genetic recombination to generate a fly stock carrying the four RE>-driven 4x-split VEnC-GAL4 pieces. This stock will carry the VEnCode-based PIL neuron driver. The new stock will be tested by crossing it to the line carrying the *20XUAS-IVS-mCD8::GFP* cassette and by direct observe of GFP expression exclusively in PIL neurons.

4.2.3 VEnCode for PTTH-producing neurons

A second population of neurons relevant for the developmental response to tissue damage is the PTTH-producing neurons (Halme et al. 2010). A new image-based neuroanatomy screen from the Janelia GAL4 collection was made for these neurons. From this screening, six GAL4 lines that putatively drive gene expression in the PTTH-producing neurons were identified: *R43A12>*, *R84E05>*, *R54C08>*, *R46C11>*, *R82G10>*, and *R24H12>* (data not shown). We further explored the fragments R43A12, R84E05, and R54C08 due to their smaller size (< 3 kb), which facilitates cloning. To test if these REs indeed drive gene expression in PTTH neurons, we crossed each GAL4 line with a stock carrying a UAS-GFP reporter (*10XUAS-IVS-myr::GFP)* and an HA-tagged PTTH protein reporter *(ptth-HA*) (McBrayer et al. 2007), as a marker for PTTH-producing cells **(Figure 4.11A)**. F1 Larval CNSs were dissected and stained with an anti-GFP and an anti-HA antibody. All three

drivers drove detectable GFP expression that colocalized with cells labelled with PTTH-HA. We conclude that the three drivers are suitable for generating a PTTH-expressing neuron VEnCode. To complete the VEnCode for PTTH neurons, a 0.9-kb fragment of the *ptth* promoter, which has been previously shown to drive expression in PTTH-expressing neurons was chosen (McBrayer et al. 2007).

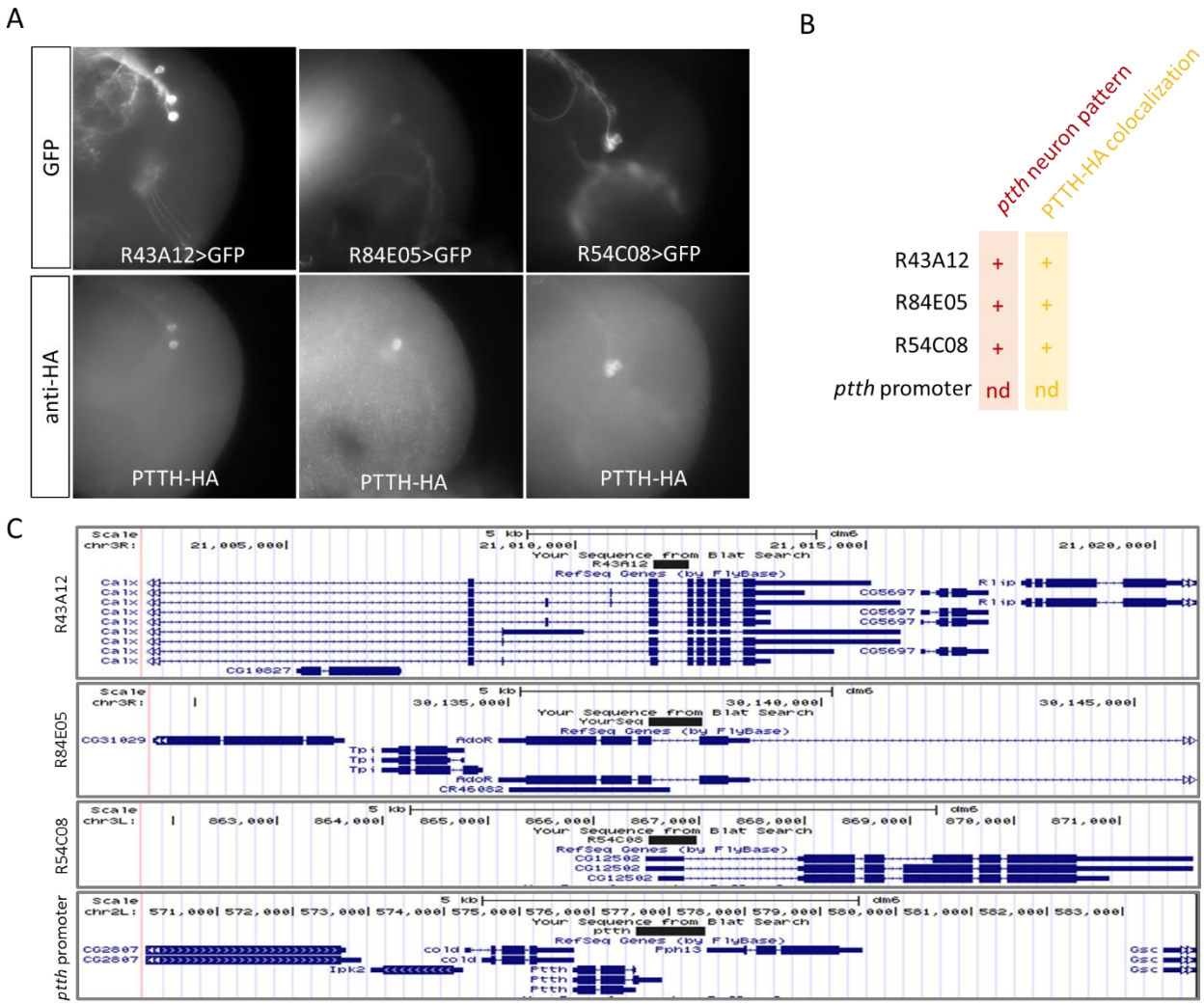

Figure 4.11. Specific REs selected to constitute a VEnCode for PTTH-producing neurons. (A) Slices stained with anti-GFP and anti-HA. *REs R43A12>, R84E05>* and *R54C08>* drive GFP and its expression colocalizes with cells expressing PTTH-HA marker (*ptth-HA* reflects sites of endogenous PTTH production. (B) Summary of the phenotypes *ptth* neurons pattern and PTTH-HA colocalization for each PTTH neuron-specific drivers. In the table "+" denotes a positive finding and "nd" denotes 'not done' (C) Genome localization of the REs chosen.

4.2.4 Quadruply-split GAL4 pieces for the VEnCode-based gene drivers

To build a gene driver based on VEnCodes, we split the GAL4 transcription factor into four pieces, generating a quadruply-split GAL4 system (4x-split VEnC-GAL4; see detailed description in Materials and Methods section). To test the hypothesis that the 4x-split VEnC-GAL4 system is able to reassemble into a functional GAL4 protein, we first placed each 4x-split VEnC-GAL4 piece under the control of the constitutive driver *tub*, generating four plasmids, each one containing one piece driven by *tub* (Tub-4x-split VEnC-GAL4 piece1-4). We then co-transfected these four plasmids together with a GFP reporter (pUAST-GFP-MS2-nl) and followed

their ability to induce GFP by staining the transfected cells with an anti-GFP antibody 48 h after co-transfection. As positive controls, we used a GAL4 driven constitutively under the control of the actin promoter (*Actin-GAL4*) and a *Tub-fused VEnC-GAL4* plasmid expressing a constitutively expressed "pre-assembled" VEnC-GAL4 version that resembles exactly what the 4x-split VEnC-GAL4 should reassemble into once expressed in the same cells. This control is important because the additional sequences inserted between the GAL4 activation and DNA-binding domains to make the 4x-split VEnC-GAL4 version could interfere with GAL4 activity (*i.e.*, the ability of GAL4 to activate UAS-driven expression). Quantification of the % of GFP-positive cells shows that the level of VEnC-GAL4-driven GFP expression (26% ± 6%, average ± standard deviation of the mean (SD)) is not statistically significantly different from the levels driven by *Act-GAL4* (22% ± 13%, average + SD), a commonly used reagent in Drosophila research ($P > 0.05$, two tailed t test with Welch's correction, after Shapiro-Wilk normality test; **Figure 4.12A and 4.12B)**. We conclude that the pre-assembled VEnC-GAL4 is a potent and functional GAL4 transcriptional factor.

Lower efficiencies and hence lower % of GFP-positive cells are expected for the co-transfection of the four 4x-split VEnC-GAL4 plasmids. This is because a cell should be transfected by five plasmids (four with one piece each plus one plasmid carrying the UAS-GFP reporter) in order to see a positive result. Furthermore, as the UAS-GFP reporter plasmid is not the optimal plasmid for this system, as we observed leakiness in transfections (*i.e.,* it can produce basal levels of GFP protein without transcriptional activation of UAS by a GAL4 molecule), it is critical to quantify the % of GFP-positive cells and to analyse the data statistically. Results show that the co-expression of the 4x-split VEnC-GAL4 pieces driven from four separate plasmids (*4x-split VEnC-GAL4>*GFP) leads to reassembly of a functional GAL4 transcription factor that can significantly activate UAS-GFP transcription over control background levels (control transfection with equimolar levels of the UAS-GFP plasmid) (4% ± 0.5% vs. 1% ± 0.2%, average ± SD relative to *fused VEnC-GAL4>GFP* control, $P = 0.0018$, two tailed t test with Welch's correction, after Shapiro-Wilk normality test; **Figure 4.12A and 4.12B**). Representative images from all conditions are depicted in **Figure 4.12A** and quantification and statistical analyses are depicted in **Figure 4.12B**.

Taken together, these results demonstrate the successful splitting of the GAL4 transcription factor into four pieces, which can reassemble, if co-expressed in the same cells, into a functional GAL4. Now, in order to generate a VEnCode-based PIL neuron or PTTH-producing neuron-specific gene expression driver that converts the activity of four different gene drivers into a single UAS-driven output, these protein-coding cDNAs will be functionally linked to the REs described above to make transgenic flies and test the system *in vivo*.

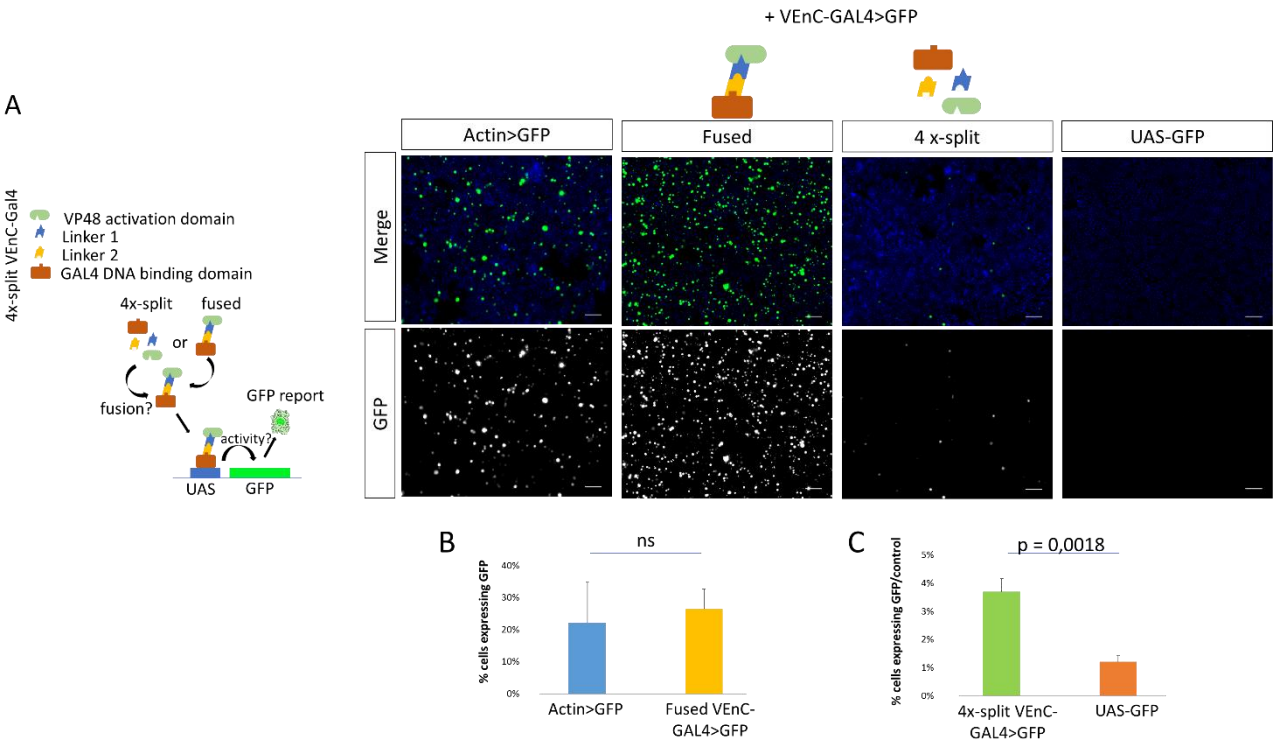

Figure 4.12. *4x-split VEnC-GAL4* activates gene transcription. (A) Representative fluorescence slices of transfected cells expressing GFP (green). A negative control was done with only the *pUAST-GFP-MS2-nl* reporter plasmid to control for the leakiness of this reporter cassette (UAS-GFP). Actin driving expression of GFP (*Actin>GFP*) was used as a positive control for GFP expression. The fused VEnC-GAL4 represents the quadruply-split GAL4 transfected already pre-fused to induce GFP expression. The quadruply-split VEnC-GAL4 system co-transfected in four separate plasmids is 4x-split VEnC-GAL4. Scale bars, 50 µm. (B) Average ± SD % of GFP-positive cells. (C) Average ± SD, in %, of GFP-positive cells relative to Fused VEnC-GAL4>GFP control. (B, C) *P = 0.3508,* and *P* = 0.0018, respectively, two tailed t test with Welch's correction, after Shapiro-Wilk normality test.

4.3 PIL NEURON ANATOMICAL CONSIDERATIONS

PIL neurons are good candidates to mediate the Dilp8-dependent developmental delay. They are a bilateral pair of neurons localized at the *pars intercerebralis* region of the Drosophila larval CNS. We sought to learn more about their anatomy and how they anatomically interact with other neurons at the same region. We used a tool that enables multicolor stochastic labelling of neurons, named MultiColor FlpOut (MCFO) (Nern et al. 2015). With MCFO we can control the expression of multiple membrane-targeted and distinct epitope-tagged proteins (HA, V5 and FLAG) by a transcriptional driver and by concomitant (and stochastic) recombinase-mediated excision of transcription-terminating cassettes, using the Flp-out system. The Flp-out technology uses the yeast site-specific recombinase, flippase (Flp), and its recognition target sequence, FRT (Golic & Lindquist 1989). The transgenes are silenced by a transcriptional stop cassette flanked by FRT sites, which can be removed by the random expression of Flp, thereby activating the gene of interest. Epitope tags are inserted in groups into a non-fluorescent sfGFP, which just serves as a protein scaffold in this system. The resultant proteins are named smGFPs (for "spaghetti monster GFP") **(Figure 4.13A)**. This approach can be used to reveal cell shapes and relative cell positions.

With a panneuronal driver *R57C10>* used to activate the expression of a flippase variant (FLPL) and the restricted RE R19B09.3D, which drives strongly expression in PIL neurons **(Figure 4.13B-E)**, we could stochastically mark single *R19B09.3D>*-expressing cells. For this, we performed immunofluorescence assays with CNSs dissected from F1 larvae from the crosses between the line *R57C10-FLPL; 10xUAS(FRT.stop)myr::smGFP-HA, 10xUAS(FRT.stop)myr::smGFP-V5, 10xUAS(FRT.stop)myr::smGFP-FLAG* and the line *R19B09.3D>*. With this technique, a better anatomical understanding of PIL neurons was achieved, because we could see the different cells labelled with different colours and differentiate the neuroanatomy of each labelled cell. While there is an apparent contralateral neuroanatomical symmetry between the pairs of PIL neurons, we find that the two PIL neurons from the same side of the brain are fundamentally different. Namely, while both PIL neurons send both ipsilateral and contralateral anterior projections (labelled with asterisks), only one PIL neuron from each side projects posteriorly to the subesophageal zone (SEZ), as can be seen in the **Figures 4.13E** (asterisk), where two PIL neurons are observed, but only one SEZ projection is detected. With this system, we could see neurons closer to PIL neurons and possible candidates that could interact with them **(Figure 4.13C, E**, arrows). One neuron was observed that sent ipsilateral projections to the same region in which the PIL neurons arborize anteriorly **(Figure 4.13C**, arrow), and a neuron with a cell body localized in the same anatomical region as the PIL neurons cell bodies, which projected to both sides and to the SEZ **(Figure 4.13E**, arrow), similarly to the PIL neurons, were observed. A model summarizing the results about each PIL neuron neuroanatomy is described in **Figure 4.13F**.

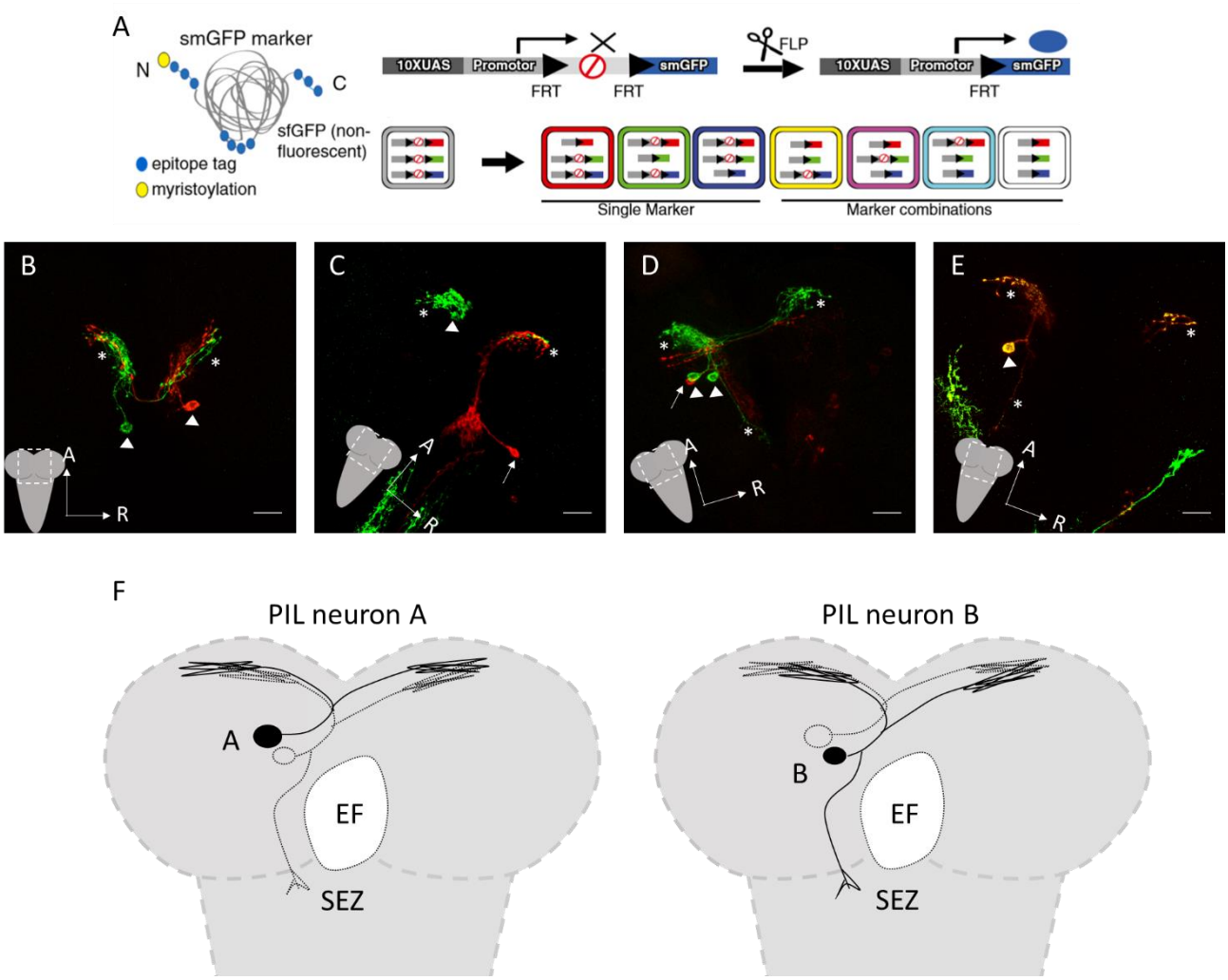

Figure 4.13. PIL neuron neuroanatomy. (A) Schematic representation of the MCFO system (image from the Rubin lab website, Janelia Research Campus). Multiple copies of a single epitope tag (HA, FLAG, MYC, V5, blue circles) are inserted in groups into a backbone of myristoylated (yellow circle) nonfluorescent sfGFP (gray). The MCFO reporter with 10XUAS and a core promoter for GAL4-activated expression, a transcriptional terminator flanked by FRT sites, and an smGFP marker. Flp-recombinase excision of the terminator permits marker expression (adapted from (Nern et al. 2015)). (B-E) Sum of confocal z-stack slices of MCFO labelling of L3 neurons with R57C10-driven expression of FLP and R19B09.3D driven expression of GFP (green) and V5 (red). Arrowheads highlight PIL neuron cell bodies. Asterisks labels PIL neurons projections. Arrows highlight PIL neuron closer cells. Scale bars, 50 µm. (F) Model describing PIL neuron neuroanatomy. Circles represent the cell body of each PIL neuron (PIL neuron A and B), sending ipsilateral and contralateral anterior projections. Only PIL neuron B sends also a posterior projection to the subesophageal zone (SEZ), localized below the esophageal foramen (EF).

Another question we asked about PIL neuron neuroanatomy is whether their neuroanatomy changes during larval development. To answer this question, we crossed *R19B09.3D>* animals with *10XUAS-IVS-mCD8::RFP* animals, dissected the CNS of the F1 larvae at different stages, and performed immunohistochemistry **(Figure 4.14)**. Our results show that, throughout larval and prepupal development, the PIL neurons appear to maintain the same neuroanatomy of ipsilateral and contralateral expression at the *pars intercerebralis* region observed in the previous immunofluorescence experiments using L3 stage CNS preparations.

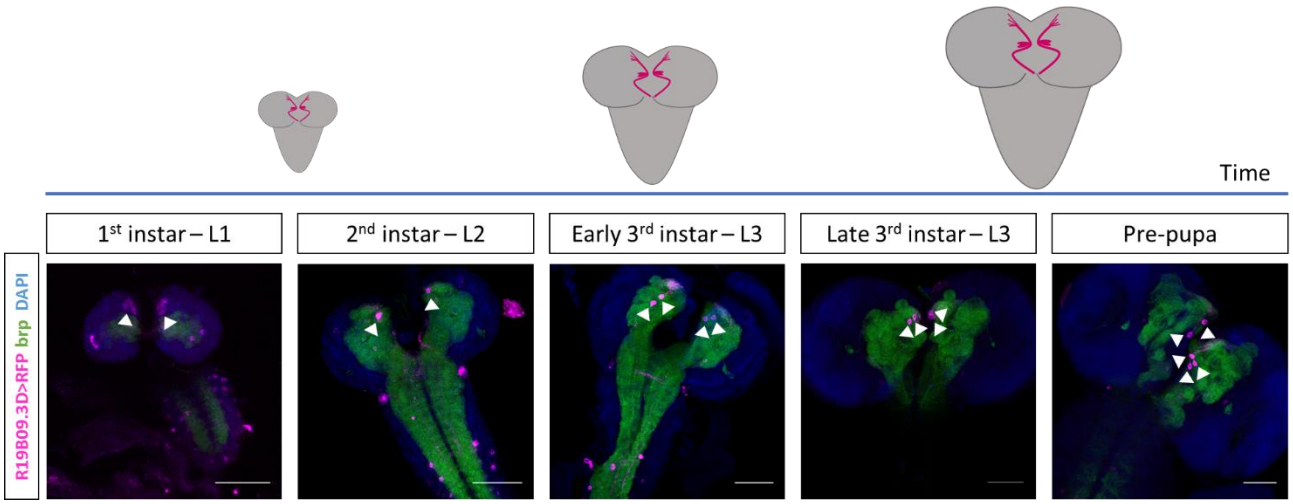

Figure 4.14. PIL neuron neuroanatomy during larval development. Sum of confocal z-stack slices of CNSs from different developmental stages, stained with nc82 (anti-brp, green) and DAPI-labelled nuclei (blue). The *Lgr3* RE *R19B09.3D>* drives RFP expression (magenta). The neuropil is labelled with nc82 antibody, which recognizes the Bruchpilot protein that localizes to synaptic active zones (Wagh et al. 2006).

4.4 BACKUP METHODOLOGIES

To achieve the main goal of this thesis, which is to find drivers capable of targeting specifically the PIL neurons, we also used other methodologies as a backup strategy to restrict the expression of GAL4 drivers to PIL neurons.

4.4.1 Recombination mediated (R19B09-MZ699) expression restriction

Garelli *et al*. showed that PIL neurons represent two neurons of a population of neurons defined by the *MZ699-GAL4* driver (*MZ699>*) (Garelli et al. 2015), called #5 neurons (Ito et al. 1997). Consistently, *MZ699>*-driven *Lgr3-IR* is able to suppress the Dilp8-dependent delay in pupariation time, just as the *R19B09>* (Garelli et al. 2015). Using an *MZ699>RFP* and a *R19B09-LexA*-driven lexAop2-GFP, Garelli *et al*. determined that both expression patterns overlap in at least 9 bilateral neurons, two of which are the PIL neurons (Garelli et al. 2015). The purpose of this next task is to functionally combine these two cell populations into a single genetic driver, so that the PIL neurons can be studied anatomically and functionally. To achieve this, we used an intersectional genetic system that combines the GAL4-UAS expression system, the LexA-LexAop expression system, and the Flp-out system (**Figure 4.15**).

First, we generated a recombinant stock carrying the transgenes *R19B09-LexA; LexAop2-FLPL, MZ699>*. To test if the system FLPL-dependent recombination system was working to restrict the expression pattern to the intersection between these drivers, schematic representation in **Figure 4.15A**, we crossed the *R19B09-LexA; LexAop2-FLPL, MZ699>* stock to the stock of the genotype *brp(FRT.Stop)GFP, UAS(FRT.stop)tdTomato.Myr*, dissected F1 larvae in the third larval stage, and stained them with antibody against GFP **(Figure 4.15B)**. With this strategy, *myr::tdTomato* expression is only produced in cells in which

both *R19B09>* and *MZ699>* drivers co-express (hereafter, named as R19B09 ∩ MZ699 cells). The *R19B09>*-expressing neurons that are synaptically active (expressing brp) are labelled with brp-GFP. Our results show that both drivers co-express in the PIL neurons and sometimes, in a few more cells (present only at the left image), as previously described (Garelli et al. 2015). One limitation of this technique is that the *myr::tdTomato* expression in R19B09 ∩ MZ699 cells is variable, not always reflecting the full intersection, because it depends on the Flp-out recombination, which is an inherently random process. Besides that, the results suggest that in some brains not all PIL neurons express detectable levels of brp-GFP, as can be seen in **Figure 4.15B** (right panel). This result was very surprising, but it can mean that PIL neurons are not always ready to signal using brp-positive active zones in response to certain types of stimuli during development, as we had thought. This hypothesis needs to be confirmed, with a similar experiment done in different stages of the larval development, to check the regulation of putative synaptic activity of PIL neurons.

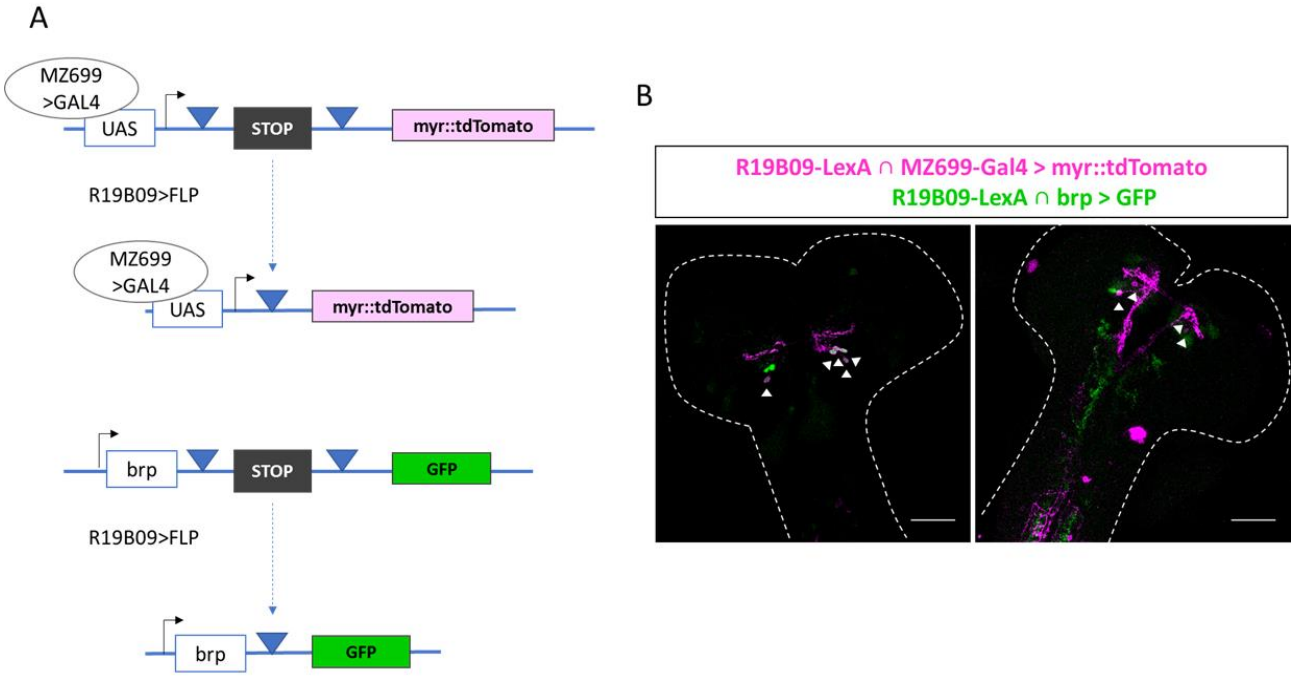

Figure 4.15. R19B09 ∩ MZ699> drives gene expression in PIL neurons. (A) Schematic representation of experiments done in (B). A spacer with a transcriptional stop is flanked by FRT sites, preventing the expression of myr::tdTomato, upon MZ699-GAL4-UAS binding. In R19B09 cells, FLP is expressed and recombines the FRT sites, removing the stop sequence and allowing *MZ699>*-dependent myr::tdTomato expression. In parallel, but in other construct, forward to brp gene, there is a transcriptional stop flanked by FRT sites, preventing the expression of GFP. In R19B09 cells, FLP is expressed and recombines the FRT sites, removing the stop sequence and allowing GFP expression. (B) Sum of confocal z-stack slices of L3 brains stained with anti-GFP (green). *R19B09 ∩ MZ699>* drives expression of myr::tdTomato (magenta) and R19B09 drives GFP (green) in brp-positive cells. PIL neurons are highlighted with arrowheads.

To test whether PIL neuron activation is sufficient to induce a delay in the onset of metamorphosis, we thermogenetically activated R19B09 ∩ MZ699 cells by expressing TrpA1 using two different strategies **(Figures 4.16)**. In the first method **(Figure 4.16B)**, we crossed *GMR19B09-LexA; LexAop2-FLPL, MZ699-GAL4* animals with *UAS-TRPA1; Tub84B(FRT.GAL80)* animals, and scored the developmental time of F1 larvae. As explained in **Figure 4.16A**, in the *Tub84B(FRT.GAL80)* cassette, GAL80, a potent inhibitor of the GAL4-UAS system, is constitutively expressed under the control of the *Tubulin* promoter, thereby constitutively

inhibiting GAL4-UAS activation. Upon FLP expression, in this case provided by the *R19B09-LexA>lexAop2-FLPL* system, the FRT sites flanking the GAL80 mediate its excision from the *Tubulin* promoter region, relieving the *MZ699-GAL4>UAS-TRPA1* system from repression, leading to cell activation. In contrast to our initial hypothesis, our results show that thermogenetic activation of R19B09 ∩ MZ699 cells by TrpA1 is not sufficient to delay the onset of metamorphosis, suggesting that PIL neuron activation is not sufficient to delay the onset of metamorphosis **(Figure 4.16B)**.

To confirm that the *Tub84B(FRT.GAL80)* system was working as expected, we crossed the *R19B09-LexA; LexAop2-FLPL, MZ699-GAL4* stock with a stock carrying the *10XUAS-IVS-myr::GFP; Tub84B(FRT.GAL80)* cassettes to express GFP rather than TrpA1 in R19B09 ∩ MZ699 cells **(Figure 4.16C)**. Results show PIL neurons plus two cells at the CNS and a few more cells at the VNC, confirming that the system is working properly and that both REs express in the PIL neurons, as expected. These findings strengthen the conclusion that TrpA1 activation of R19B09 ∩ MZ699 cells is not sufficient to delay the onset of metamorphosis.

The second method used to express TrpA1 in R19B09 ∩ MZ699 cells upon recombination is described in **Figure 4.16D**. In this method, an FRT-site-flanked spacer with a transcriptional stop is placed between UAS and the TrpA1 sequences, preventing GAL4-dependent UAS-driven TrpA1 expression. Upon *R19B09-LexA>lexAop2-FLPL* expression, the FRT-flanked STOP cassette is excised, allowing UAS-TrpA1 expression in MZ699>-expressing cells. We thus crossed *R19B09-LexA; LexAop2-FLPL, MZ699-GAL4* animals to a stock carrying the *UAS(FRT.stop)TrpA1* cassette, and concordant with the previous result, the activation of R19B09 ∩ MZ699 cells by TrpA1 does not delay the onset of the metamorphosis. On the contrary, there is a statistically significant precocious pupariation when R19B09 ∩ MZ699 cells are thermogenetically activated with TrpA1 (**Figure 4.16E**, $P < 0.0001$, Dunn's *post hoc* test, respectively). To put these results into context, it is important to recall that a significant delay is obtained when either *R19B09>* or *MZ699>* alone drives TrpA1 (**Figure 4.5A, and Figure 4.16E**, $P < 0.0001$, Dunn's *post hoc* test, respectively). These results suggest that other non-redundant cells may be involved in producing the TrpA1-dependent delay, and that the activation of PIL neurons *per se*, is not sufficient to induce the delay, and, if anything, causes a slightly precocious pupariation timing. It would be important to carry out an experiment removing Lgr3 from R19B09 ∩ MZ699 cells using *Lgr3-IR* in the context of constitutive expression of Tub-dilp8 to provide a more restricted test if *Lgr3* is indeed required in the PIL neurons to mediate the Dilp8 peripheral stress signal induced delay. Unfortunately, the construction of this stock was not finished in time for this thesis.

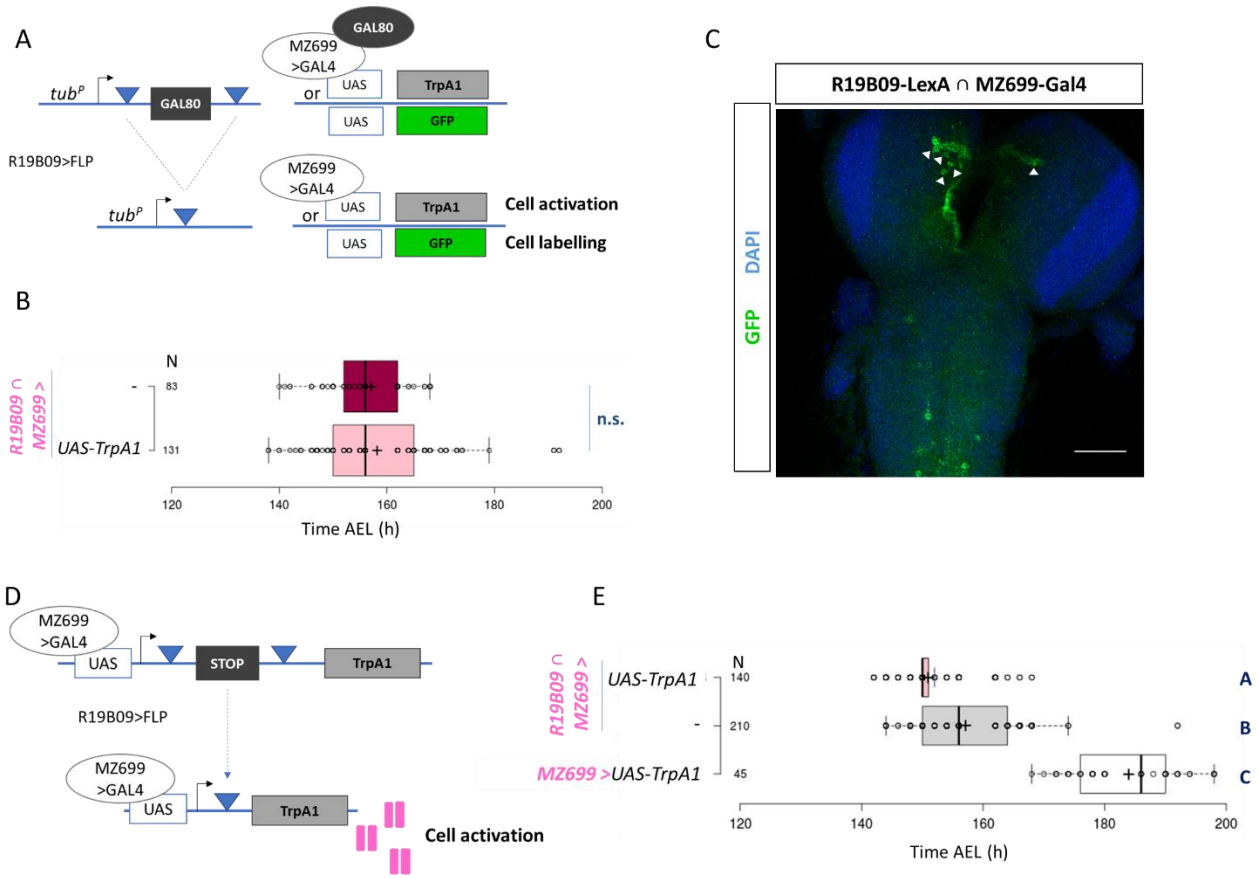

Figure 4.16. R19B09 ∩ MZ699 cells are not sufficient to induce a delay upon TrpA1 thermogenetic activation. (A) Schematic representation of the experiments done in (B,C). *Tubulin* promoter is constitutively expressing GAL80 flanked by FRT. GAL80 binds to GAL4, inhibiting the expression of TrpA1 (B) or GFP (C) in MZ699-expressing cells. R19B09 drives FLP that recombines the FRT sites, removing the GAL80 sequence. Then R19B09∩MZ699-cells are able to express TrpA1 or GFP, leading to cell activation or cell labelling, respectively. (B) Box plot showing pupariation time of (N) larvae expressing TrpA1 under the control of R19B09 ∩ MZ699 drivers. As a negative control, *GMR19B09-LexA; LexAop2-FLPL, MZ699-GAL4 (R19B09 ∩ MZ699>*) was crossed with *w[1118].* (C) Sum of confocal z-stack slices of L3 brains stained with anti-GFP (green) and DAPI (blue). *R19B09 ∩ MZ699* cells express GFP. Scale bars, 50 µm. (D) Schematic representation of the experiments done in (E). A spacer with a transcriptional stop is flanked by FRT sites, preventing the expression of TrpA1, upon MZ699-GAL4-UAS binding. In R19B09 cells, FLP is expressed and recombines the FRT sites, removing the stop sequence and allowing *MZ699>*-dependent TrpA1 expression, leading to cell activation. (E) Box plot showing pupariation time of (N) larvae expressing TrpA1 under the control of R19B09 ∩ MZ699> drivers. As a negative control, *GMR19B09-LexA; LexAop2-FLPL, MZ699-GAL4 (R19B09 ∩ MZ699>*) was crossed with *w[1118]*. As a positive control for the delay, the *MZ699>* driver was crossed with *UAS-TrpA1*. (B,E) Whiskers extend to data points that are less than 1.5 x IQR away from 1st/3rd quartile, dots represents all data, the black vertical bars represent the median and the plus sign represents the mean. (C) $P = 0.4646$, Mann-Whitney test. (F) $P < 0.0001$, Kruskal–Wallis one-way ANOVA test. Genotypes sharing the same letter (blue) are not statistically different at $\alpha = 0.01$, Dunn *post hoc* test.

The results above indicate that R19B09 ∩ MZ699> cells do not induce a delay upon TrpA1 thermogenetic activation. Instead there might even be a slightly precocious pupariation. We then wondered if silencing the R19B09 ∩ MZ699> neurons could be sufficient to rescue the Dilp8-dependent delay. To answer this question, we scored the pupariation time of non-Tb F1 larvae from the cross between *R19B09-LexA; LexAop2-FLPL, MZ699-GAL4* animals and *UAS(FRT.stop)Kir2.1;+; Tub-dilp8/TM6B* animals. Kir2.1 is an inward rectifying K^+ channel used to silence neurons via hyperpolarization (Wischmeyer et al. 1998). In the *UAS(FRT.stop)Kir2.1* construct, the expression of the Kir2.1 transgene is blocked by a spacer containing strong transcriptional stop sites, flanked by FRT sites **(Figure 4.17A)**. Upon *R19B09-LexA>lexAop2-FLPL* expression, the FRT-flanked STOP cassette is excised, allowing UAS-Kir2.1 expression in *MZ699>*-expressing cells. As a positive control for the Dilp8-dependent delay, we crossed *R19B09-LexA; LexAop2-FLPL, MZ699-GAL4* animals with *Tub-dilp8/TM3*

animals and scored pupariation time of all F1 larvae, but computed only non-Sb animals of the genotype *R19B09-LexA; LexAop2-FLPL, MZ699-GAL4/Tub-dilp8* (certified after eclosion) **(Figure 4.17B)**. The results show that the silencing of the overlapping neurons does not rescue the delay induced by the constitutive expression of Dilp8. Rather, silencing R19B09 ∩ MZ699> neurons led to a statistically significant 21-h increase in the 23-h developmental delay caused by *Tub-dilp8* ($P < 0.0001$, Dunn's post hoc test). This is a very surprising result, once it suggests that, if anything, it is the silencing, rather than the activation of R19B09 ∩ MZ699> neurons, which include the PIL neurons, that delays the onset of metamorphosis. These results are in contrast with previous findings showing that *R19B09>Kir2.1* can partially suppress the delay caused by EMS-induced tissue damage (Garelli *et al*., 2015). These results show the importance of having drivers with restricted expression patterns to test hypotheses regarding neuronal function in vivo. These results also highlight the need for *de facto* PIL neuron-specific drivers, as even though the *R19B09 ∩ MZ699>* intersection provides 1-2 orders of magnitude more restricted expression pattern, it is still driving expression in a dozen of cells other than the PIL neurons (see **Figure 4.15B and 4.16C**). In this sense, the work presented herein defining REs for the generation of a VEnCode-based PIL neuron driver is likely to significantly improve the resolution, and hence bring more definitive answers to these questions.

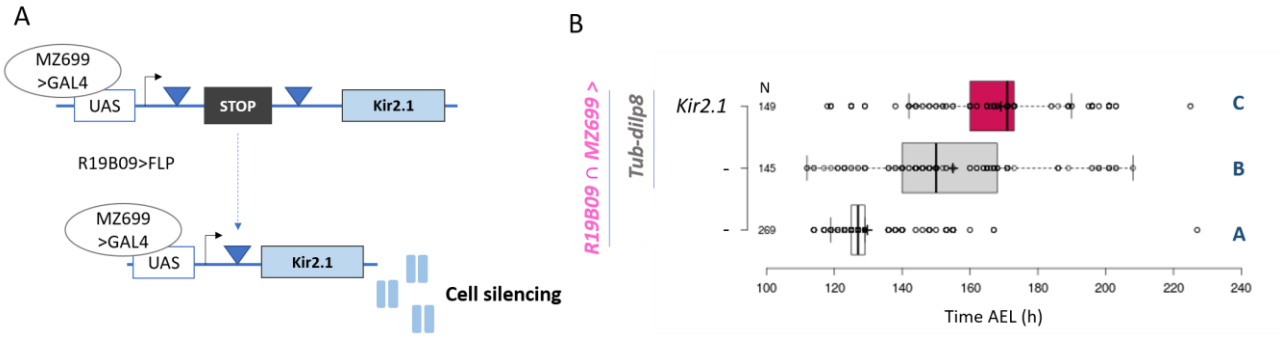

Figure 4.17. Kir2.1 silencing of R19B09 ∩ MZ699 cells does not rescue the Dilp8-dependent delay. (A) Schematic representation of the experiments done in (B). A spacer with a transcriptional stop is flanked by FRT sites, preventing the expression of Kir2.1, upon MZ699-GAL4-UAS binding. In R19B09>-expressing cells, FLP is expressed and recombines the FRT sites, removing the stop sequence and allowing *MZ699*>-dependent Kir2.1 expression, leading to neuronal silencing via hyperpolarization. (B) Box plot showing pupariation time of (N) larvae expressing Kir2.1 under the control of R19B09 ∩ MZ699 drivers, and Dilp8 under the control of *Tubulin* promoter (*Tub-Dilp8*). As a negative control, *R19B09-LexA; LexAop2-FLPL, MZ699-GAL4 (R19B09 ∩ MZ699*>) animals were crossed with *w[1118]* animals. As a positive control for the Dilp8-dependent delay, *R19B09-LexA; LexAop2-FLPL, MZ699-GAL4 (R19B09 ∩ MZ699*>) animals were crossed with *Tub-dilp8* animals. Whiskers extend to data points that are less than 1.5 x IQR away from 1st/3rd quartile, dots represent all data, the black vertical bars represent the median and the plus sign represents the mean. $P < 0.0001$, Kruskal–Wallis one-way ANOVA test. Genotypes sharing the same letter (blue) are not statistically different at $\alpha = 0.01$, Dunn *post hoc* test.

4.4.2 Split GAL4

One of the available techniques to restrict reporter expression is the usage of the ternary system Split GAL4 (Luan *et al*. 2006). In this system, two critical functional domains (DNA binding domain and activating domain) of the GAL4 protein are separated into distinct polypeptides (Brent & Ptashne 1985), restoring its activity only with protein-protein interactions between the two pieces. This method allows the expression of the GAL4 DNA binding domain and the GAL4 activation domain separately, each one under the control of

different REs. An active GAL4 protein is only reconstituted in the cells where both REs are active. Pfeiffer *et al*. improved the efficacy of this method by replacing the activation domain for p65 activation domain, creating two new Split GAL4 vectors, pBPZpGAL4DBDUw and pBPp65ADZpUw (Barret D. Pfeiffer et al. 2010a). Using three of the four REs found for PIL neurons (section 4.2.2): R19B09.3A, R19B09.3C and R29B09, we developed the following plasmids:

1) pBPZ_R19B09.3A_pGAL4DBDUw;
2) pBPZ_R29B09_pGAL4DBDUw;
3) pBP_R19B09.3C_p65ADZpUw;
4) pBP_R19B09.3A_p65ADZpUw.

These plasmids were injected into flies to generate transgenic flies carrying a Split-GAL4 specific for PIL neurons. These flies are still being developed, but the main goal is to use different combinations and test the specificity of the Split GAL4 system towards PIL neurons. To confirm that the system is working we will do imaging assays with R19B09.3A>GAL4DBD ∩ R19B09.3C>p65AD, R29B09>GAL4DBD ∩ R19B09.3C>p65AD, and R29B09>GAL4DBD ∩ R19B09.3A>p65AD, selectively driving the reporter gene UAS-GFP in overlapping cells. The expected result is that the overlapping neurons will compromise the PIL neurons and only a few or no other neurons in the CNS. This tool could help the study of the function of these Lgr3-positive neurons in the Dilp8-Lgr3 pathway.

4.5 New elements of the Dilp8-dependent delay

As described in the section 1.2.2, we found evidence for new (non-PIL neuron) cells capable of delaying the onset of metamorphosis when thermogenetically-activated with TrpA1. Namely, we found that *R48H10>* or *R69F02>-expressing cells*, when stimulated with calcium, induce a strong delay in pupariation time **(Figure 4.8C)**. We used sensitive functional and anatomical assays to show that neither *R48H10>* or *R69F02>* drives detectable expression in the PIL neurons **(Figure 4.8A)**. These findings raise a series of questions that we try to address in this chapter. First, is Lgr3 required in these cells for them to induce a delay? Second, is the delay produced due to the activation of Dilp8-Lgr3 pathway? Third, are these two REs active in distinct cell populations? Fourth, are these new TrpA1-sensitive cells, neurons?

To answer the first question, whether Lgr3 is required in these cells or not for the delay observed, we crossed the *R48H10>* and *R69F02>* lines with a stock of the genotype *UAS-TRPA1; UAS-Lgr3-IR-V22*, and scored the timing of pupariation of F1 larvae **(Figure 4.18A)**. *R19B09>* was used as a positive control, because it induces a delay when thermogenetically activated with TrpA1. Consistent with the results show above **(Figure 4.8C)**, both *R48H10>* and *R69F02>* induced a 16-h and 15-h delay in pupariation timing, respectively, when driving TrpA1, even though the *R69F02>*-induced delay did not reach statistical significance in this large experiment ($P < 0.0001$ and $P > 0.01$. (n.s.), respectively, Dunn *post hoc* test, **Figure 4.18A**). Each GAL4 line crossed with

UAS-Lgr3-IR-V22 was used as negative control. Our results show that *R48H10>TrpA1, Lgr3-IR* is lethal, because all larvae die upon TrpA1 system activation (when the temperature increases from 18°C to 29°C). This interesting result reveals that Lgr3 becomes essential in *R48H10>*-expressing cells upon their thermogenetic activation, suggesting that Lgr3 can have different roles besides its role in developmental stability. As regards the *R69F02>* line, we found evidence for an intrinsic delay in this line, which increases when the cells are thermogenetically activated (*R69F02>TrpA1*), and when *Lgr3-IR* is co-expressed with TrpA1 (*R60F02>TrpA1; Lgr3-IR*) ($P < 0.01$, Dunn *post hoc* test). With these preliminary results, we can hypothesise that Lgr3 is not required for the delay induced by the thermogenetic activation of *R69F02>*-expressing cells. o Similar results were obtained by thermogenetically activating *R48H10>* and *R69F02>*-expressing cells with TrpA1 in animals completely lacking *Lgr3 (Lgr3(-/-) = Lgr3[ag1]*, a null *Lgr3* allele generated by Garelli *et al*., (Garelli et al. 2015) and comparing them to the control background for *Lgr3 (Lgr3(+/-) = Lgr3[ag2/ag1])* **(Figure 4.18B)**. Interestingly, as observed in the experiment above with *Lgr3* RNAi, *R48H10>TrpA1* activation in animals lacking Lgr3 (*Lgr3[ag1]*) is also lethal. When only half of Lgr3 is dysfunctional (*R48H10>Trpa1, Lgr3[ag2/ag1]*), a small delay can be induced but it remains strongly lethal, suggesting that the *R48H10>TrpA1* condition makes *R48H10>*-expressing cells exquisitely sensitive to *Lgr3* levels. We conclude that the delay observed upon TrpA1 activation of *R69F02>*-expressing cells is Lgr3-independent. We also conclude that *R48H10>*-expressing cells become highly sensitive to *Lgr3* levels upon their TrpA1 thermogenetic activation, leading to larval lethality. However, this interesting property does not seem to be related to the Dilp8-Lgr3-developmental stability pathway.

A

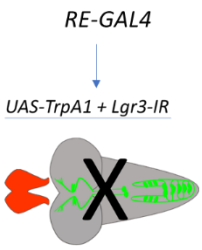
RE-GAL4
UAS-TrpA1 + Lgr3-IR

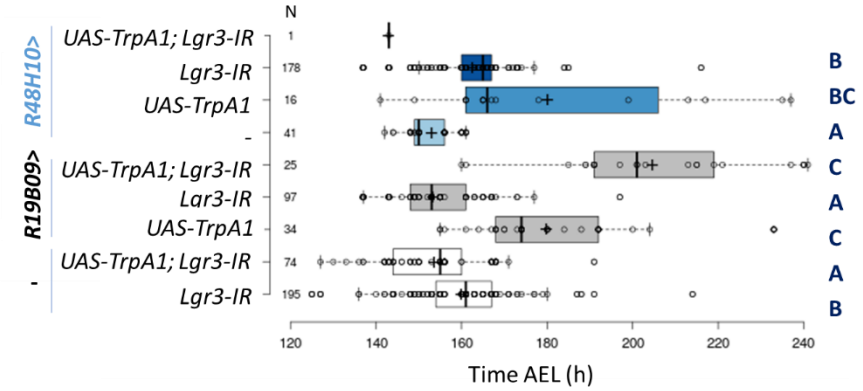
N
R48H10>
UAS-TrpA1; Lgr3-IR
Lgr3-IR
UAS-TrpA1
-
R19B09>
UAS-TrpA1; Lgr3-IR
Lar3-IR
UAS-TrpA1
-
UAS-TrpA1; Lgr3-IR
Lgr3-IR
1
178
16
41
25
97
34
74
195
B
BC
A
C
A
C
A
B
120
140
160
180
200
220
240
Time AEL (h)

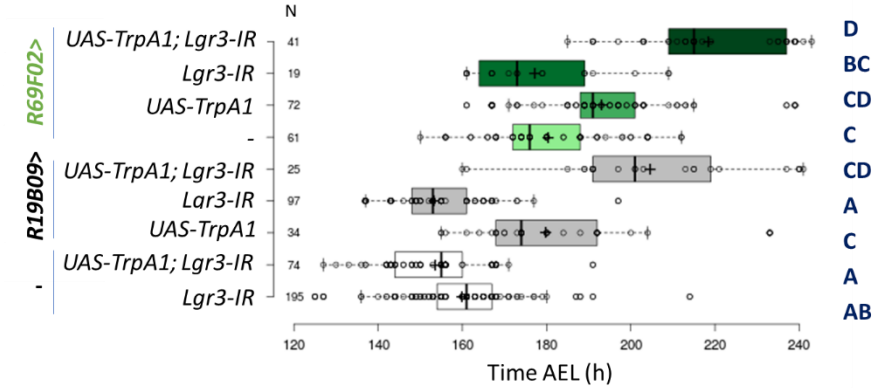
N
R69F02>
UAS-TrpA1; Lgr3-IR
Lgr3-IR
UAS-TrpA1
-
R19B09>
UAS-TrpA1; Lgr3-IR
Lar3-IR
UAS-TrpA1
-
UAS-TrpA1; Lgr3-IR
Lgr3-IR
41
19
72
61
25
97
34
74
195
D
BC
CD
C
CD
A
C
A
AB
120
140
160
180
200
220
240
Time AEL (h)

B

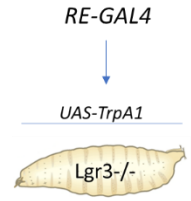
RE-GAL4
UAS-TrpA1
Lgr3-/-

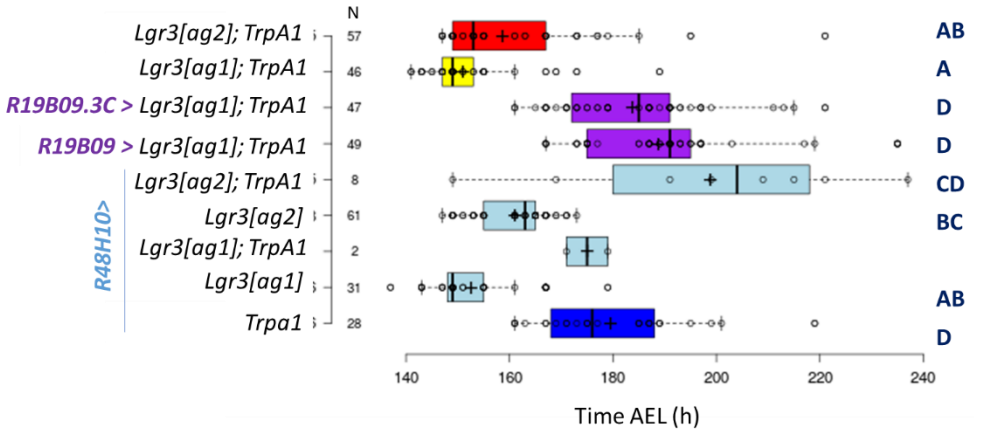
N
Lgr3[ag2]; TrpA1
Lgr3[ag1]; TrpA1
R19B09.3C > Lgr3[ag1]; TrpA1
R19B09 > Lgr3[ag1]; TrpA1
R48H10>
Lgr3[ag2]; TrpA1
Lgr3[ag2]
Lgr3[ag1]; TrpA1
Lgr3[ag1]
Trpa1
57
46
47
49
8
61
2
31
28
AB
A
D
D
CD
BC
AB
D
140
160
180
200
220
240
Time AEL (h)

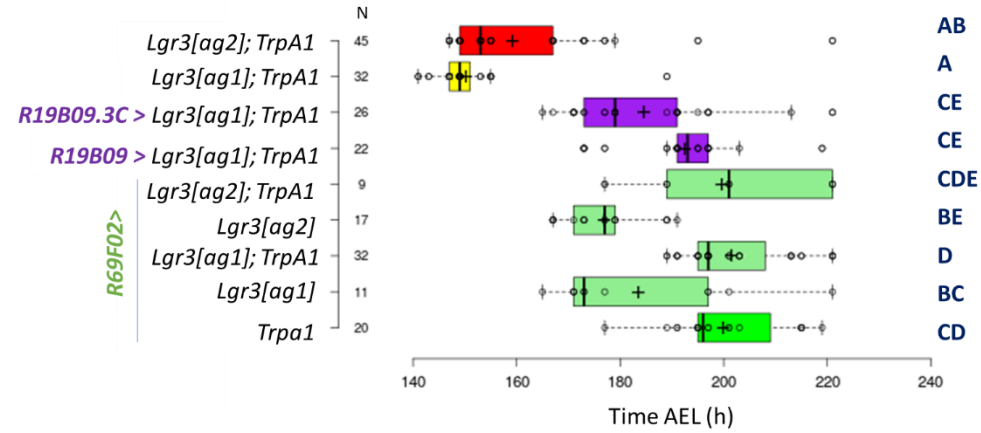
N
Lgr3[ag2]; TrpA1
Lgr3[ag1]; TrpA1
R19B09.3C > Lgr3[ag1]; TrpA1
R19B09 > Lgr3[ag1]; TrpA1
R69F02>
Lgr3[ag2]; TrpA1
Lgr3[ag2]
Lgr3[ag1]; TrpA1
Lgr3[ag1]
Trpa1
45
32
26
22
9
17
32
11
20
AB
A
CE
CE
CDE
BE
D
BC
CD
140
160
180
200
220
240
Time AEL (h)

Figure 4.18. Discovery of new cell populations able to induce an Lgr3-independent delay in developmental timing. (A) Box plot showing pupariation time of (N) larvae expressing TRPA1 and *Lgr3-IR* driven by the REs *R19B09>*, *R48H10>*, and *R69F02>*. As a negative control, a stock carrying the *UAS-TrpA1* transgene was crossed to *w[1118]* animals. *R19B09>* was used as a positive control. For the sake of presentation, I separated the data obtained with the *R48H10>* and *R69F02>* drivers into two separate graphs, but it is important to keep in mind that the experiments were done in parallel so that the positive and negative controls denoted in both graphs are the same. (B) Box plot showing pupariation time of (N) larvae expressing TRPA1 driven by the REs *R19B09>*, *R48H10>*, and *R69F02>* in a control background for Lgr3 (*Lgr3(+/-)* = *Lgr3[ag2/ag1]*) or mutant for *Lgr3 (Lgr3(-/-)* = *Lgr3[ag1]*). *R19B09>* and *R19B09.3C>* were used as positive controls for the delay. TrpA1 lines (*Lgr3[ag2]; UAS-TrpA1 and Lgr3[ag1]; UAS-TrpA*1) without drivers were used as negative controls for TrpA1 activation. (A,B) Whiskers extend to data points that are less than 1.5 x IQR away from 1st/3rd quartile, dots represents all data, the black vertical bars represent the median and the plus sign represents the mean. $P < 0.0001$, Kruskal–Wallis one-way ANOVA test. Genotypes sharing the same letter (blue) are not statistically different at $\alpha = 0.01$, Dunn *post hoc* test.

To confirm that Lgr3 is not required in the *R48H10>* and *R69F02>*-expressing cells to mediate the Dilp8-dependent delay in pupariation time, we removed *Lgr3* in *R48H10>* and *R69F02>*-expressing cells using RNAi (*Lgr-IR*) in a *Tub-dilp8* background **(Figure 4.19)**. Larvae of the *R19B09>Lgr3-IR, Tub-dilp8* genotype served as controls for suppression. Our preliminary results show that both lines expressing *Lgr3-IR* did not suppress the Dilp8-dependent delay. This result still needs to be repeated to increase the number of pupae scored (N). However, taking into consideration the previous anatomical results, it seems very unlikely that these cells in which these REs are expressed required *Lgr3* to mediate the Dilp8-dependent delay. Moreover, it also seems safe to conclude that R*48H10>* and *R69F02>*-expressing cells represent new populations of cells that can delay the onset of pupariation in an Lgr3-independent manner.

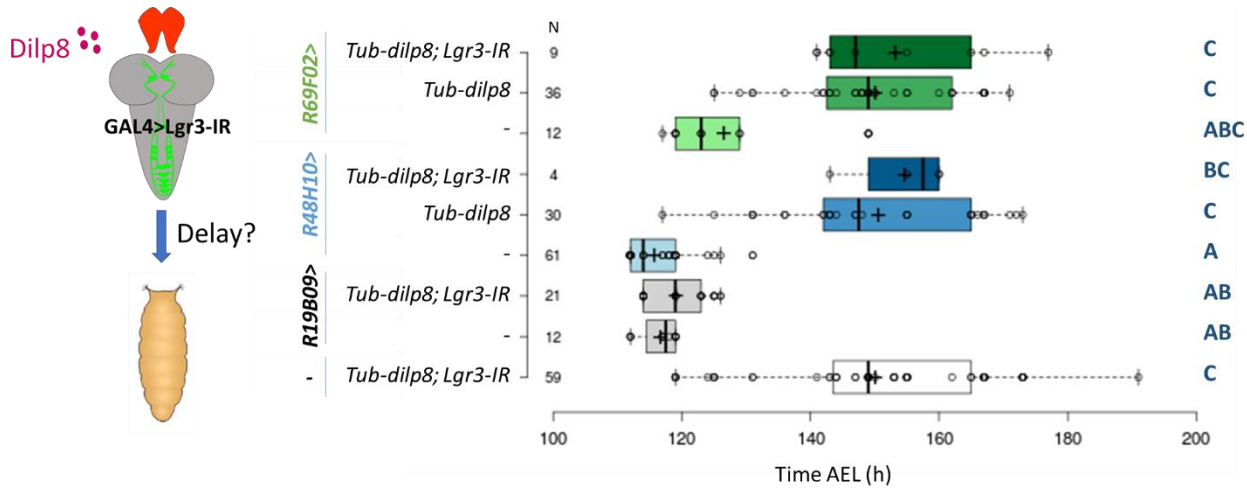

Figure 4.19. Lgr3 is not required in *R48H10>*- or *R69F02>*-expressing cells to delay development in response to Dilp8 activity. (A) Box plot showing pupariation time of (N) larvae expressing *Lgr3-IR* driven by the REs *R19B09>*, *R48H10>*, and *R69F02>* in a *Tub-dilp8* background. As negative and positive controls for the delay, we crossed each GAL4 line with *w[1118]* and with *Tub-dilp8*, respectively. Whiskers extend to data points that are less than 1.5 x IQR away from 1st/3rd quartile, dots represent all data, the black vertical bars represent the median and the plus sign represents the mean. $P < 0.0001$, Kruskal–Wallis one-way ANOVA test. Genotypes sharing the same letter (blue) are not statistically different at $\alpha = 0.01$, Dunn *post hoc* test.

Another relevant question about the *R48H10>*- and *R69F09>*-expressing cells that mediate a delay is whether these cells are neurons or other type of cells. We used GAL80, under the control of the panneuronal promoter *elav* (*elav-GAL80*), to inhibit the GAL4 activity in *R48H10>*- and *R69F09>*-expressing neurons. *R19B09>*-expressing neurons were used as a control. First, we did immunohistochemistry of 3rd instar larvae CNSs

from the F1 obtained by crossing a stock of the genotype *elav-GAL80; R19B09>* with *elav-GAL80; UAS-mCherry* animals, and compared the mCherry-labeled cells to the ones obtained by crossing *R19B09>* with *UAS-mCherry* **(Figure 4.20A)**. Curiously, despite efficiently blocking most of the R19B09>-driven mCherry expression, high amounts of mCherry are still detectable in the PIL neurons (and some other brain cells) despite the presence of 2x-elav-GAL80. As PIL neurons are definitively neurons, we conclude that the competence and/or efficiency of elav-GAL80 to inhibit GAL4 activity varies between neurons. In other words, some neurons might be elav-GAL80-"resistant". One way this can be achieved is if we consider R19B09 regulatory activity in PIL neurons to be strong enough to bypass the GAL80 expression levels produced by two *elav-Gal80* transgenes. Another alternative is that *elav* expression is temporally modulated in PIL neurons during larval development, but we have no evidence for this.

We also performed immunohistochemistry of larvae obtained from the crosses between *elav-GAL80; R48H10>* or *elav-GAL80; R69F02>* and *20XUAS-IVS-mCD8::GFP* to compare the cell patterns with F1 larvae from the crosses between *R48H10>* or *R69F02>* and *20XUAS-IVS-mCD8::GFP,* respectively **(Figure 4.20B)**. We observed that elav-GAL80 effectively blocks GFP expression of all *R48H10>*-expressing cells in the brain. This result suggests that *R48H10>* drives expression mostly, or exclusively, in neurons in the CNS. Contrary to *R48H10>*, *R69F02>* seems to drive expression in two elav-GAL80-resistant cells **(Figure 4.20B)**. In parallel, we assessed if only the elav-GAL80-resistant cells in which each RE drives expression could induce the TrpA1-dependent delay **(Figure 4.20C)**. For this, we crossed *elav-GAL80; R19B09>, elav-GAL80; R48H10>*, and *elav-GAL80; R69F02>* stocks with stocks of the genotype *elav-GAL80, UAS-TrpA1*, and scored the pupariation time of resulting F1 larvae. Surprisingly, and contrary to our initial expectations, the results show that two copies of *elav-GAL80* do not inhibit the *R19B09>TrpA1* delay in pupariation (10-h vs 24-h delay relative to controls for *R19B09>TrpA1* and *2x-elav-GAL80*; *R19B09>TrpA1*, respectively, $P > 0.01$ (n.s.), Dunn's *post hoc* test). As *2x-elav-GAL80* blocks *R19B09>mCherry* expression in most but a few neurons in the CNS **(Figure 4.20A)**, it is likely that one of these neurons is responsible for the TrpA1 delay. As we have mostly ruled out the possibility that PIL neuron thermogenetic activation leads to a delay, this leaves the other elav-GAL80-resistant cells as good candidate cells to produce the TrpA1-dependent delay in pupariation. Another possibility is that the TrpA1-sensitive cells causing the delay are indeed not neurons and are not even located in the CNS. Similarly to *R19B09>, 2x-elav-GAL80* did not affect the thermogenetically-induced delay caused by *R69F02>TrpA1* expression, as this genotype caused an increase in pupariation time relative to *2x-elav-GAL80, R69F02>* controls ($P < 0.01$, Dunn's *post hoc* test). Again, notwithstanding, an important control, *R69F02>TrpA1* was missing, and is required to confirm this result. If confirmed, this delay can be caused by the 2x-elav-GAL80-resistant cells observed in the **Figure 4.20B**. These cells can act in an independent pathway to regulate developmental timing of the developmental stability in *Drosophila* larvae.

In contrast to *R19B09> and R69F02>*, *2x-elav-GAL80* significantly abrogated the ability of *R48H10>TrpA1* to induce a statistically significant delay in the onset of pupariation ($P > 0.01$, Dunn's *post hoc* test*)*. However,

important controls were lacking in these preliminary experiments, such as the *R48H10>TrpA1* positive control, to evaluate if there is indeed a suppression of the delay upon *2x-elav-GAL80* expression.

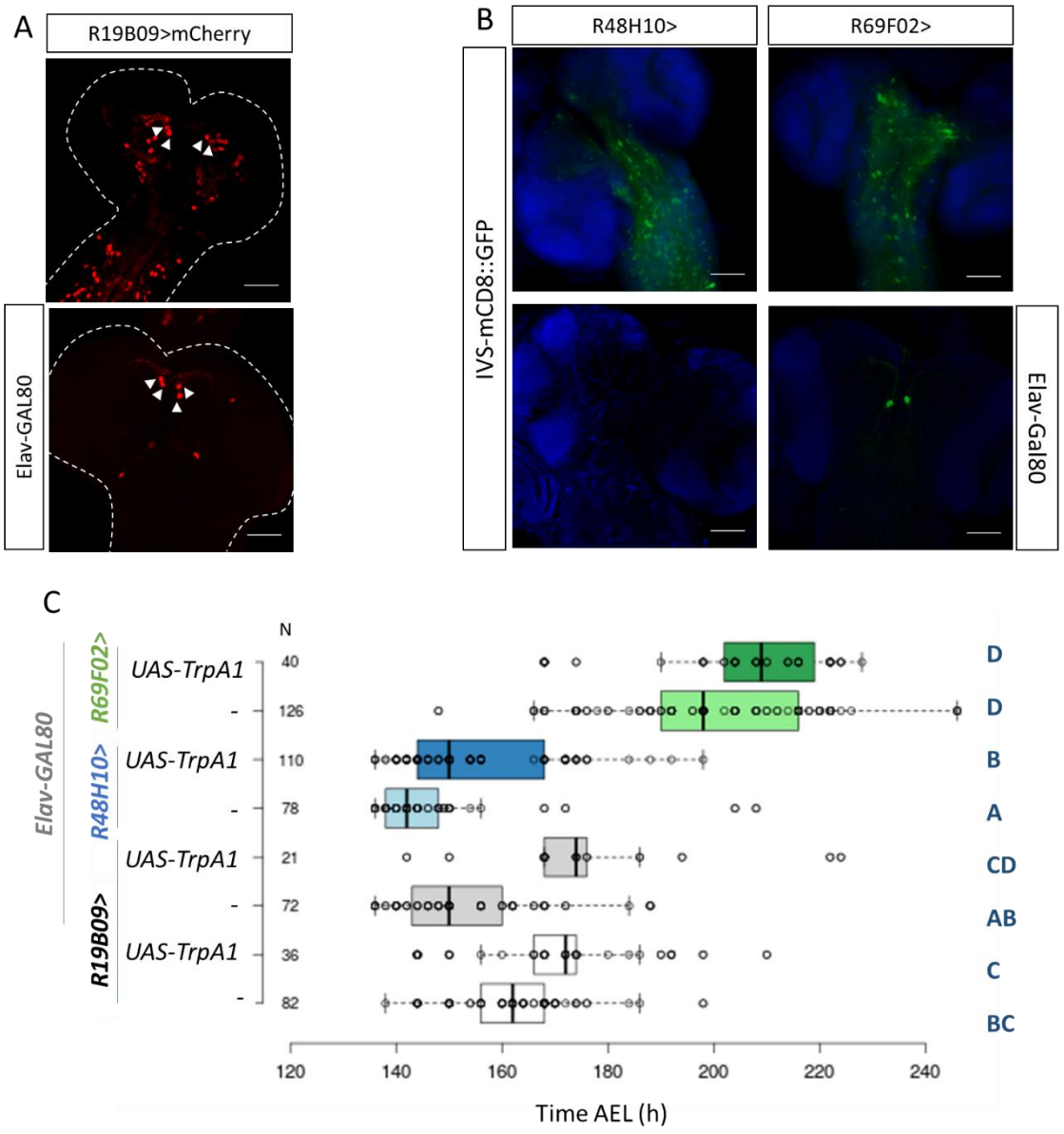

Figure 4.20. Preliminary evidence that some TrpA1-sensitive 2x-elav-GAL80-resistant cells drive developmental delays. (A) Sum of confocal z-stack slices of L3 brains stained with Living Colors DsRed antibody against mCherry (red), driven by *R19B09>*. CNS images were obtained from F1 larvae of the crosses between *R19B09>* and *UAS-mCherry* animals (left panel), and *elav-Gal80; R19B09>* and *elav-GAL80; UAS-mCherry* animals (right panel). PIL neurons are highlighted with arrowheads. (B) Sum of confocal z-stack slices of L3 brains stained with anti-GFP (green), driven by *R48H10>* or *R69F02>.* DAPI counterstain (blue). CNS images were obtained from F1 larvae of the crosses between *R48H10>* or *R69F02>* and 20XUAS-IVS-mCD8::GFP (left columns), and between *elav-Gal80; R48H10>* or *eav-Gal80; R69F02>* and 20XUAS-IVS-mCD8::GFP animals (right panels). (A,B) Scale bars, 50 µm. (C) Box plot showing pupariation time of (N) larvae expressing *UAS-TrpA1* driven by the REs *R19B09>*, *R48H10>*, and *R69F02>* in the presence of *2x-elav-GAL80.* As negative controls, animals of the genotype *elav-GAL80; RE>* were crossed with *w[1118]* animals. Additional controls were made for the *R19B09>* driver. This experiment requires similar controls, and must thus be repeated and the current data considered preliminary. Whiskers extend to data points that are less than 1.5 x IQR away from 1st/3rd quartile, dots represent all data, the black vertical bars represent the median and the plus sign represents the mean. $P < 0.0001$, Kruskal–Wallis one-way ANOVA test. Genotypes sharing the same letter (blue) are not statistically different at $\alpha = 0.01$, Dunn's *post hoc* test.

5 MAJOR CONCLUSIONS

The Dilp8-Lgr3 pathway is critical to ensure developmental stability in *D. melanogaster*. PIL neurons are among the population of Lgr3-positive cells requiring Lgr3 for the Dilp8-dependent developmental delay activity, which respond to Dilp8 by increasing cAMP levels (Colombani et al. 2015; Garelli et al. 2015; Vallejo et al. 2015). This, together with the finding that PIL neurons respond to ectopic Dilp8 expression by increasing cAMP levels, makes PIL neurons good candidates to mediate the response of Lgr3 to the Dilp8-dependent delay (Garelli et al. 2015; Vallejo et al. 2015). This led to a model where the Dilp8 signal, produced from aberrantly-growing imaginal-discs, somehow reaches the brain and signals to membrane-bound Lgr3 in the PIL interneurons, leading to an increase in cAMP levels in the PIL neurons. This would then "activate" PIL neurons to send a downstream signal that delays ecdysone biosynthesis in the ring gland, causing a delay in the onset of pupariation (see "Previous Model" in **Figure 5.1**). Our main goal was to test this model by generating PIL neuron-specific gene drivers. Some of the questions we tried to answer were: Are PIL neurons the only Lgr3-positive neurons involved in Dilp8-Lgr3 pathway? If yes, then how do they relay information to the ring gland? Is PIL neuron activation sufficient to delay the onset of metamorphosis?

Our data support the fact that Lgr3 is required in PIL neurons to convey the Dilp8 peripheral stress signal and delay development. By fragmenting and mapping the *R19B09>* driver, a 3-kb DNA fragment corresponding to the seventh intron of the *Lgr3* gene that had been previously shown to drive gene expression in ~270 CNS neurons, four of which are the PIL neurons (Colombani et al. 2015; Garelli et al. 2015; Vallejo et al. 2015), we found at least two ~300-bp fragments containing shadow enhancers that are active in PIL neurons. Driving RNAi against *Lgr3* under the control of each of these enhancers was sufficient to suppress the delay induced by the constitutive expression of *Tub-Dilp8*, suggesting that Lgr3 is required in the cells where these REs are active, which included the PIL neurons. One cautionary finding, however, was that we also found an ~1-kb fragment, R19B09.2, that suppresses the Dilp8-dependent delay when driving *Lgr3-IR*, but has only barely detectable expression in PIL neurons. While this result needs to be confirmed and better quantified, it does not allow the rejection of the hypothesis that PIL neurons are the neurons where Lgr3 is required to induce the delay in pupariation, because there is at least some *R19B09.2>*-driven gene expression in PIL neurons, which could be enough to reduce *Lgr3* levels to a level that rescues the Dilp8-dependent delay. Consistent with this rationale, *Lgr3* RNAi experiments using constructs of different strength have shown that the Dilp8 delay is indeed exquisitely sensitive to Lgr3 dosage (Garelli et al. 2015).

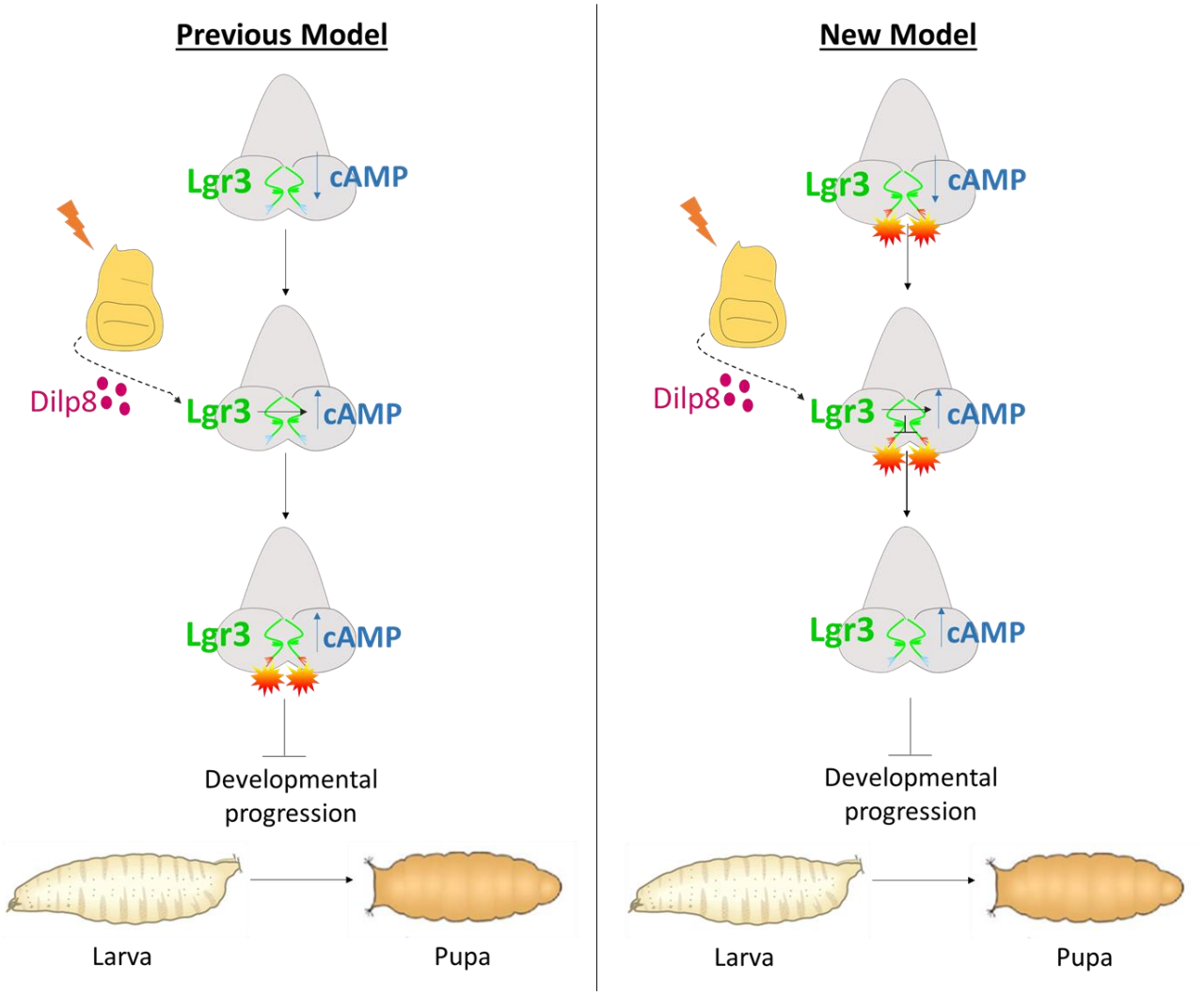

Figure 5.1. Models of the Dilp8-Lgr3 pathway, leading to a delay in the developmental progression. The current initial model (Previous Model) suggests that Lgr3 neurons, including PIL neurons, are in an inactive state (inactive zone, blue) with low concentration of cAMP, until the Dilp8 peripheral tissue stress signal activates Lgr3 receptor in PIL neurons. This activation leads to an increase of cAMP in PIL neurons and consequently its synaptic activation (orange star represents synaptic activation; active zone, orange). PIL neuron activation induces a delay in developmental progression (larval to pupal transition). The new model, based on the results obtained in this thesis, suggests that PIL neurons are permanently active (or gain this property during development). The Dilp8 peripheral tissue stress signal activates Lgr3 receptor in PIL neurons which leads to an increase of cAMP levels as in the previous model. However, instead of activating the PIL neurons, Lgr3-dependent cAMP activation leads to PIL neurons silencing, which inhibits developmental progression, resulting in a delay in the onset of metamorphosis.

In contrast, one hypothesis that we rejected based on the results obtained in this thesis is that PIL neuron activation leads to a delay in development. This rejection is based on the following pieces of evidence. We found different drivers (*R19B09.3B>, 3C>, 3D>,* and *3E>*), all of which drive gene expression in cells where Lgr3 is required to mediate the Dilp8-dependent delay, drive expression in cells capable of inducing a delay when thermogenetically activated with TrpA1, and anatomically drive expression in PIL neurons. Our initial hypothesis, based on the current model of the Dilp8-Lgr3-pathway, was that the subset of cells performing both Lgr3 and TrpA1-dependent functions was the same: PIL neurons. However, this hypothesis is incompatible with our findings with the drivers *R19B09.2>* and *R19B09.3A>*, as neither drives expression in TrpA1-sensitive cells that induce a developmental delay, but do drive expression in *Lgr3*-sensitive cells and PIL neurons as described above **(Figure 5.2)**. Hence, we can conclude that the cells that respond to TrpA1

thermogenetic activation by delaying the onset of metamorphosis are neither the PIL neurons nor the cells in which Lgr3 is required to respond to the Dilp8 delay signal. These data are consistent with PIL neurons being the cells in which Lgr3 is required for the delay as proposed in the previous model, but lead to the following question: if PIL neuron activation does not delay development, what does Lgr3 activation upon Dilp8 signalling do the PIL neurons apart from increasing cAMP levels?

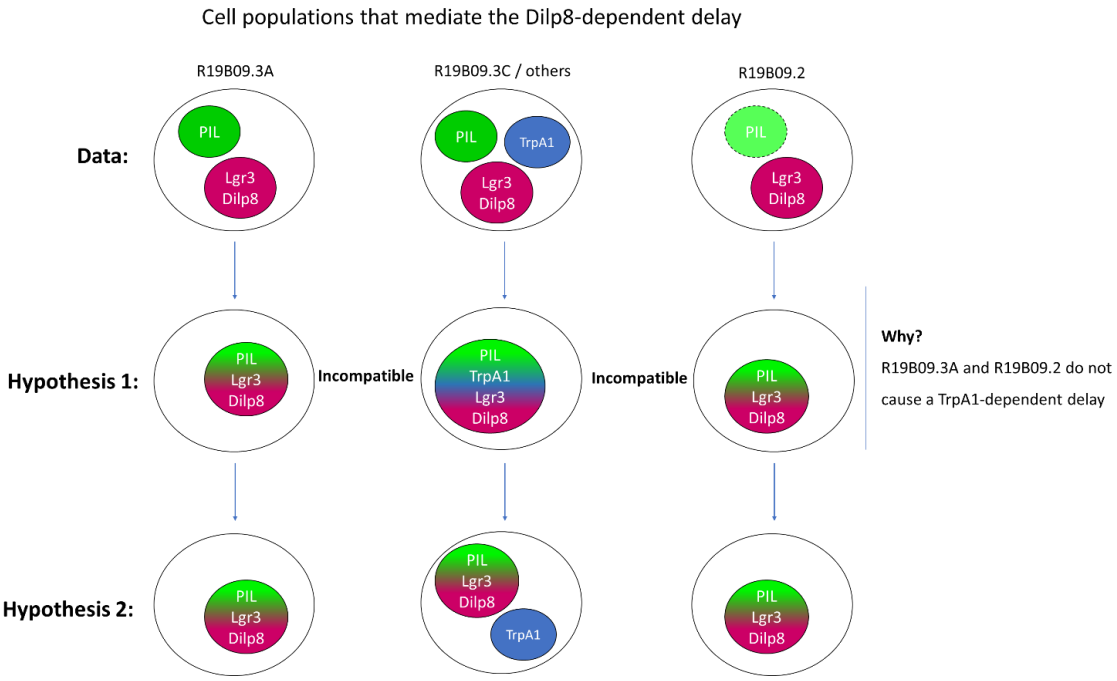

Figure 5.2. Summary of the cell populations found that mediate the Dilp8-dependent delay. Each RE drives expression in a limited population of cells (black circle). Our data suggests that R19B09.3A> drives expression in PIL neurons (green circle) and in cells where Lgr3 is required for the Dilp8-dependent delay ("Lgr3-Dilp8" cells, magenta circle); that R19B09.3C> and the remaining R19B09.3> REs drive expression in PIL neurons, in cells where Lgr3 is required for the Dilp8-dependent delay, and in TrpA1-sensitive cells (blue circle); and that R19B09.2> drive weak expression in PIL neurons (yet to be quantified, green circle with dashed lines) and in Lgr3-Dilp8 cells. Our first hypothesis (Hypothesis 1) was that all these populations were the same, however this is not possible, because R19B09.3A> and R19B02.2> do not cause a TrpA1-dependent delay. We therefore came up with a new hypothesis (Hypothesis 2) in which there are two different cell populations: 1) PIL neurons being the cells where Lgr3 is required for the Dilp8-dependent delay; and 2) the TrpA1-sensitive cells that induce a delay.

A possible answer to this question came from experiments using a Flp-out recombination system to restrict gene expression towards PIL neurons so we could manipulate it genetically with more precision. Namely, we generated a driver to manipulate cells where the expression pattern of the R19B09> and MZ699> drivers intersect (*MZ699 ∩ RB19B09>)*. As expected from previous anatomical and functional experiments (Garelli et al. 2015), *MZ699 ∩ RB19B09>* drove expression a restricted number of cells which included the PIL neurons and a dozen of VNC cells. We used *MZ699 ∩ RB19B09>* to thermogenetically activate the PIL neurons with TrpA1, and not only a delay was not observed, but instead, *MZ699 ∩ RB19B09>TrpA1* larvae even pupariated precociously in some experiments. As with either driver alone, TrpA1 thermogenetic activation causes a delay, we can conclude that non-redundant cells may be involved in producing the TrpA1-dependent delay, masking the actual effect of TrpA1 on PIL neurons. These results were consistent with the fact that silencing the few *MZ699 ∩ RB19B09>*-expressing cells with Kir2.1-mediated neuronal hyperpolarization extended the developmental delay caused by *Tub-dilp8* expression. Taken together, these results suggest a model where,

contrary to what we thought, PIL neurons have a constitutive activity that promotes pupariation, which is temporarily silenced upon Dilp8-Lgr3 signalling. In this new model, we can suggest that PIL neurons are indeed pupariation-promoting neurons. However, despite being the most sparsely-expressed PIL neuron driver yet made, the *MZ699 ∩ RB19B09>* driver still carries limitations: it is expressed in other neurons that can still interfere with our ability to understand PIL neuron function and it is based on a recombination strategy that leads to variable and incomplete expression in the intersecting cells. Therefore, new experiments need to be performed to confirm this hypothesis and the use of new drivers with better and more restricted expression patterns is essential.

With the aim of making such specific PIL neuron drivers, we launched an effort to find new REs driving expression in PIL neurons, which resulted in the characterization of four REs: R19B09.3A, R19B09.3C, R25E10 and R29B09. These would allow the construction of new recombinase-mediated intersectional drivers, Split-Gal4 intersectional drivers, or the new and hopefully highly specific VEnCode-based gene drivers, which should allow the manipulation of cells in which up to four expression patterns intersect.

In this thesis, I also found evidence for different cell populations, characterized by the drivers *R48H10>* and *R69F02>,* that are capable of delaying pupariation time in an Lgr3-independent manner. Whether or not these cells are the same as the non-PIL neuron *R19B09>*-expressing cells that delay development when thermogenetically activated with TrpA1, is not clear. My finding of GAL80-resistant *R19B09>* and *R69F02>*-expressing cells capable of induce a TrpA1-dependent delay could help in the identification and further characterization of these cell populations. It is important to state that we do not have any evidence that these cells act in the Dilp8-Lgr3 pathway, but is still formally possible that they might act downstream of PIL neurons. They could also regulate other developmental pathways related with feeding behaviour or insulin-producing cell physiology. Another important conclusion that can be drawn from my thesis regards PIL neuron neuroanatomy. I observed, using single-cell MCFO labelling that the bilateral pairs of PIL neurons are different: while both send ipsilateral and contralateral projections to the anterior-dorsalmost compartments of the neuropil, only one bilateral PIL neuron sends ipsilateral projections towards the subesophageal zone. These results open up the very interesting possibility that each PIL neuron has a different function. Is Lgr3 really required in both PIL neuron subtypes? Why one PIL neuron apparently receives input from the subesophageal zone (SEZ) and the other one doesn't? Is this different neuroanatomy functionally relevant for the Dilp8-Lgr3 pathway? It will be very interesting to generate drivers to genetically manipulate either PIL neuron subtype separately.

A broadly-applicable take-home message about my work is to highlight the importance of generating cell type specific gene drivers to understand cell function in complex organs as the CNS: activating and silencing large populations of neurons can lead to erroneous conclusions about cell function and can mask single-neuron properties. In this sense, VEnCode-based cell-specific drivers offer a promising avenue to studying the function of components of neuronal circuits in Drosophila CNS as well as in other animals.

REFERENCES

Adams, M.D. et al., 2000. The Genome Sequence of Drosophila melanogaster. *Science*, 287(5461).

Agui, N. et al., 1979. Cellular localization of the insect prothoracicotropic hormone: In vitro assay of a single neurosecretory cell. *Proceedings of the National Academy of Sciences of the United States of America*, 76(11), pp.5694–5698.

Anraku, Y., Mizutani, R. & Satow, Y., 2005. Protein Splicing: Its Discovery and Structural Insight into Novel Chemical Mechanisms. *IUBMB Life*, 57(8), pp.563–574.

Bathgate, R.A.D. et al., 2013. Relaxin Family Peptides and Their Receptors. *Physiological Reviews*, 93(1), pp.405–480.

Brand, A.H. & Perrimon, N., 1993. Targeted gene expression as a means of altering cell fates and generating dominant phenotypes. *Development*, 118(2), pp.401–15.

Butala, M., Žgur-Bertok, D. & Busby, S.J.W., 2009. The bacterial LexA transcriptional repressor. *Cellular and Molecular Life Sciences*, 66(1), pp.82–93.

Cannavò, E. et al., 2016. Shadow Enhancers Are Pervasive Features of Developmental Regulatory Networks. *Current biology : CB*, 26(1), pp.38–51.

Cao, C. & Brown, M.R., 2001. Localization of an insulin-like peptide in brains of two flies. *Cell and tissue research*, 304(2), pp.317–321.

Carvajal-Vallejos, P. et al., 2012. Unprecedented rates and efficiencies revealed for new natural split inteins from metagenomic sources. *Journal of Biological Chemistry*, 287(34), pp.28686–28696.

Cheriyan, M. et al., 2013. Faster protein splicing with the nostoc punctiforme DnaE intein using non-native extein residues. *Journal of Biological Chemistry*, 288(9), pp.6202–6211.

Colombani, J. et al., 2015. Drosophila Lgr3 Couples Organ Growth with Maturation and Ensures Developmental Stability. *Current Biology*, 25(20), pp.2723–2729.

Colombani, J., Andersen, D.S. & Léopold, P., 2012. Secreted Peptide Dilp8 Coordinates. *Science*, 336, pp.582–586.

Combes, P. et al., 2002. The streptomyces genome contains multiple pseudo-attB sites for the (phi)C31-encoded site-specific recombination system. *Journal of bacteriology*, 184(20), pp.5746–52.

Dassa, B. et al., 2009. Fractured genes: A novel genomic arrangement involving new split inteins and a new homing endonuclease family. *Nucleic Acids Research*, 37(8), pp.2560–2573.

Davidowitz, G., D'Amico, L.J. & Nijhout, H.F., 2003. Critical weight in the development of insect body size. *Evolution & Development*, 5(2), pp.188–197.

Duffy, J.B., 2002. GAL4 system indrosophila: A fly geneticist's swiss army knife. *Genesis*, 34(1-2), pp.1–15.

Edgar, B.A., 2006. How flies get their size: genetics meets physiology. *Nat Rev Genet*, 7(12), pp.907–916.

Evanko, D., 2007. Controlling proteins the intein way. *Nat Meth*, 4(2), pp.112–113.

Fischer, J.A. et al., 1988. GAL4 activates transcription in Drosophila. *Nature*, 332(6167), pp.853–856.

Fish, M.P. et al., 2007. Creating transgenic Drosophila by microinjecting the site-specific ϕC31 integrase mRNA and a transgene-containing donor plasmid. *Nature Protocols*, 2(10), pp.2325–2331.

Garelli, A. et al., 2015. Dilp8 requires the neuronal relaxin receptor Lgr3 to couple growth to developmental timing. *Nature communications*, 6, p.8732.

Garelli, A. et al., 2012. Imaginal Discs Secrete Insulin-Like Peptide 8 to Mediate Plasticity of Growth and Maturation. *Science*, 336(6081), pp.579–582.

Gokhale, R.H. & Shingleton, A.W., 2015. Size control: the developmental physiology of body and organ size regulation. *Wiley Interdisciplinary Reviews: Developmental Biology*, 4(4), pp.335–356.

Golic, K.G. & Lindquist, S., 1989. The FLP recombinase of yeast catalyzes site-specific recombination in the Drosophila genome. *Cell*, 59(3), pp.499–509.

Groth, A.C. et al., 2004. Construction of transgenic Drosophila by using the site-specific integrase from phage phiC31. *Genetics*, 166(4), pp.1775–1782.

Hackney, J.F., Zolali-Meybodi, O. & Cherbas, P., 2012. Tissue Damage Disrupts Developmental Progression and Ecdysteroid Biosynthesis in Drosophila. *PLoS ONE*, 7(11).

Halme, A., Cheng, M. & Hariharan, I.K., 2010. Retinoids Regulate a Developmental Checkpoint for Tissue Regeneration in Drosophila. *Current Biology*, 20(5), pp.458–463.

Hamada, F.N. et al., 2008. An internal thermal sensor controlling temperature preference in Drosophila. *Nature*, 454(7201), pp.217–220.

Henderson, D.S., 2004. The Chromosomes of Drosophila melanogaster. In D. S. Henderson, ed. Totowa, NJ: Humana Press, pp. 1–43.

Herboso, L. et al., 2015. Ecdysone promotes growth of imaginal discs through the regulation of Thor in D. melanogaster. *Scientific Reports*, 5, p.12383.

Hong, J.-W., Hendrix, D.A. & Levine, M.S., 2008. Shadow Enhancers as a Source of Evolutionary Novelty. *Science*, 321(5894), pp.1314–1314.

Hussey, R.G., Thompson, W.R. & Calhoun, E.T., 1927. The influence of x-rays on the development of drosophila larvae. *Science*, 66(1698), pp.65–66.

Ikeya, T. et al., 2016. Nutrient-Dependent Expression of Insulin-like Peptides from Neuroendocrine Cells in the CNS Contributes to Growth Regulation in Drosophila. *Current Biology*, 12(15), pp.1293–1300.

Ito, K. et al., 1997. GAL4-responsive UAS-tau as a tool for studying the anatomy and development of the Drosophila central nervous system. *Cell and tissue research*, 290(1), pp.1–10.

Jaszczak, J.S. et al., 2015. Nitric oxide synthase regulates growth coordination during Drosophila melanogaster imaginal disc regeneration. *Genetics*, 200(4), pp.1219–1228.

Jenett, A. et al., 2012. A GAL4-Driver Line Resource for Drosophila Neurobiology. *Cell Reports*, 2(4), pp.991–1001.

Katsuyama, T. et al., 2015. During Drosophila disc regeneration, JAK/STAT coordinates cell proliferation with Dilp8-mediated developmental delay. *Proceedings of the National Academy of Sciences of the United States of America*, 112(18), pp.2327–2336.

Li, H.-H. et al., 2014. A GAL4 Driver Resource for Developmental and Behavioral Studies on the Larval CNS of Drosophila. *Cell Reports*, 8(3), pp.897–908.

Li, Y., 2015. Split-inteins and their bioapplications. *Biotechnology Letters*, 37(11), pp.2121–2137.

Luan, H. et al., 2006. Refined spatial manipulation of neuronal function by combinatorial restriction of transgene expression. *Neuron*, 52(3), pp.425–436.

McBrayer, Z. et al., 2007. Prothoracicotropic hormone reegulates developmental timing and body size in Drosophila. *Dev. Cell*, 13(6), pp.857–871.

Meissner, G.W. et al., 2016. Sex-specific regulation of Lgr3 in Drosophila neurons. *Proceedings of the National Academy of Sciences*, 2016, p.201600241.

Menut, L. et al., 2007. A mosaic genetic screen for Drosophila neoplastic tumor suppressor genes based on defective pupation. *Genetics*, 177(3), pp.1667–1677.

Mills, K. V et al., 1998. Protein splicing in trans by purified N- and C-terminal fragments of the Mycobacterium tuberculosis RecA intein. *Proceedings of the National Academy of Sciences of the United States of America*, 95(7), pp.3543–3548.

Mirth, C., Truman, J.W. & Riddiford, L.M., 2016. The Role of the Prothoracic Gland in Determining Critical Weight for Metamorphosis in Drosophila melanogaster. *Current Biology*, 15(20), pp.1796–1807.

Mirth, C.K. & Riddiford, L.M., 2007. Size assessment and growth control: how adult size is determined in insects. *BioEssays*, 29(4), pp.344–355.

Nern, A., Pfeiffer, B.D. & Rubin, G.M., 2015. Optimized tools for multicolor stochastic labeling reveal diverse stereotyped cell arrangements in the fly visual system. *Proceedings of the National Academy of Sciences of the United States of America*, 112(22), pp.2967–2976.

Nijhout, H.F. & Williams, C.M., 1974. Control of Moulting and Metamorphosis in the Tobacco Hornworm, Manduca Sexta (L.): Cessation of Juvenile Hormone Secretion as a Trigger for Pupation. *Journal of Experimental Biology*, 61(2), pp.493–501..

Parvathi V, D., Amritha, A. & Paul, S.F., 2009. Wonder animal model for genetic studies - Drosophila melanogaster – its life cycle and breeding methods – a review. *Sri Ramachandra Journal of Medicine*, II(2).

Pfeiffer, B.D. et al., 2010. Refinement of Tools for Targeted Gene Expression in Drosophila. *Genetics*, 186(2).

Pfeiffer, B.D. et al., 2008. Tools for neuroanatomy and neurogenetics in Drosophila. *Proceedings of the National Academy of Sciences*, 105(28), pp.9715–9720.

Poodry, C.A. & Woods, D.F., 1990. Control of the developmental timer forDrosophila pupariation. *Roux's archives of developmental biology*, 199(4), pp.219–227.

Pozo, J. & Argente, J., 2002. Delayed puberty in chronic illness. *Best Practice & Research Clinical Endocrinology & Metabolism*, 16(1), pp.73–90.

Pulver, S.R. et al., 2009. Temporal dynamics of neuronal activation by Channelrhodopsin-2 and TRPA1 determine behavioral output in Drosophila larvae. *Journal of neurophysiology*, 101(6), pp.3075–3088.

Reiter, L.T. et al., 2001. A Systematic Analysis of Human Disease-Associated Gene Sequences In Drosophila melanogaster. *Genome Research*, 11(6), pp.1114–1125.

Rosenzweig, M. et al., 2005. The Drosophila ortholog of vertebrate TRPA1 regulates thermotaxis. *Genes & Development*, 19(4), pp.419–424.

Rulifson, E.J., Kim, S.K. & Nusse, R., 2002. Ablation of Insulin-Producing Neurons in Flies: Growth and Diabetic Phenotypes. *Science*, 296(5570), pp.1118–1120.

Saleh, L. & Perler, F.B., 2006. Protein splicingIn Cis andIn Trans. *The Chemical Record*, 6(4), pp.183–193.

Shingleton, A.W., 2010. The regulation of organ size in Drosophila: Physiology, plasticity, patterning and physical force. *Organogenesis*, 6(2), pp.76–87.

Shingleton, A.W. et al., 2005. The Temporal Requirements for Insulin Signaling During Development in Drosophila. *PLoS Biol*, 3(9), p.289.

Shuman, S., 1994. Novel approach to molecular cloning and polynucleotide synthesis using vaccinia DNA topoisomerase. *The Journal of biological chemistry*, 269(51), pp.32678–32684.

Shuman, S., 1991. Recombination mediated by vaccinia virus DNA topoisomerase I in Escherichia coli is sequence specific. *Proceedings of the National Academy of Sciences of the United States of America*, 88(22), pp.10104–1018.

Simpson, P., Berreur, P. & Berreur-Bonnenfant, J., 1980. The initiation of pupariation in Drosophila: dependence on growth of the imaginal discs. *Journal of embryology and experimental morphology*, 57, pp.155–165.

Slaidina, M. et al., 2009. A Drosophila Insulin-like Peptide Promotes Growth during Nonfeeding States. *Developmental Cell*, 17(6), pp.874–884.

Soller, M., Bownes, M. & Kubli, E., 1999. Control of Oocyte Maturation in Sexually Mature Drosophila Females. *Developmental Biology*, 208(2), pp.337–351.

Stieper, B.C. et al., 2008. Imaginal discs regulate developmental timing in Drosophila melanogaster. *Developmental Biology*, 321(1), pp.18–26.

Tennessen, J.M. & Thummel, C.S., 2011. Coordinating growth and maturation - Insights from drosophila. *Current Biology*, 21(18), pp.750–757.

Thiel, I. V. et al., 2014. An atypical naturally split intein engineered for highly efficient protein labeling. *Angewandte Chemie - International Edition*, 53(5), pp.1306–1310.

Thornhill, R. & Møller, a P., 1997. Developmental Stability, Disease and Medicine. *Biological Reviews of the Cambridge Philosophical Society*, 72(4), pp.497–548.

Thorpe, H.M., Wilson, S.E. & Smith, M.C., 2000. Control of directionality in the site-specific recombination system of the Streptomyces phage phiC31. *Molecular microbiology*, 38(2), pp.232–241.

Thummel, C.S., 2001. Molecular Mechanisms of Developmental Timing in C. elegans and Drosophila. *Developmental Cell*, 1(4), pp.453–465.

Truong, D.-J.J. et al., 2015. Development of an intein-mediated split–Cas9 system for gene therapy. *Nucleic Acids Research*, 43(13), pp.6450–6458.

Del Valle Rodriguez, A., Didiano, D. & Desplan, C., 2012. Power tools for gene expression and clonal analysis in Drosophila. *Nat Meth*, 9(1), pp.47–55.

Vallejo, D.M. et al., 2015. A brain circuit that synchronizes growth and maturation revealed through Dilp8 binding to Lgr3. *Science (New York, N.Y.)*, (October), pp.1–16.

Wagh, D.A. et al., 2006. Bruchpilot, a Protein with Homology to ELKS/CAST, Is Required for Structural Integrity and Function of Synaptic Active Zones in Drosophila. *Neuron*, 49(6), pp.833–844.

Walker, G.C., 1984. Mutagenesis and inducible responses to deoxyribonucleic acid damage in Escherichia coli. *Microbiological reviews*, 48(1), pp.60–93.

Walkiewicz, M.A. & Stern, M., 2009. Increased Insulin/Insulin Growth Factor Signaling Advances the Onset of Metamorphosis in Drosophila. *PLoS One*, 4(4), p.5072.

Wischmeyer, E., Döring, F. & Karschin, A., 1998. Acute suppression of inwardly rectifying Kir2.1 channels by direct tyrosine kinase phosphorylation. *The Journal of biological chemistry*, 273(51), pp.34063–34068.

Zhang, H. et al., 2009. Deletion of Drosophila insulin-like peptides causes growth defects and metabolic abnormalities. *Proceedings of the National Academy of Sciences of the United States of America*, 106(46), pp.19617–19622.

Zhou, X. et al., 2006. Optimization of the Tet-On system for regulated gene expression through viral evolution. *Gene Therapy*, 13, pp.1382–1390.